THE ROLE OF TWO-PORE POTASSIUM TRESK CHANNELS IN THE REGULATION OF CIRCADIAN RHYTHMS IN MAMMALS

AISTE STEPONENAITE

A thesis submitted in partial fulfilment of the requirements of the University of Kent and the University of Greenwich for the Degree of Doctor of Philosophy

October 2019

The Declaration

I certify that the work contained in this thesis, or any part of it, has not been accepted in substance for any previous degree awarded to me and is not concurrently being submitted for any degree other than that of Doctor of Philosophy being studied at the University of Kent and Greenwich. I also declare that this work is the result of my own investigations, except where otherwise identified by references and that the contents are not the outcome of any form of research misconduct.

Acknowledgements

There are so many people that were involved in helping me to be where I am now and helping to shape my personality. I believe that there is a purpose for each person we meet and I could not thank enough for each one of them and their input to my life.

First of all, I would like to thank my supervisor, Gurprit Lall. Thank you for the trust, support and guidance throughout these years, for always finding an encouraging word to say when I need it the most, for being my mentor and a role model. I have been truly blessed to have you as my supervisor and I could not imagine having a better work environment to the one I had working with you.

To Zameel Cader and Tatjana Lallic – thank you for the invaluable experience I had while being in Oxford and continuous support. Thank you for the opportunity to join your team and learn from your expertise. Thanks for Cader lab members (Yukyee, Grace, Paula, Elena, Galbha, Tina, Satyan, Bryan and others) for being so welcoming and friendly. And I would like to say thank you to Stuart Peirson and Sridhar Vasudevan for their help in facilitating my research and for the valuable advice.

To Alistair Mathie – I feel privileged to have you as part of my supervisory team. Your wise advice and knowledge have helped me to shape and plan my project and to always seek knowledge beyond my understanding.

I want to thank Charles River: their technicians, project coordinators and cheerful security staff. Thank you for taking care of the facility, for helping to run the experiments when I was away and for always making sure that I am safe and alive when working at nights.

Thanks to all fellow PhD students on Medway campus, especially Ahmad Taha, Amira Eltokhy and Sona Vyskocilova for helping to run the Postgraduate café. Without your commitment, dedication and creative ideas, PhD journey would not have been so enjoyable.

I want to say a special thank you for Lynne Martin – Medway campus chaplain. You have been by my side for the last six years, because of you and your work, I had a chance to meet so many wonderful people throughout the world – I feel like they are part of my family now. Thank you for your friendship, your hard work making sure that students are happy and taken care of, thank you for constantly listening to all of the never-ending problems of PhD students and for spreading happiness to our lives. Thank you for making us feel like at home.

To my partner, best friend and a life mate Basel Barakat. You have been by my side since the beginning of my University journey, always encouraging and supportive. Without your help, I

could have never believed that I can do a PhD, but you kept believing in me and making me believe in myself. Thank you for finding ways to brighten my day, to make me smile and to build my confidence more and more every day.

I would like to especially thank my parents, Antanas and Rima and to my brother Arunas. You have always believed in me and never stopped from achieving my dreams, even if it meant us living a thousand miles apart. Thank you for your unconditional love and your trust. None of this would have been possible without your support.

Preface

This thesis consists of a general introduction followed by nine data chapters, final discussion and future work chapters. Most of the data presented in experimental chapters will be included in the manuscript for publication.

This research programme was carried out in collaboration with the Zameel Cader's group at the University of Oxford, where I have spent 9 months of my PhD and still work in close collaboration with them.

Data presented in all results chapters was either obtained while working at the University of Kent or University of Oxford.

Abstract

The suprachiasmatic nucleus (SCN) is a principal circadian pacemaker synchronising our daily routines to environmental cues, such as the day/night cycle. The SCN relies on an endogenously generated electrical output rhythm as one of its timekeeping mechanisms. This consists of higher neuronal spontaneous activity during the day, which then silences during the night. Excitation of the SCN neurons is tightly regulated by two-pore domain potassium channels (K2P). These K2P channels play a role in establishing resting membrane potential and have been implicated in driving the excitability of SCN neurons.

TRESK – calcium regulated leak two-pore potassium channels are highly enriched in the SCN compared to other brain regions. We employed a TRESK knock-out mouse model to assess alterations in SCN molecular changes, behaviour output and electrical properties. [REDACTED]

Table of Contents

List of figures and tables

Abbreviations

5-HT	5-Hydroxytryptamine
AA's	Amino acids
AII	Angiotensin II
AMPA	α-amino-3-hydroxyl-5-methyl-4-isoxazole-propionate
ATP	Adenosine triphosphate
AVP	Arginine vasopressin
BMAL1	Brain muscle arnt-like 1
CALB	Calbidin
CALR	Calretinin
cGMP	Cyclic guanosine monophosphate
CK1	Casein kinase 1
CLOCK	Circadian locomotor output cycles kaput
CRE	cAMP response element
CREB	cAMP response element-binding protein
CRTC	CREB-regulated transcription coactivator
CRY	Cryptochrome
CT	Circadian time
Ct	Threshold cycle
DAG	Diglyceride
DD	Constant dark
EW	Edinger-Westphal
FDR	Fast delayed rectifier
GABA	γ-aminobutyric acid
GFAP	Glial fibrillary acidic protein
GHT	Geniculohypothalamic tract
GOI	Gene of interest
GRP	Gastrin releasing peptide
GTP	Guanosine triphosphate
HCN	Hyperpolarization activated cyclic nucleotide gated
i.p.	Intraperitoneal
IGL	Intergeniculate leaflet
iGluR	Ionotropic glutamate receptor
IP3	Inositol trisphosphate

IPL	Inner plexiform layer
ipRGCs	Intrinsically photosensitive retinal ganglion cells
iPSCs	Induced pluripotent stem cells
IR	Infrared
IRC	Irradiance response curve
K2P	Two-pore domain K+ channels
KO	Knock-out
LD	Light-dark
LL	Constant light
LUC	Luciferase
MARK	Microtubule affinity regulating kinases
mENK	Met-enkephalin
Meta II	Metarhodopsin II
mGluR	Metabotropic glutamate receptor
ND	Neutral density
NIF	Non-image forming
NK	Natural killer
NMDA	N-methyl-D-aspartate
NMDAR	N-methyl-D-aspartate receptor
NPY	Neuropeptide Y
NT	Neurotensin
OCT	Optimal cutting temperature
OPL	Outer plexiform layer
OPN	Olivary pretectal nucleus
PACAP	Pituitary adenylate cyclase-activating polypeptide
PCR	Polymerase chain reaction
PER	Period
PIP2	Phosphatidylinositol 4,5-bisphosphate
PKC	Protein kinase C
PLC	Phospholipase C
PLR	Pupillary light reflex
PRC	Phase response curve
PRL	Photoreceptor layer
PVN	Paraventricular nucleus of the hypothalamus
rAAV	Recombinant adeno-associated virus

RGC	Retinal ganglion cells
RHT	Retinohypothalamic tract
RMP	Resting membrane potential
RORE	Retinoic acid-related orphan receptor response element
RT-qPCR	Real-time quantitative polymerase chain reaction
RW	Running wheel
SCN	Suprachiasmatic nuclei
SPZ	Subparaventricular zone
TASK	TWIK-related acid-sensitive K+ channel
TM	Transmembrane
TRESK	TWIK-related spinal cord K+ channel
TTFL	Transcription/translation feedback loops
TWIK	Tandem of pore domains in a weak inward rectifying K+ channel
VIP	Vasoactive intestinal polypeptide
VPAC	Vasoactive Intestinal Peptide Receptor
WT	Wildtype
ZT	Zeitgeber time

1 Introduction

1.1 Environmental and biological rhythms around us

Many living systems possess elements of rhythmicity – from bacteria to complex mammal species, such as humans. These rhythms can be shorter or longer than 24 hours or repeating every 24 hours.

For example, in humans, the heart beats on average 80 times per minute, with a single cardiac cycle lasting about 0.8 seconds. This is a representation of an ultradian cycle because in 24-hour period multiple cycles of activity will occur. The opposite of this would be infradian rhythms as they cycle with a frequency lower than 24 hours, such as female's menstrual cycle or lunar rhythms.

Cyanobacteria perform photosynthesis during the daylight and nitrogen fixation at night, as there is no oxygen produced that would inhibit enzymes needed for nitrogen fixation. Plants also display daily rhythmicity, where rhythmic leaf movements and flower opening are an example. Humans exhibit multiple rhythmic activities that involve hormonal secretion at certain times of the day (for example, cortisol peaking in early morning and melatonin production increasing at night), body temperature or blood pressure changes throughout the day. All of these examples represent circadian rhythms – processes that happen on a 24-hour cycle.

In this thesis I will conduct behavioural and molecular work aiming at further deepening the understanding of mice circadian rhythms and will look at how they are regulated by leak potassium channels.

1.2 Regulation of circadian rhythms

We know that circadian rhythms maintain their 24-hour pattern even in the absence of sun, so how are they controlled?

Circadian rhythms are endogenously generated and regulated by a pacemaker called the suprachiasmatic nucleus (SCN). It has a self-sustained oscillation (variation in activity), therefore it is able to run even in the absence of light input or any other environmental cues. It also helps to synchronise the body to the external world and maintain its internal and external rhythms. In most non-mammalian species (e.g. birds) the pineal gland and retina act as a clock, with the pineal gland having rhythmic melatonin secretion.

In mammals the molecular clock is made of 20 000 tightly interconnected cells, it is self-autonomous, can indefinitely sustain circadian oscillations when isolated *in vitro* and it acts as circadian orchestrator linking behaviour and physiology to the surrounding world.

1.3 The suprachiasmatic nucleus (SCN)

The SCN is located in the rostral region of the hypothalamus, below the third ventricle and just above the optic chiasm (Figure 1). The average size of the human SCN is approximately 0.65mm^2 (Hofman *et al.*, 1988). Being in close proximity to the optic chiasm enables the SCN to receive visual inputs for light-dark entrainment through the direct and indirect retina to SCN pathways (Reppert and Weaver, 2001).

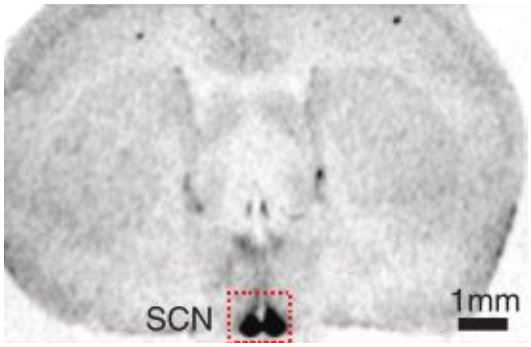

Figure 1: The mouse SCN (black structure boxed in red).

SCN is located above the optic chiasm, is at the base of anterior hypothalamus and below the third ventricle. Each nucleus consists of 10 000 cells. Staining shows the binding of SCN neuropeptide Prokineticin 2 to its receptor (image taken from Patton and Hastings (2018)).

Majority of SCN neurons are capable of generating an action potential. This indicates that the SCN is composed of autonomous, single-cell circadian oscillators driven by circadian clock genes, that upon photic stimulation facilitate transcription and translation of those gene products (Welsh et al. 1995; Antle & Silver 2005; Mohawk et al. 2012).

The SCN is a bilateral structure composed of two nuclei. Lesion experiments in rats helped to identify the SCN as the region responsible for circadian entrainment (Moore and Eichler, 1972; Stephan and Zucker, 1972). Following a bilateral ablation of SCN, it was observed that preoperative nocturnal drinking rhythms, as well as nocturnal activity rhythms, were completely eliminated, confirming the role of SCN as a circadian pacemaker.

1.3.1 SCN structure

SCN can be divided into two zones: the dorsomedial shell and ventrolateral core (Figure 2).

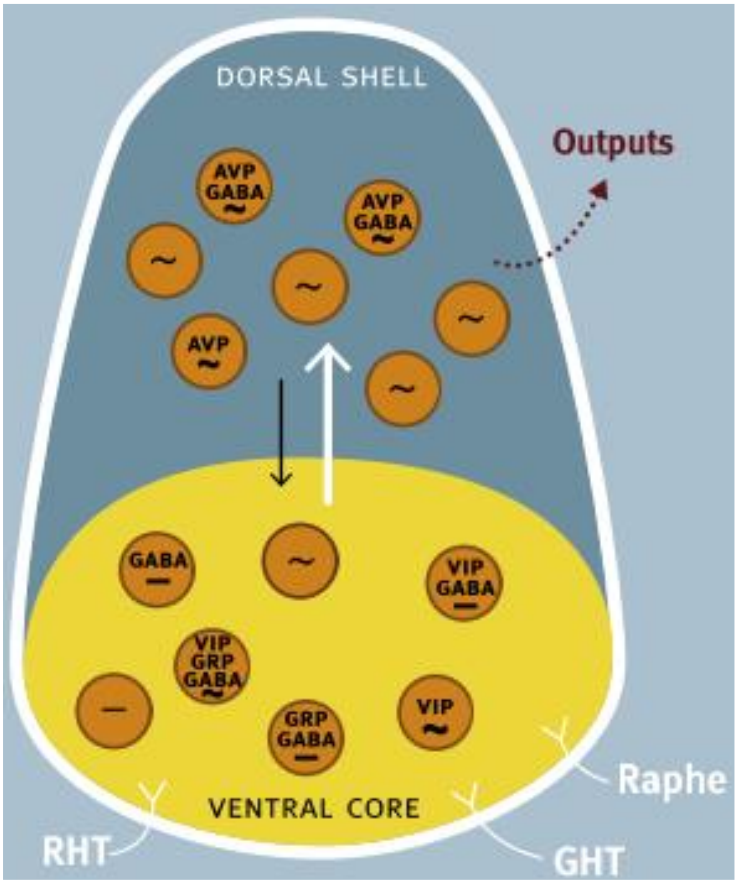

Figure 2: Schematic diagram of the dorsal/ventral division of the SCN.

Inputs from retinohypothalamic tract (RHT), geniculohypothalamic tract (GHT) and raphe nucleus are primarily received by the core of SCN. Core neurons contain vasoactive intestinal peptide (VIP) and gastrin-releasing peptide (GRP). The shell contains arginine-vasopressin (AVP) with GABA being ubiquitously expressed across the entire SCN. There is more communication happening between ventral to dorsal part of the SCN. However, the information could also be sent from dorsal part to the ventral (Albers et al., 2016).

The shell receives neuronal input from the basal forebrain, brainstem and thalamus. The core receives input from the hypothalamus and thalamus, it has a dense projection from midbrain raphe and it also receives both direct and indirect visual inputs (Figure 3) (Leak *et al.*, 1999). SCN core has dense projections to the shell, but there is little signalling coming from shell to the core (Welsh *et al.*, 2010).

The SCN is triggered by a number of different neurotransmitters that can act in an excitatory or inhibitory way. The ventrolateral core receives direct visual/photic input from the retina that comes through the retinohypothalamic tract (RHT), as well as indirect visual input coming from the intergeniculate leaflet (IGL) through the geniculohypothalamic tract (GHT). The core also receives non-photic inputs sent from raphe nuclei. The dorsomedial shell receives inputs from limbic, hypothalamic and brainstem nuclei, basal forebrain and hippocampus (Leak *et al.*, 1999; Abrahamson and Moore, 2001; Yan *et al.*, 2007).

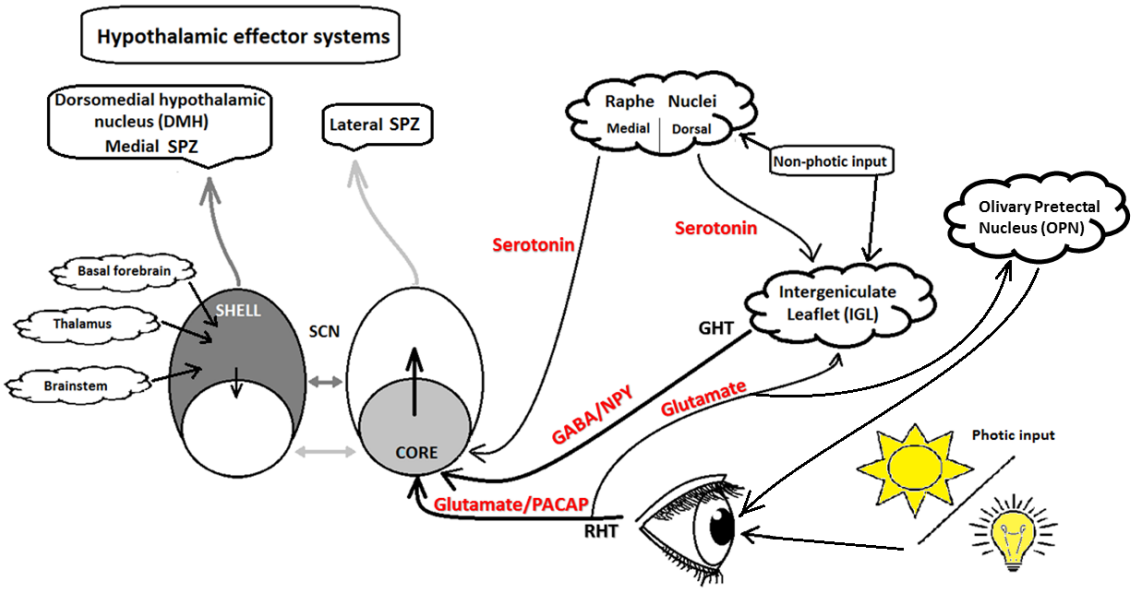

Figure 3: Main SCN innervation pathways.

ipRGCs use protein PACAP and glutamate for photic information transmission from the retina to the core of SCN through the optic nerve projection called retinohypothalamic tract (RHT) and to the intergeniculate leaflet. SCN also receives direct input from IGL transmitted by GABA and NPY through geniculohypothalamic tract (GHT) and from medial raphe nuclei transmitting signals by using serotonin that are stimulated by non-photic inputs. The shell of SCN also receives input which arises from brainstem, thalamus and basal forebrain. There are neurons connecting core and shell of SCN and so the signal from core can be transmitted to the shell and subparaventricular zone of the hypothalamus, which can be innervated by both, core or shell neurons leading to circadian regulation of body temperature, sleep and locomotor activity (Moga and Moore, 1997; Leak *et al.*, 1999; Moore *et al.*, 2002; Lall *et al.*, 2012; Morin, 2013a).

1.3.1.1 Glia cells in the SCN

Glia cells occupy about 65% of mouse and 90% of the human brain (Allen and Barres, 2009). Even though they do not fire action potentials, glia interact with neurons and surrounding blood vessels playing a crucial role in maintaining well-functioning neurons. To briefly summarise the key glia cells, microglia are immune cells of the brain and they engulf dead cells and debris. Oligodendrocytes enhance interneuron signalling by enwrapping axons with their lipid-rich membrane – myelin. Astrocytes provide energy, substrates for neurons and modulate synaptic function. Astrocytes in the SCN also express clock proteins that respond to light stimuli impacting phase of expression of these genes (Prolo, 2005). The presence of such circadian rhythms in astrocytes suggests that they might be involved in the control of circadian timekeeping.

Work by Brancaccio *et al.* (2017) and Tso *et al.* (2017) has proven the importance of astrocytes in the circadian clock. Unlike SCN neurons, astrocytes are active during the circadian night, thereby suppressing the neuronal activity through release of extracellular glutamate acting on NR2C receptors (a type of NMDA ionotropic glutamate receptor). Astrocytic glutamate could

potentially lead to changes in the molecular clock through modulating the clock gene expression. It could also be possible that during the night, when astrocytic glutamate is present, neurons increase the glutamate threshold level needed to result in clock gene expression changes. To prevent or dampen unnecessary neuronal excitation it is possible that leak potassium channels hyperpolarise molecular clock neurons, therefore it is harder to excite them at night. TRESK is one if the leak potassium channels and it is expressed in the SCN. Hence, there is a possibility that TRESK might contribute to silencing SCN neurons during the night. Astrocytes are also involved in determining the period length in the SCN. Ablating one of the molecular clock genes Bmal1 or deleting casein kinase 1 (enzyme facilitating protein phosphorylation) from astrocytes only led to an increase in circadian period of clock gene expression and locomotor activity. Recently, even more prominent role of astrocytes was published by Brancaccio *et al.* (2019). Their work has shown that in absence of neuronal cellular clocks, astrocytes are able to autonomously drive SCN oscillations and indefinitely sustain the neuronal and locomotor activity circadian patterns.

1.3.2 Intrinsic signalling within SCN

The dorsomedial shell of the circadian pacemaker is populated with small, closely packed neurons having arginine vasopressin (AVP), met-enkephalin (mENK) and angiotensin II (AII) as neurotransmitters. These neurons encapsulate ventrolateral core neurons that are loosely aggregated and can be distinguished by presence of vasoactive intestinal polypeptide (VIP), neuromedin S, gastrin-releasing peptide (GRP), neurotensin (NT) and calretinin (CALR) (Leak *et al.*, 1999; Abrahamson and Moore, 2001; Mohawk and Takahashi, 2011). Moreover, both, shell and core neurons contain γ-aminobutyric acid (GABA) and calbindin (CALB), where GABA is important for communication of non-photic information coming from IGL via the GHT to SCN (Lall and Biello, 2003).

There are also neurons connecting the dorsomedial and ventrolateral regions of the pacemaker. A number of projections from core to shell of the SCN have been found, but there are fewer signals sent from shell to the core (Mohawk and Takahashi, 2011). Differences in the SCN regions also arise at the level of synchronisation. Under typical 12:12 LD photoperiods, shell neurons are less tightly synchronised than the core which receives direct retinal input. Housing under increased day length (for example, 16:8 LD cycle) affects synchronisation of core neurons but not the shell and leads to expanded phase distribution. Long day housing also affects the duration of neuron activity and it is increased in the dorsal SCN. This shows that the ventral (core) photoperiod of the SCN is encoded at the network level, but dorsal (shell) SCN is coded at the individual cell level (Brown and Piggins, 2009).

1.4 Physiology of light decoding

1.4.1 Visual detection of light

We now know that the SCN controls our circadian rhythms and helps us to adapt to the surrounding world, but how does it happen? The only photoreceptive organ in our body is the eye. Light information is processed by photoreceptor cells present in the retina (Figure 4). Composition of retina perfectly serves its dual function – it conveys the visual image of surroundings through the optic nerve to the lateral geniculate nucleus in the thalamus and it is also crucial for encoding irradiance leading to non-image forming (NIF) behavioural and physiological responses to light (Lall *et al.*, 2010).

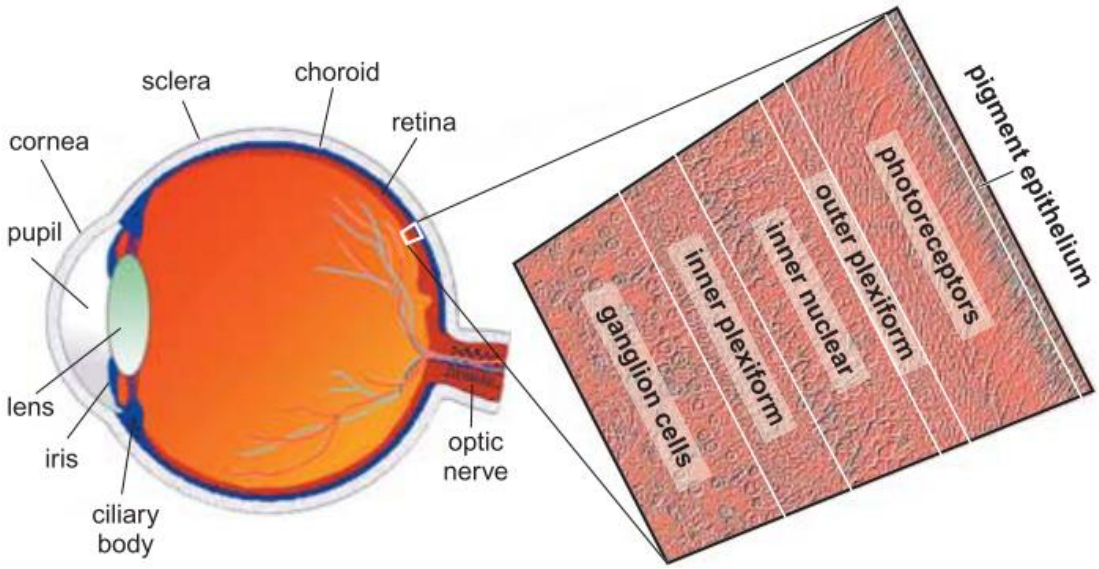

Figure 4: Human eye diagram and layers of the retina.

The retina at the back of the eye is composed of multiple layers with photoreceptors located in the deepest layer, next to the pigment epithelium. In inner nuclear layer, there are horizontal, bipolar and amacrine cells. In outer plexiform layer are synapses linking photoreceptors with dendrites of bipolar and horizontal cells. In the inner plexiform layer, bipolar and amacrine cells connect with the ganglion cells (Kolb, 2003).

Light passes to the retina through the pupil, which is the opening of the pigmented structure iris. The amount of light entering the eye through the pupil is regulated by antagonistic action of smooth muscles of iris. Constriction of sphincter or dilator muscles that are innervated by the autonomic nervous system controlled by the OPN changes pupil diameter thus regulating the amount of light entering the eye. This is also known as pupillary light reflex (PLR).

When light reaches the retina, it has to pass the entire retinal layer known as the photoreceptor layer that lies at the back of the retina. The location of photoreceptor cells

allows direct contact with pigment epithelial layer providing retinol (also known as vitamin A) needed for phototransduction (Kolb, 2003).

1.4.2 Non-image forming effects of light

There are three types of photoreceptors – rods, cones and melanopsin located in intrinsically photosensitive retinal ganglion cells (ipRGCs) (Figure 5).

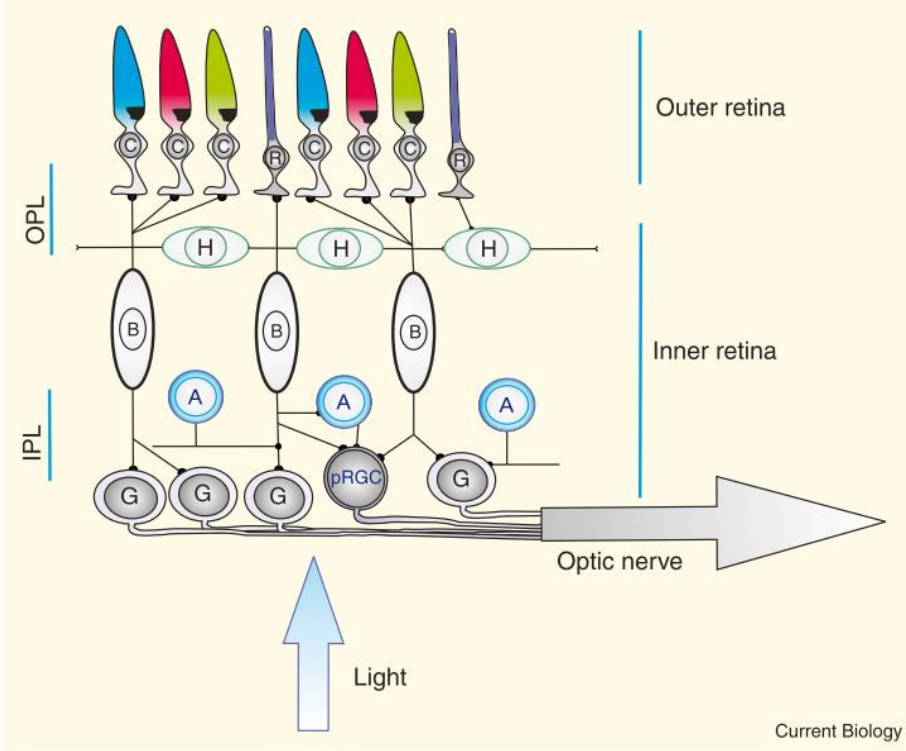

Figure 5: Light detection in the retina.

Rod (R) and cone (C) photopigments detect the light that causes conformational change enabling interaction between opsin and G-protein. Light information is further sent through the bipolar cells (B), to ganglion cells (G) in the inner plexiform layer (IPL). Horizontal cells (H) located at the outer plexiform layer (OPL) laterally connect photoreceptors and facilitate feedback. Amacrine cells (A) located at the IPL enable the lateral connection between bipolar and ganglion cells. In addition, there are intrinsically photosensitive retinal ganglion cells (ipRGCs) – they can detect the light directly, which is done with melanopsin photopigment. As a result, photodetection happens in both outer and inner retina (Foster and Hankins, 2007).

Light detected by rods and cones is transmitted through a multisynaptic pathway to the brain via retinal ganglion cells (RGC). Non-image forming (NIF) function of the retinal output mediates circadian photoentrainment as well as pupillary light reflex (PLR) (Lucas *et al.*, 2003; Güler *et al.*, 2008). These NIF functions are mediated by retinal photoreceptors rods and cones, as well as intrinsically photosensitive retinal ganglion cells (ipRGCs) containing melanopsin, which is responsible for intrinsic photosensitivity at high irradiances, as it was found by Lucas *et al.*, (2003). ipRGCs are directly photosensitive and can also be activated through rod/cone input (Güler *et al.*, 2008). Axons of ipRGCs project to the SCN, as well as to

the IGL and OPN thus contributing to the NIF responses to light. These structures are the key centres in circadian entrainment and pupillary light reflex (Hattar *et al.*, 2003).

Rods are the most sensitive and the most abundant retinal photoreceptors (Figure 6, left) (Masland, 2012). They are sensitive to dim light and respond to relatively slow changes. However, rods can distinguish light from dark even in bright light (500 photopic lux), as discovered in cone and melanopsin lacking animal models. This enables rods to drive non-image forming visual functions across a wide range of light intensities (Altimus *et al.*, 2010).

Cones start working at higher light intensities, when rods get saturated, with cones being able to detect rapid light fluctuations (Figure 6, right). Primates have three types of cones sensitive to different lights: blue, green and red. In order to enable good daylight vision, the fovea is densely packed with cones. Moreover, cones present in peripheral parts of the retina facilitate the detection of even very small amount of photons at night (Kolb, 2003).

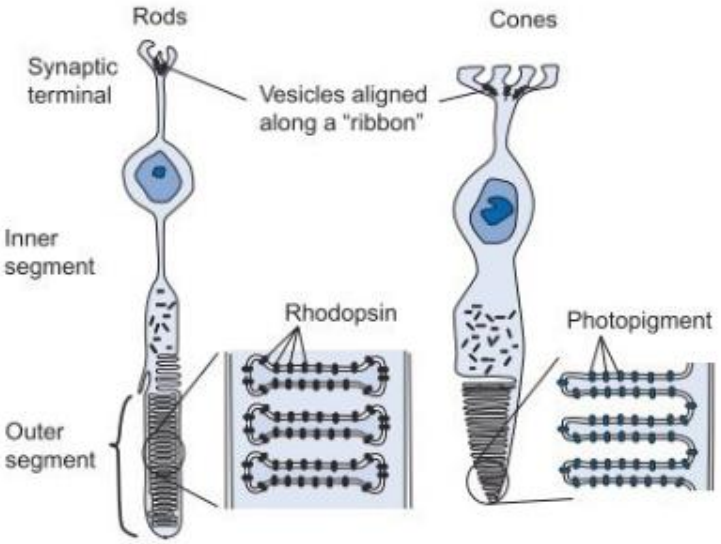

Long outer segment	Shorter outer segment
Large synaptic terminal	Larger synaptic terminal
High sensitivity	Low sensitivity
Scotopic vision	Photopic vision
Saturates in daylight	Saturates only in intense light
Lower temporal resolution (20 Hz)	High temporal resolution (70 Hz)
Rhodopsin	Erythrolabe Chlorolabe Cyanolabe
Low spatial acuity	High spatial acuity
Color blind	Color sensitive

Figure 6: Schematic diagram of rod and cone structures.

Rods and cones have an outer segment that contains light-sensitive opsins, as well as inner segment containing nucleus and mitochondria. Cones allow colour vision in the bright light (photopic vision) and rods allow vision in dim light (scotopic vision) (Feher, 2016).

Melanopsin is the least sensitive photoreceptor, therefore it is activated in the presence of bright light. In mice, melanopsin expressing cells comprise only 1% of the ganglion cell population, but this 1% plays a major role in NIF responses to light at the circadian level and pupillary responses (Sekaran *et al.*, 2003). Apart from being directly photosensitive, melanopsin containing ipRGCs also receive an input from rods and cones sending the signal to the brain (Güler *et al.*, 2008).

1.4.2.1 Phototransduction pathway

In summary, the following cascade of events happens in photoreceptors following light detection in the eye (Figure 7). Upon light stimulation, a photon is absorbed by a visual pigment molecule. It is located in outer segments of photoreceptor – a specialised ciliary structure in rods and cones. The visual pigment is a G-coupled receptor that consists of opsin

attached to vitamin A-derived chromophore, 11-cis-retinal. Absorption of a photon causes isomerisation from 11-cis to -trans, making it a physiologically active metarhodopsin II (Meta II). Meta II triggers a transduction cascade that leads to the closure of non-selective cation cGMP gated channels; it hyperpolarises photoreceptor and reduces the release of glutamate from the synapse (Kefalov, 2012).

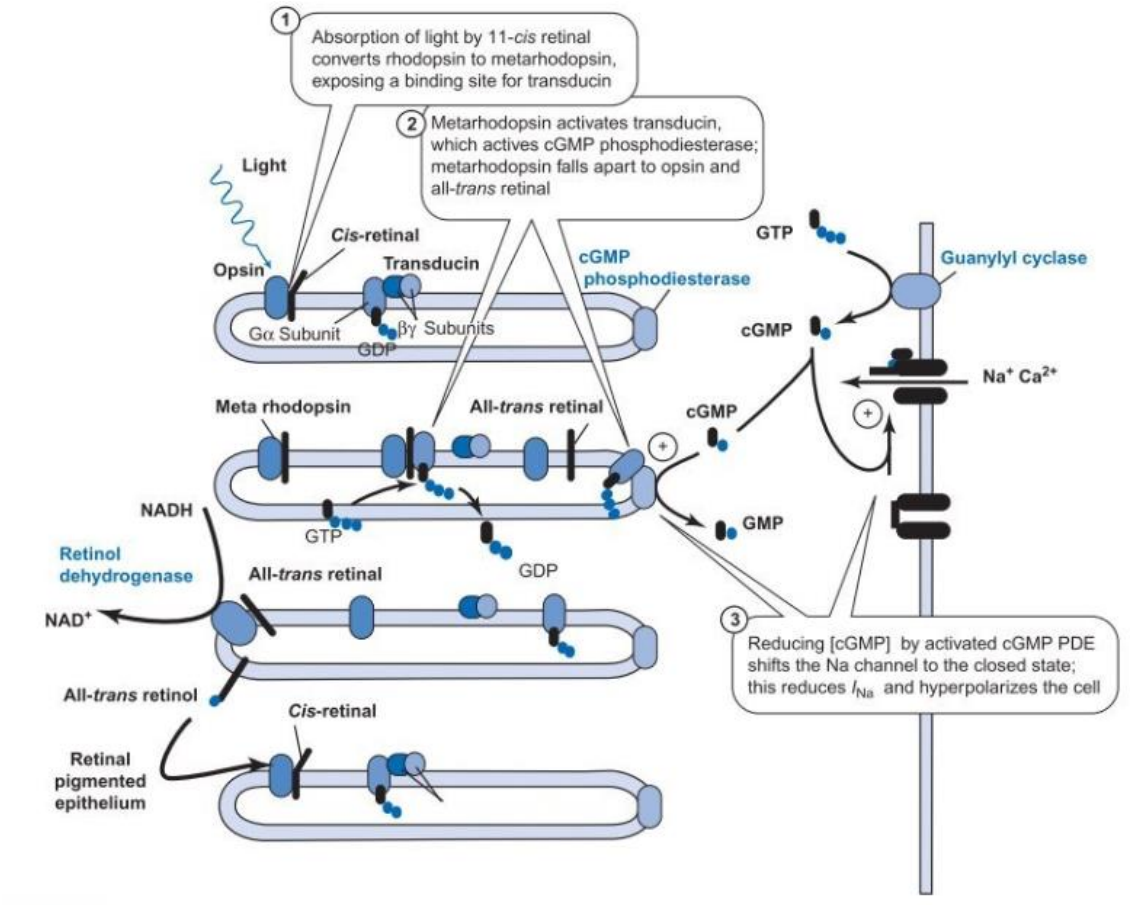

Figure 7: Photobleaching of rhodopsin and photodetection.

Rhodopsin contains opsin and its chromophore 11-cis retinal. Upon light absorption (1) 11-cis retinal isomerises to all-trans retinal and rhodopsin is therefore converted to metarhodopsin. (2) Metarhodopsin activates transducin, a heterotrimeric G-protein and its subunit activates cGMP phosphodiesterase. This lowers cGMP concentration (3), which in turn reduces inward sodium current, because of sodium channels closure. Metarhodopsin dissociates to form opsin and all-trans retinal, with all-trans retinal eventually converted back to cis-retinal (Feher, 2016).

In the dark photoreceptors are in a depolarised state. This is different from neurons, because they are hyperpolarised in their resting state and become depolarised when activated. Photoreceptors hyperpolarise in response to light, which is a calcium mediated response. Once the cascade is initiated, the opsin has to be restored to be active again. This involves regeneration of 11-cis-retinal from its -trans state. Figure 8 shows a cascade of events happening in photoreceptors during the dark and when light is present.

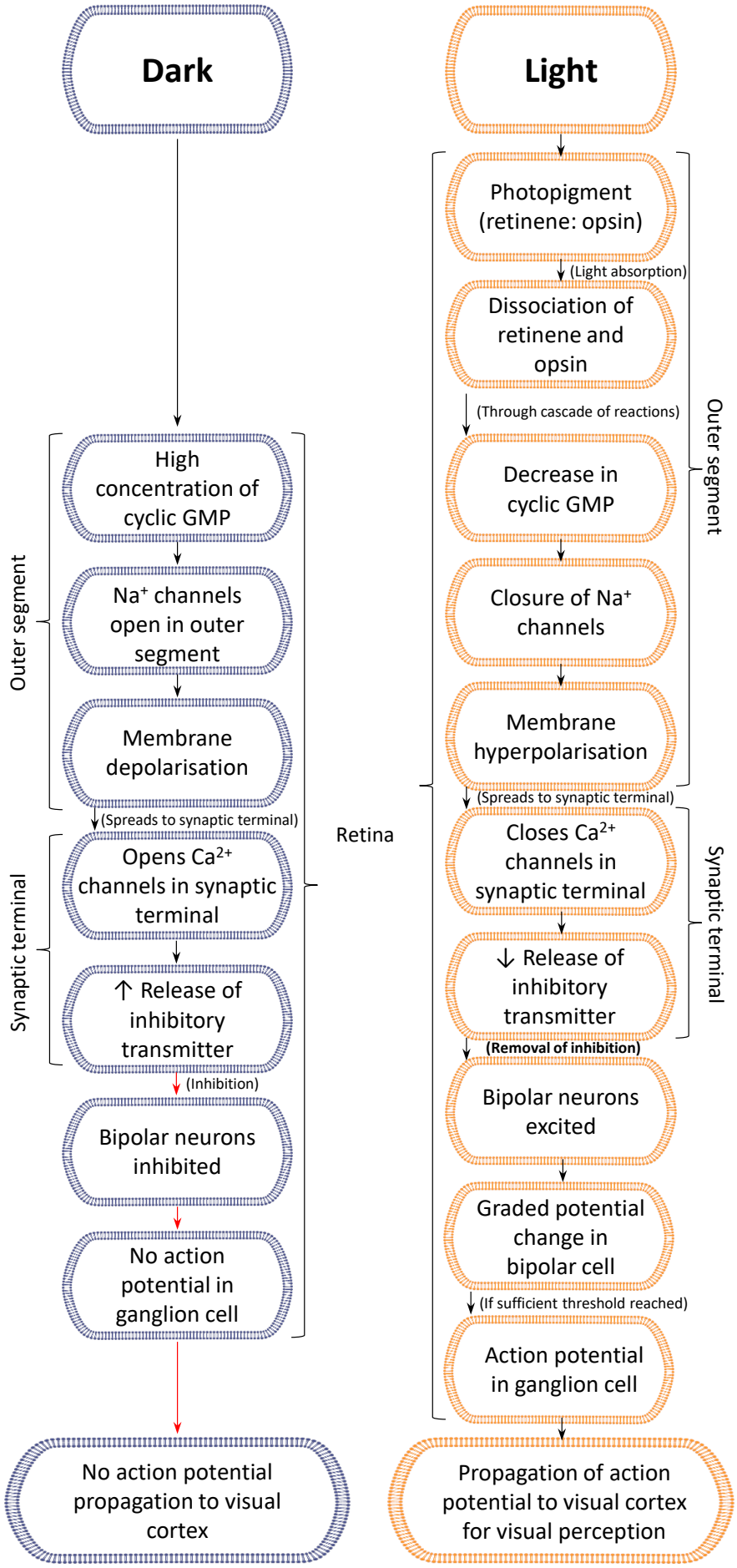
Dark
High concentration of cyclic GMP
Na+ channels open in outer segment
Membrane depolarisation
(Spreads to synaptic terminal)
Opens Ca2+ channels in synaptic terminal
↑ Release of inhibitory transmitter
(Inhibition)
Bipolar neurons inhibited
No action potential in ganglion cell
No action potential propagation to visual cortex
Outer segment
Synaptic terminal
Retina
Light
Photopigment (retinene: opsin)
(Light absorption)
Dissociation of retinene and opsin
(Through cascade of reactions)
Decrease in cyclic GMP
Closure of Na+ channels
Membrane hyperpolarisation
(Spreads to synaptic terminal)
Closes Ca2+ channels in synaptic terminal
↓ Release of inhibitory transmitter
(Removal of inhibition)
Bipolar neurons excited
Graded potential change in bipolar cell
(If sufficient threshold reached)
Action potential in ganglion cell
Propagation of action potential to visual cortex for visual perception
Outer segment
Synaptic terminal

Figure 8: Phototransduction and initiation of the action potential in the visual pathway.

Light-induced biochemical changes in photopigment close sodium channels located in the membrane of the outer segment, with the concentration of cGMP regulating the state of sodium channels. Light-induced hyperpolarisation spreads from the outer segment to the synaptic terminal of photoreceptor resulting in reduced neurotransmitter release that is light intensity-dependent (Sherwood, 1993).

1.4.2.2 Pupillary constriction

Pupil constriction regulates the amount of light entering the eye: pupils are constricted at high light intensities and dilated in dark-adapted conditions. During low light intensity, pupils can constrict about 50% compared to the fully dilated diameter and this is mediated by rod and cone input. However, for full constriction melanopsin present in ipRGC is needed (Güler *et al.*, 2008).

Branches of the RHT transmitting photic information project not only to the SCN, but also to the olivary pretectal nucleus (OPN) which regulates iris response to light (McNeill *et al.*, 2011). This provides an excellent way of assessing retinal decoding for non-image forming events such as circadian entrainment and the pupillary light reflex, enables the analysis of the photoreceptors and melanopsin function (Lucas *et al.*, 2003; Güler *et al.*, 2008).

OPN contains luminance sensitive neurons that have increased firing pattern during higher light irradiance, facilitating pupillary light reflex. Pathway mediating constriction of the pupils goes via Edinger-Westphal (EW) nuclei and ciliary ganglion (Klooster *et al.*, 1995). The postsynaptic fibres from OPN go to the EW nuclei. From each of the EW nucleus, CNIII nerve fibres enter the orbit and synapse at ciliary ganglion. Beyond the synapse, postsynaptic fibres form ciliary nerves innervate sphincter muscle facilitating pupillary constriction.

Pupil dilator muscles are innervated by the sympathetic nervous system. The sympathetic pupillary fibres originating in hypothalamus descend along the spinal cord and enter the centre of Budge present in the cervicothoracic region, where they synapse. Preganglionic fibres from the cord synapse at the superior cervical ganglion and postganglionic fibres via the ophthalmic branch of fifth cranial nerve. Some of the fibres directly go to long ciliary nerves innervating the dilator pupillae, whereas some of the fibres firstly go through ciliary ganglion and only then to the long ciliary nerves (Janisse, 2013).

Mice opsins have the highest sensitivity to a very similar wavelength (Figure 9). The peak sensitivity for S-cone opsin is 360nm, melanopsin – 480nm, rod opsin – 498nm and M-cone opsin – 508nm (Lucas *et al.*, 2012). Using light in between 480-500nm enables to achieve maximum pupillary constriction.

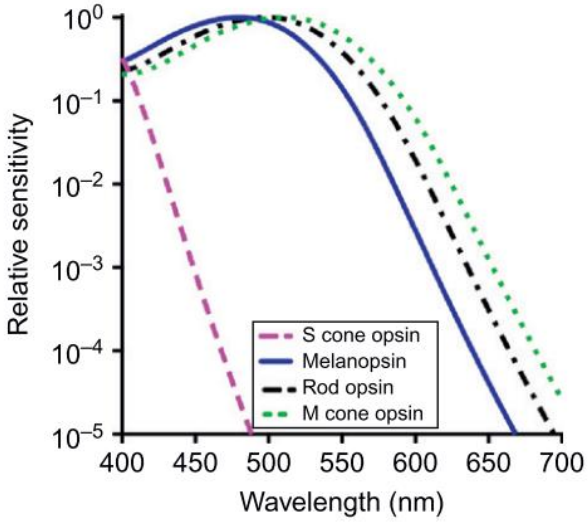

Figure 9: Spectral sensitivity of four mouse retinal photopigments.

Three of the photopigments - melanopsin, rod opsin and M cone opsin (middle wavelength sensitive) – have a very close peak of sensitivity. Therefore, the use of wavelengths between 480nm and 500nm would result in maximum pupil constriction (Lucas *et al.*, 2012).

In the absence of melanopsin, pupillary constriction is reduced, as shown by Lucas *et al.* (2003). To test whether there is a defect in constriction mechanism, parasympathetic agonist, such as carbachol, can be used. Application of parasympathetic agonist to the cornea results in maximum pupil constriction if there is no defect present in the constriction mechanism. Failure of the pupil to respond to light pulses, but positive response obtained after parasympathetic agonist application indicates that defect can be present in retinal decoding of light (such as non-functional photoreceptors, melanopsin, or absence of neurotransmitters) (Hattar *et al.*, 2003).

1.4.3 Photoentrainment

As discussed earlier, light information from our surroundings is directly conveyed to the SCN through the retinohypothalamic tract. This light input helps to synchronise our body to the external light-dark cycle, eventually leading to entrainment – full adaptation to the environment that is achieved through factors like the light information, social interactions and food availability.

Daily rhythm of animals is highly determined by one of the main zeitgebers – light (zeitgeber: zeit (time) + geber (giver), originating from German). Zeitgeber is any periodically occurring environmental factor that synchronises circadian periodicity. This can be a presence of light at the same time of the day, a short signal every 24 hours (e.g. husbandry happening at the same time of the day), or even continuously changing factors, such as temperature (Aschoff, 1960). Animals can adapt their rhythm based on the light source, whether it is the sun or artificial

light used in laboratories. As a result, the intrinsic rhythm is synchronised to the light, what is called photoentrainment. As light is a very strong zeitgeber defining the molecular clock rhythm, time under specific light conditions is called Zeitgeber Time (ZT). During 12 hours of light and 12 hours of dark conditions (12:12 LD), ZT0 is the time when the lights turn on and ZT12 is end of the light phase.

One of the entrainment measurements performed when housing under light-dark cycle is phase angle. The phase angle of entrainment is a relationship between the timing cue (light-dark cycle) and the timing of the biological clock. It could be expressed in degrees (24 hr = 360 degrees), but most commonly minutes are used.

1.5 Endogenous period

In the absence of all the zeitgebers (time-givers) molecular clock is still able to generate circadian rhythms because of its neurons being autonomous circadian oscillators. Therefore, in conditions when the organism's circadian rhythm is solely controlled by the circadian pacemaker, the organism is free-running.

The free-running period (tau, τ – the duration of the cycle in the absence of light entrainment) differs across species. For example, it is about 23.81-24.31 hours in humans (Markwell *et al.*, 2010), 23.36 hours in deer mouse, 23.5 hours in the house mouse (Pittendrigh and Daan, 1976b). However, not only interspecific variation in tau is present, but the same individual is prone to period variation, which in some cases can be explained by ageing (for example, testosterone levels in males change with age and this hormone was found to have an effect on SCN frequency), or different light conditions (Pittendrigh and Daan, 1976a).

Periods of entrainment can be easily adjusted within T=23-25 hours, but animals are not able to entrain to extreme periods, such as T=5/T=40. To be able to know the range of entrainment, the phase response curve (PRC) is used. PRCs can be generated by repeating stimulus at different time points in free-running animals. And even though different species have variation in the level of their phase advance and delay, animals follow very similar pattern: light pulses falling during late subjective day and early subjective night cause phase delays, whereas light pulses administered during late subjective night and early subjective day lead to phase advances (Daan and Pittendrigh, 1976). Light pulses administered during the subjective day (CT-2-10) have no influence on phase-shifting, however, non-photic stimulation can cause phase changes (Figure 10). It has been shown that photic and non-photic associated mediators (such as NPY and glutamate, respectively) can block each other's phase shifting abilities (Biello *et al.*, 1997; Lall and Biello, 2002).

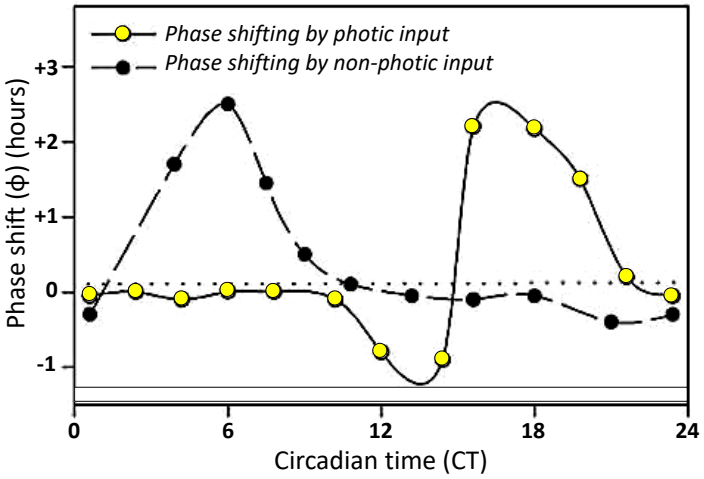

Figure 10: Phase response curve to photic and non-photic stimuli across 24 hours.

Photic input during the light does not cause any changes in the phase, whereas light administered during early hours of dark would cause a phase delay and phase advance when administered closer to dawn. In contrast, non-photic stimulation advances the phase when presented in the first 12 hours of day.

The range of entrainment is calculated by finding maximal advance and delay from the PRC and knowing the inner running period (tau, τ) of the animal. Each species have their own range of entrainment, which can be very narrow, like in Glaucomys Volans (Southern flying squirrel) and Peromyscus leucopus (White-footed mouse) (both 23.5-24.9 hrs). The range of entrainment can also be widely spread out, as it is observed in Sarcophaga argyrostoma (Flesh fly) (11.8-35.8 hrs) or Coturnix coturnix (Common quail) (16.5-33.8 hrs) (Refinetti, 2006). Even though using PRC for the range of entrainment is not very accurate, it enables us to know approximate values that might be useful when designing experiments.

1.6 Afferent pathways to the SCN

The entrainment of the SCN to light originates from the retina, where signals are transmitted through optic nerve projections via the RHT (Figure 3). Rod and cone photoreceptors within the retina absorb light translating it into neurochemical signals that are passed to the retinal ganglion cells. However, some of the retinal ganglion cells are photoreceptive themselves, therefore they can respond directly to light, even in isolation (Hattar *et al.*, 2002; Güler *et al.*, 2008). Opsin based photopigment melanopsin is present in intrinsically photosensitive retinal ganglion cells (ipRGCs). Upon light absorption melanopsin causes activation of G-protein cascade leading to cellular depolarisation and increased firing rate (Lucas *et al.*, 2012). It is believed that upon light-mediated activation of melanopsin, it interacts with Gq/G11 leading to PLC-β activation. PLC-β generates IP3 and DAG modulating TRPC channel that generates light activated photocurrent in presence of melanopsin (Foster and Hankins, 2007).

It was found that ipRGCs are dominant cells in RHT; therefore, they act as the main route delivering light information to the SCN. Some of the ipRGCs projections extend from RHT to IGL of the lateral geniculate complex, as well as the olivary pretectal nucleus (OPN) (Schmidt *et al.*, 2011). Cells from the IGL project to the SCN providing feedback regulation of the circadian pacemaker via GHT (Moore *et al.*, 1995). This non-image forming mechanism of retina drives the behavioural and physiological circadian entrainment mechanisms, such as pupillary light reflex, circadian photoentrainment and phase shifting (Güler *et al.*, 2008; Keenan *et al.*, 2016).

Glutamate and pituitary adenylate cyclase-activating polypeptide (PACAP) are principal RHT neurotransmitters (Hannibal, 2002). Roles of PACAP and glutamate have been confirmed by the exogenous application of agonists and antagonists of these neurotransmitters. Furthermore, just neurotransmitters alone are able to phase shift the clock even in the absence of light (Harrington *et al.*, 1999).

1.6.1.1 PACAP and its receptors

PACAP is part of vasoactive intestinal polypeptide (VIP)/secretin family and it is widely distributed in both, central and peripheral nervous systems. It was found that PACAP is co-stored together with glutamate in glutamatergic retinal ganglion cells and the ventrolateral SCN nerve terminals (Hannibal, 2002) and it plays an important role in SCN entrainment to the solar day. PACAP works on two classes of G-protein coupled receptors. Type I receptor (PAC1) is coupled to adenylate cyclase and phospholipase C. It binds PACAP with 1000-fold higher affinity comparing to VIP and it is widely distributed in the brain and spinal cord. Whereas type II receptors (VPAC1 and VPAC2) are coupled to adenylate cyclase and they bind both PACAP and VIP with the same affinity (Harmar *et al.*, 1998).

Retinal ganglion cells synthesising PACAP show rhythmic expression, with low levels present during the daytime and high levels of PACAP at night in the SCN of animals housed under a 12:12 light-dark cycle. On the other hand, keeping animals in constant dark eliminates PACAP expression rhythmicity, which results in stable PACAP expression over 24 hours (Fukuhara *et al.*, 1997). It has been shown that mice lacking functional VPAC2 receptors for VIP and PACAP are unable to maintain daily locomotor activity rhythms. They do not have coordinated clock gene expression in the SCN and other areas of the brain. VPAC2 receptor knockouts present masking-like behaviour during LD housing and phase advance protocol and they are arrhythmic during constant dark housing with no clear activity onset (Harmar *et al.*, 2002).

1.6.1.2 Glutamate and the glutamate receptor family

Glutamate is highly abundant excitatory neurotransmitter that participates in a number of functions, some of which are learning, memory, synaptic plasticity and conveying light information to the SCN or even phase shifting (Meijer *et al.*, 1988; Ebling, 1996; Willard and Koochekpour, 2013).

Glutamate receptors belong to two families of receptors. These are ionotropic glutamate receptors, such as N-methyl-D-aspartate (NMDA), α-amino-3-hydroxyl-5-methyl-4-isoxazole-propionate (AMPA) and kainate, or metabotropic glutamate receptors, which are G-protein coupled receptors (Figure 11)(Kew and Kemp, 2005). Some of the receptors have subtypes that are only expressed in certain regions. For example, in rat SCN GluN1 (a.k.a. NMDAR1C) is expressed in all SCN, but GluN2C (a.k.a. NMDAR2C) is only detected in dorsomedial SCN (Hannibal, 2002).

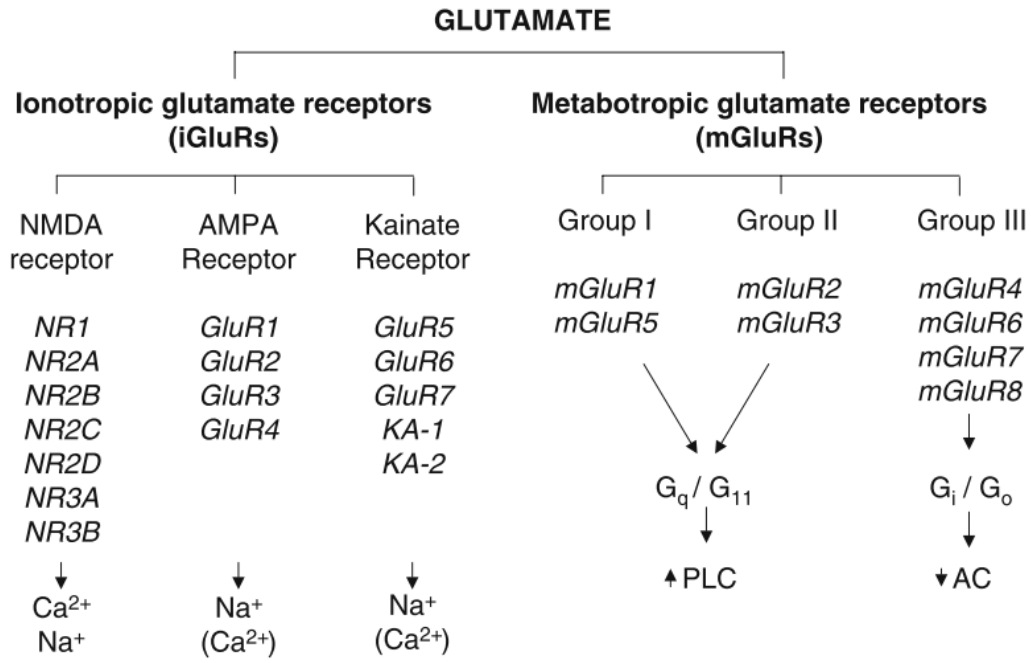

Figure 11: Overview of the glutamate receptor family.

Members of ionotropic and metabotropic receptors with their subunits and primary signal transduction mechanism. Glutamate receptors are divided into ionotropic (NMDA, AMPA and Kainate) and metabotropic (Group I, II and III) receptors. Glutamate gates ionotropic receptors that in turn activate metabotropic receptors through the G proteins. This leads to phospholipase C (PLC) activation and inhibition of adenylate cyclase (AC) (Kew and Kemp, 2005).

Ionotropic glutamate receptors (iGluRs) are widely expressed in the SCN with AMPA receptors mediating fast synaptic transmission (Benke *et al.*, 1998), NMDA receptors involved in Ca^{2+} influx into post-synaptic cells leading to activation of intracellular signalling (Paoletti and Neyton, 2007), they are also permeable to sodium and potassium ions (Figure 12, A). Glycine is

an important cofactor needed for the opening of the channel and NMDA receptor is voltage-dependent. During resting membrane potential magnesium blocks ionic current by binding at pore of the channel and when membrane is depolarised magnesium is expelled from the channel allowing movement of sodium and calcium ions. NMDA receptors also have binding sites for zinc and phencyclidine (PCP) that work as antagonists (Kandel *et al.*, 2012). Kainate receptors act both, pre-synaptically and post-synaptically as well as being involved in synaptic plasticity (Contractor *et al.*, 2000, 2011; Mayer, 2005). Upon glutamate activation, they are permeable to sodium and potassium ions.

Metabotropic glutamate receptors (mGluRs) consist of 8 genes that are split into three groups, with more gene variability present through the splice variants (Niswender and Conn, 2010). Group I consists of mGluR1 and mGluR5, Group II is mGluR2 and mGluR3 and Group III is made of mGluR4, mGluR6-8. mGluRs indirectly gate ion channels through activation of GTP binding protein that interacts with effector molecules changing channel activity (Figure 12, B).

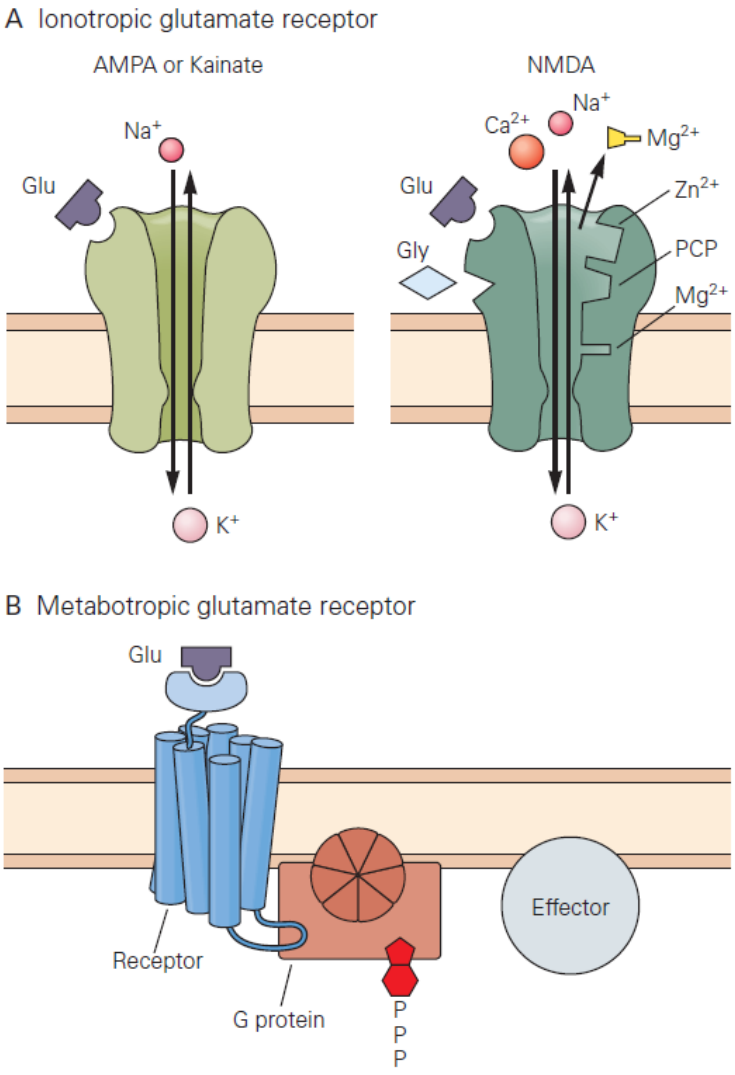

Figure 12: Schematic structures of different classes of glutamate receptors.

(A) Ionotropic glutamate receptors consist of AMPA, Kainate and NMDA receptors. AMPA and Kainate bind glutamate agonists that result in a flow of sodium and potassium ions. NMDA receptors are more complicated. They are permeable to calcium, sodium and potassium, but they are also tightly regulated by glycine, magnesium, zinc and phenylcycline binding. (B) Metabotropic glutamate receptors work by indirectly gating ion channels through activation of GTP binding protein (Kandel *et al.*, 2012).

Group I mGluRs couple to $G\alpha_q$ activating phospholipase C that results in the generation of IP3 and diacylglycerol (DAG). This, in result, increases calcium levels and activates protein kinase C (PKC) (Mathie, 2007) (Figure 13). mGluR1 and mGluR5 receptors play an important role in normal brain functions and neuronal development, whereas disturbance in action of these receptors results in diseases like epilepsy, anxiety, depression, schizophrenia and even neurodegenerative diseases with involvement in prolonged and chronic pain (El-Kouhen *et al.*, 2006). mGluR1 knockout mice display severe motor deficit, learning impairments (Conquet *et al.*, 1994), whereas pharmacological inhibition using A-841720 had reversed chronic inflammation-induced hyperalgesia as well as mechanical allodynia, but it also caused motor and cognitive functions impairment (El-Kouhen *et al.*, 2006).

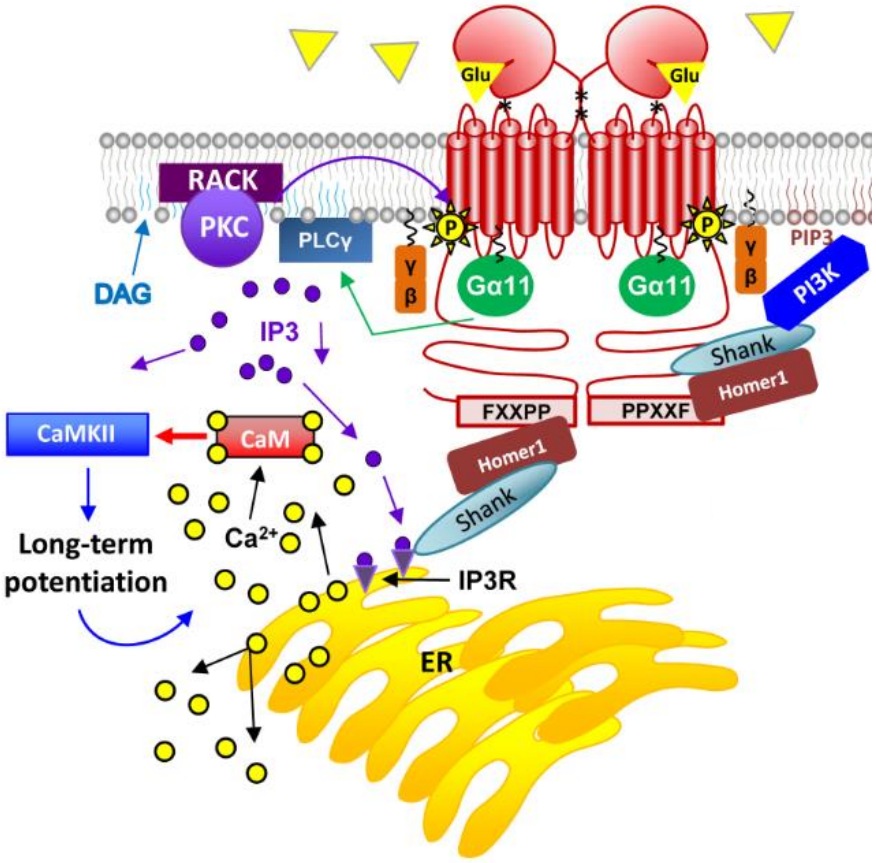

Figure 13: mGluR1a activation of G-coupled signalling pathways.

A diagram presenting the overview of G-protein signalling pathways activated by mGluR1 as a result of glutamate biding. The key outcome of glutamate binding to mGluR is an increase in intracellular calcium levels that can happen through indirect channel opening or by second messenger signalling. For example, activation of phospholipase (PLC) by Gα11 protein cleaves PIP2 (phosphatidylinositol 4,5-bisphosphate) into IP3 (Inositol triphosphate) and DAG (diacylglycerol). IP3 binds its receptor IP3R present in the endoplasmic reticulum leading to release of Ca^{2+} from intracellular store sites. DAG recruits PKC (protein kinase C) attaching it to the plasma membrane. One of the roles of PKC is to desensitise the mGluR1 receptor so that the neuron could return to the resting membrane potential (Willard and Koochekpour, 2013).

1.6.1.3 Other SCN neurotransmitters

The intergeniculate leaflet uses GABA, neuropeptide Y (NPY) and enkephalin as neurotransmitters through the GHT to the SCN, whereas the raphe nuclei utilise serotonin as a transmitter of non-photic input to the SCN (Leak *et al.*, 1999; Reppert and Weaver, 2001; Moore *et al.*, 2002; Lall and Biello, 2003).

GABA is the only neurotransmitter produced and received by nearly all SCN neurons (Moore and Speh, 1993). There are two major classes of GABA receptors: ligand-gated chloride (Cl^-) $GABA_A$ and metabotropic G-protein coupled $GABA_B$ receptors. Both classes are found in the SCN and can be found presynaptically, postsynaptically, or on extrasynaptic membranes in the brain (Albers *et al.*, 2016). Roles of GABA within SCN include coupling of individual SCN

neurons and modulating of input and output of circadian oscillation in the SCN (through plasticity changes in the retinohypothalamic tract to SCN synapses and changes in neuronal excitability) (Ono *et al.*, 2018). Normally, in the adult brain GABA is primarily an inhibitory neurotransmitter, however it acts as an excitatory neurotransmitter during early development. In rodents, the switch between depolarising to hyperpolarising GABA effects happens at around second postnatal week. However, in the SCN excitatory GABA actions remain present even in the adulthood. GABA acts as excitatory neurotransmitter when intracellular Cl^- concentrations are higher compared to extracellular Cl^- levels causing outward current and membrane depolarisation. The inhibitory effect of GABA is present when the Cl^- levels are higher at the extracellular side compared to intracellular. Cation chloride cotransporters, such as Na-K-2Cl cotransporters (NKCC) and K-Cl cotransporters (KCCs), play a critical role in determining the role of GABA in neurons by mediating the Cl^- uptake (Albers *et al.*, 2016). In the SCN GABA has two signalling components. Following an action potential, large quantities of GABA are released (phasic release). In addition to this, some neurons would become depolarised that would result in sustained low-level GABA release (tonic release). The tonic GABA release is capable of affecting circadian rhythms that would be driven by neurons that have achieved a high level of depolarisation. In contrast, phasic GABA signal does not affect circadian rhythms. This could be important for efferent signalling from SCN without affecting the timekeeping of the molecular clock itself (DeWoskin *et al.*, 2015).

NPY is one of the principal neurotransmitters utilised by the intergeniculate leaflet (IGL). From IGL through geniculohypothalamic tract (GHT) NPY transmits non-photic signals to the clock. Molecular clock genes discussed in the next section play a key role in driving circadian rhythms. Non-photic signals that advance the phase of molecular clock can achieve this only if administered during the daytime and if given in isolation (with no light signalling and glutamate input). This is because during the day one of the key clock genes *Per* is very highly expressed, but non-photic signalling, such as the one induced with NPY, can reduce the expression of *Per*, in this way advancing the clock. At night, this clock protein has very low expression, therefore NPY would not be able to have much effect, that is why non-photic signalling does not affect molecular clock at night (Maywood *et al.*, 2002). However, if animals would receive light during the dark phase of the day, NPY would be able to inhibit light-induced phase shifts. Therefore photic and non-photic signalling can cancel each other's effects (Yannielli and Harrington, 2000; Lall and Biello, 2002, 2003).

The raphe nuclei transmit non-photic input and utilise serotonin (5-Hydroxytryptamine (5-HT)) for signal transmission that can directly act on the SCN from the raphe nucleus, or can have an indirect effect through IGL signalling (Figure 3). Serotonin or its agonist application during the

day results in a non-photic response, which is typically a phase advance (Ehlen *et al.*, 2001). These effects are mediated through serotonin receptor 5-HT_7, as shown by Gardani and Biello (2008).

1.7 The molecular clock

Irrespective of light availability, the molecular clock drives intrinsic circadian rhythms based on transcription/translation feedback loops. They result in protein formation, which can inhibit its own transcription directly or indirectly. In 1971 *Period* gene was found to be responsible for period length in *Drosophila*, as published by Konopka and Benzer (1971). They used mutant flies having disrupted 24-hour cycle (arrhythmic mutant, short-period mutant (19 hours) and long-period mutant (28 hours)) and by performing genetic mapping, managed to locate the mutant genes on the X chromosome. However, the period gene has only been isolated, sequenced and cloned in 1984 (Bargiello and Young, 1984; Reddy *et al.*, 1984). This and future discoveries of the molecular mechanisms controlling circadian rhythms in fruit flies have been recognised by the wider scientific community. As a result, Jeffrey C. Hall, Michael Rosbash and Michael W. Young received the 2017 Nobel Prize in Physiology or Medicine.

There are three interlocking transcription/translation feedback loops (TTFL) that work together to generate 24-hour rhythm of gene expression (Figure 14) (Honma *et al.*, 2002; Ukai-Tadenuma *et al.*, 2011; Buhr and Takahashi, 2013; Partch *et al.*, 2014; Jagannath *et al.*, 2017).

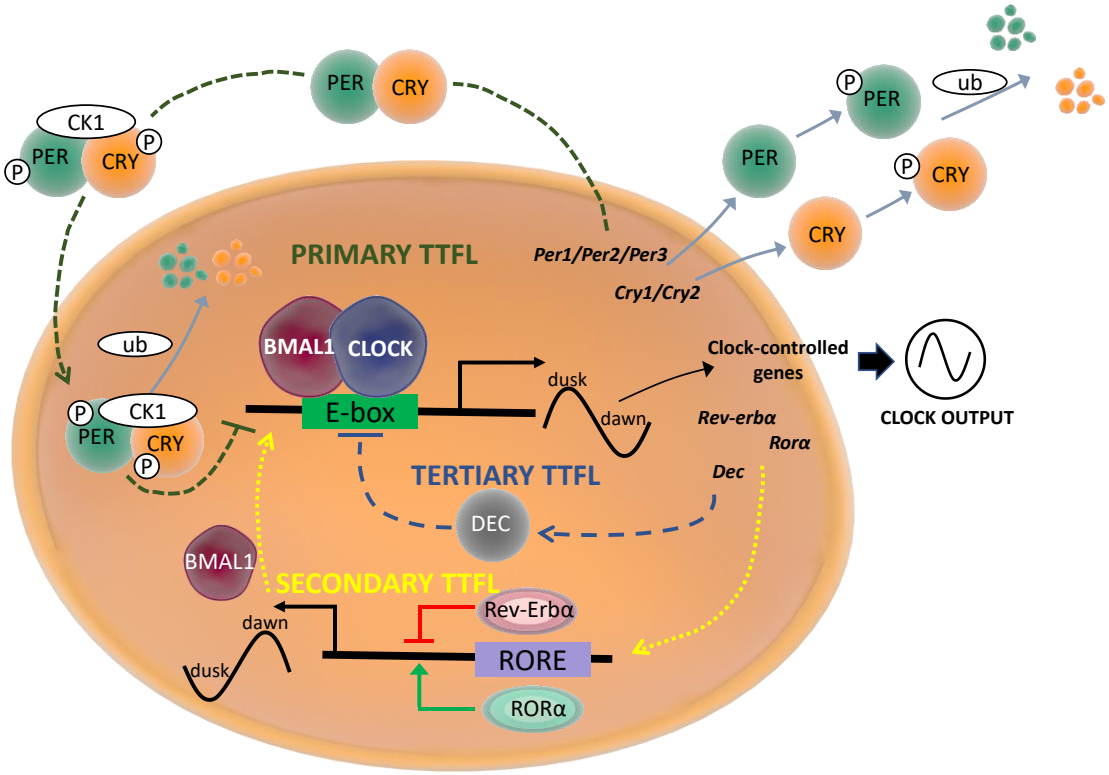

Figure 14: Representation of three mammalian TTFL.

Three transcription/translation feedback loops work together to maintain tight regulation of circadian entrainment through the production of molecular clock genes. Primary TTFL is made of a CLOCK-BMAL1 protein complex, facilitating clock gene expression. Its products PER and CRY feed-back to inhibit further transcription, with tertiary TTFL involving DEC proteins reinforcing the inhibition. Secondary TTFL regulates BMAL1 expression levels throughout the day with RORα facilitating and Rev-Erbα inhibiting Bmal1 production.

The main TTFL is driven by two proteins: Circadian Locomotor Output Cycles Kaput (CLOCK) and Brain muscle arnt-like 1 (BMAL1). CLOCK and BMAL1 form heterodimers that bind to E-box promoters driving the transcription of Period (*Per1-3*) and Cryptochrome (*Cry1/2*) genes. PER and CRY proteins dimerise to inhibit CLOCK-BMAL1 induced transcription. PER-CRY complex is phosphorylated by Casein kinase 1 family of kinases (CK1) allowing entry to the nucleus and acting as negative suppressors of BMAL1/CLOCK complex. PER and CRY surplus is degraded in cytoplasm. Throughout the day PER-CRY-CK1 levels greatly vary with the peak at dusk and nadir following the dawn.

Light plays a major role in primary TTFL as it leads to upregulation of *Per1* and *Per2* transcription. This enables the molecular clock to entrain to dawn/dusk cycle, which is very important in seasonal adaptation and jet-lag.

A second interlocked TTFL is important for regulation of BMAL1 expression. CLOCK-BMAL1 complex induces transcription of retinol related orphan nuclear receptor genes *Rev-ERBα/β*

and *RORα/β.* The REV-ERBα and RORα receptors compete for **r**etinoic acid-related **o**rphan receptor **r**esponse **e**lement (RORE) binding sites that are present in *Bmal1* promoter. Binding of the REV-ERBα to ROREs represses *Bmal1* gene transcription, whereas RORα receptor binding to ROREs facilitates *Bmal1* transcription. To ensure the peak of BMAL1 levels at dawn, RORα levels peak at dawn, whereas REV-ERBα, suppressing Bmal1 transcription, peaks at dusk. This ensures the presence of the antiphasic relationship between BMAL1 and CRY/PER.

A third TTFL is involved in CLOCK-BMAL1 regulation involving D-box elements in the promoter of the pseudoautosomal region (PAR) basic leucine zipper domain (bZIP) genes. Dec1 and Dec2 genes give rise to DEC1/2 proteins inhibiting CLOCK-BMAL1 transcription, reinforcing the inhibitory action of PER-CRY-CK1 complex.

The combination of TTFLs and the cooperative effect of clock proteins drive the rhythmicity of mammalian circadian clock, help to maintain accurate circadian timing and contributes to phase shifts induced by both, photic and non-photic inputs (Maywood *et al.*, 1999; Maywood and Mrosovsky, 2001).

1.8 Electrical regulation of the clock

1.8.1 Membrane and action potentials

The suprachiasmatic nucleus with its clock proteins alone would not be able to maintain stable circadian rhythmicity. For example, experiments using tetrodotoxin (TTX), voltage gated sodium channels blocker, have shown that TTX infusion in the rat SCN abolishes free-running locomotor activity rhythms without affecting the phase of clock gene expression (Schwartz 1987). Therefore, a major contribution is done by ion channels. They control membrane potential and enable signal transduction essential for running of the molecular clock.

Neurons have the ability to maintain stable resting membrane potential with the help of leak and gated ion channels by controlling the distribution of ions inside and out of the cell (Figure 15). At rest, the extracellular side of neurons has more positive charge comparing to the negatively charged cytoplasm. Because of electrical charge difference across the membrane, membrane potential (V_m) is defined as V_{in} (intracellular potential) minus the V_{out} (extracellular membrane potential).

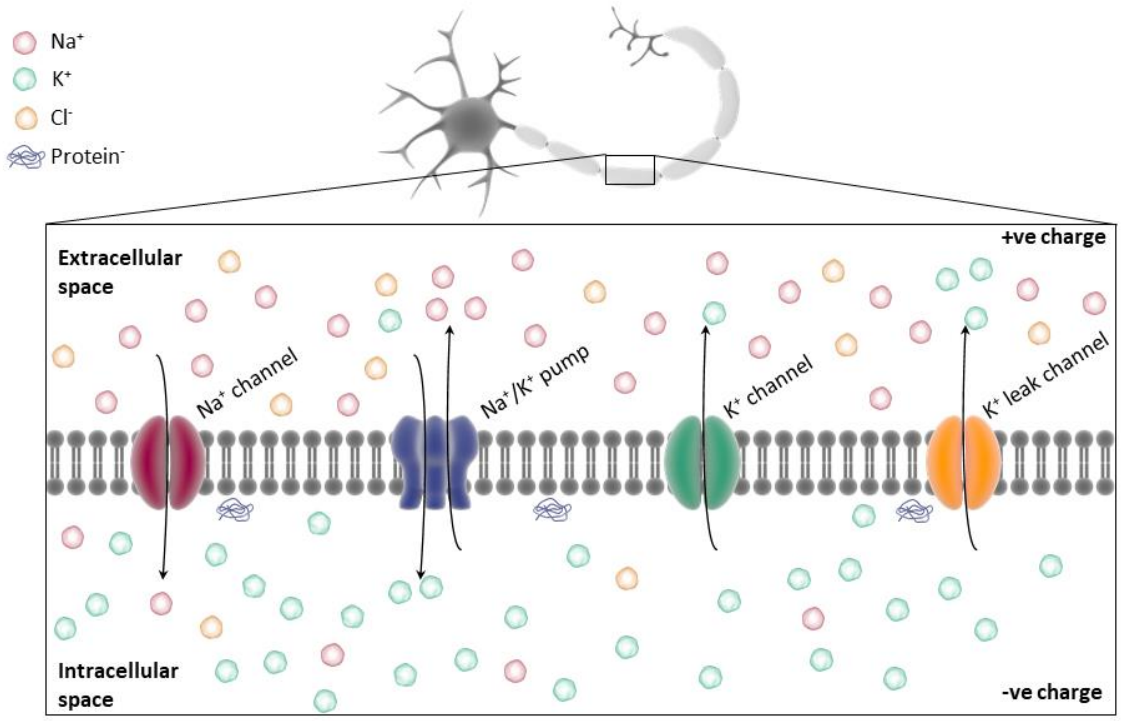

Figure 15: Maintenance of the resting membrane potential (RMP).

Resting membrane potential is regulated by the ions – their concentration gradients across the membrane, as well as the permeability of neuron's membrane to the ions. Potassium (K^+, presented as green spheres) and organic anions (for example, proteins, presented as blue structures) are more concentrated in cytosol of the neuron, whereas sodium (Na^+, presented as red spheres) and chloride (Cl^-, presented as orange spheres) have higher extracellular concentration. As a result, in relation to outside of the membrane, intracellular side of the neuron is more negative, with the mean resting membrane potential between -60 to -70mV. To maintain a stable RMP Na^+/K^+ pumps move Na^+ and K^+ ions against their concentration gradient – with each ATP used, three Na^+ ions are moved out of the cell and two K^+ ions are moved into intracellular space.

The membrane potential is maintained by the passive flux of ions with Na^+ and Cl^- abundant on extracellular side of neurons, whereas K^+ together with organic anions, such as proteins and amino acids, are concentrated on the intracellular side. This gives a difference in charge, which is between -60 to -70 mV and is known as resting membrane potential (RMP). However, the passive movement of K^+ out of the cell and Na^+ into the cell through leak channels disrupts the gradient needed to maintain resting membrane potential. Therefore with the use of ATP, Na^+-K^+ pump moves these ions against their electrochemical gradients maintaining the RMP (Kandel *et al.*, 2012).

During the stimulus, changes in neuronal membrane potential generate the action potential (Figure 16). Membrane depolarisation towards the threshold for action potential disrupts the normal Na^+ / K^+ balance with Na^+ influx into the cell through voltage-gated sodium channels. This brings the membrane potential towards Na^+ equilibrium potential of +55mV. After 1ms, when Na^+ channels are closing, K^+ leak, as well as voltage-gated channels, open allowing potassium to move down its concentration gradient to outside of the cell. This brings

membrane potential back to the hyperpolarised state (Fletcher, 2014). Depolarisation of one region in the membrane triggers the opening of neighbouring sodium channels in this way creating a wave of depolarisation travelling along the cell; therefore, action potential is self-propagating.

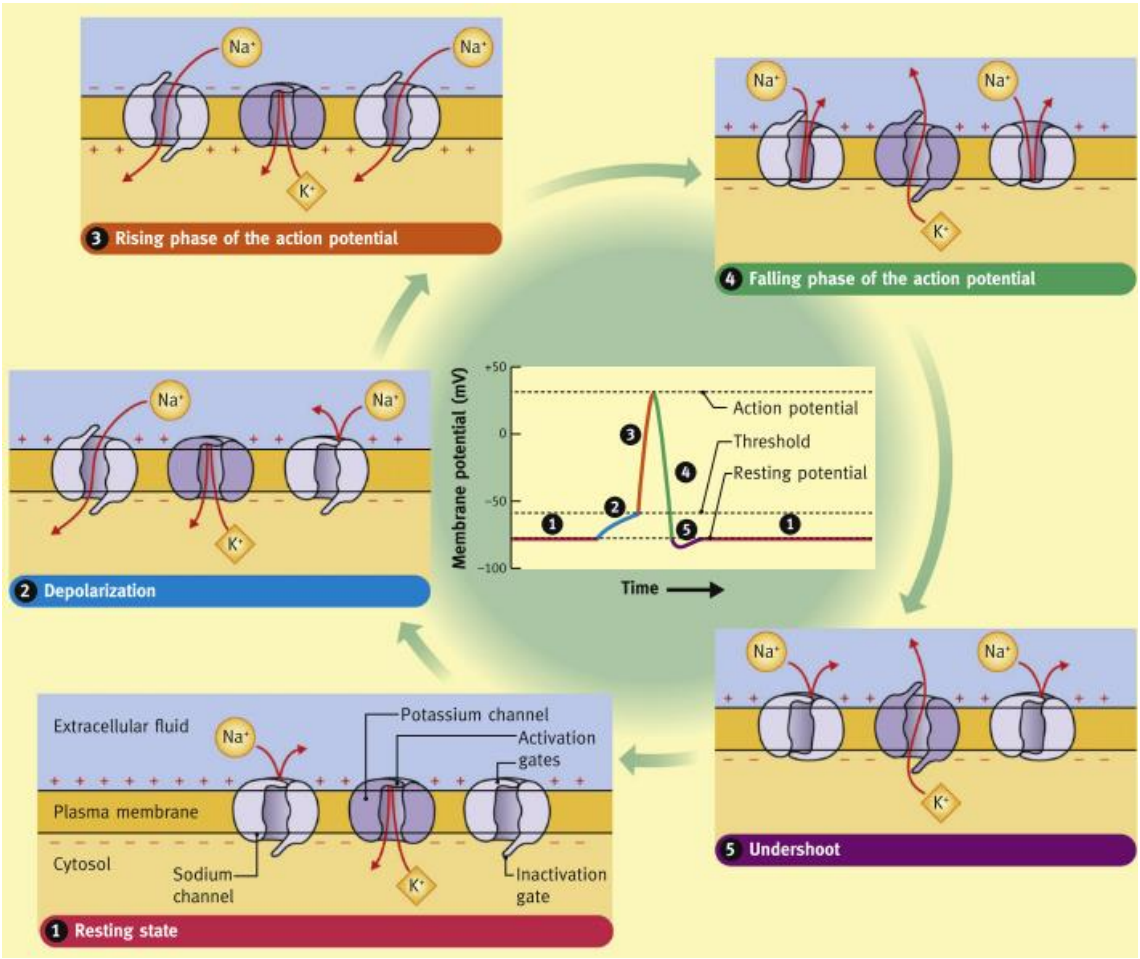

Figure 16: Generation of an action potential.

The central graph is representation of intracellular voltage changes. (1) During the resting state, RMP is approximately -70mV and the voltage-gated Na^+ and K^+ channels are closed. (2) After stimulus-induced depolarisation of the membrane some of Na^+ channels open which eventually depolarises the membrane beyond the threshold (3) triggering action potential. Sodium influx brings intracellular part of the neuron towards Na^+ equilibrium potential (approximately 60mV). (4) After about 1 ms after opening, Na^+ channels close, before the Na^+ equilibrium potential is reached, voltage-gated potassium channels open leading to potassium moving to the extracellular side of neuron and this repolarises the membrane. As the sodium channels are inactivated, neuron would be unresponsive to any depolarising stimulus (refractory period). The voltage-gated K^+ channels remain open long enough to hyperpolarise the membrane (5), but once voltage-gated Na^+ channels are responsive again, a new depolarising stimulus could facilitate an action potential (Fletcher, 2014).

During excitation and electrical signalling in the nervous system Na^+, K^+, Ca^{2+} and Cl^- ions play a major role. The change in membrane potential eventually leads to opening or closing of Ca^{2+} permeable channel altering Ca^{2+} flux into the cytoplasm in this way changing intracellular free calcium concentration. This final transduction pathway is common across different systems

receiving neural control, for example, in the secretion of neurotransmitters, digestive enzymes or even muscle fibre contraction (Hille, 2001).

In the late XIXth century, it was suggested that the movement of ions across the membrane causes electrical currents. However, the first quantitative understanding of action potential and involvement of different ion channels, as well as leak currents (though they were not known as leak currents back then), was published by Alan Hodgkin and Andrew Huxley. Their work on squid giant axon has proposed a mechanism of nerve excitation and it was a basis on which many researchers have further deepened the understanding of channels involved in action potentials (Hodgkin and Huxley, 1952; Hodgkin and Keynes, 1955). An example could be Clay Armstrong and Bertil Hille discovering that ion channels can be voltage-gated and selective for specific ions (Armstrong and Hille, 1972; Armstrong, 1974) or Roderick MacKinnon who was the first to determine high-resolution structure of a potassium channel (Doyle *et al.*, 1998).

There are many types of different ion channels involved in the regulation of electrical properties of neurons, but in this thesis, we will focus on a specific subtype of potassium channels called leak two-pore potassium channels.

1.8.2 Potassium channels

Potassium (K^+) ions are always the primary current carriers, but there is a wide diversity of voltage-gated K^+ channels that differ in their opening speed, modulation by neurotransmitters and intracellular messengers. As a result, excitable membrane uses a variety of K^+ channel subtypes based on their needs (Hille, 2001). Potassium channels stabilise the membrane potential by keeping the membranes hyperpolarised and opening of these channels make actions potentials short, lower effectiveness of excitatory input, whereas closure leads to enhanced excitability.

All K channels have common features, such as pore-lining P-loops with the same amino acid sequence (Figure 17) (Heginbotham *et al.*, 1992; Hille, 2001; Choe, 2002). The simplest is the two-transmembrane (2TM) K-channel. As can be known from the name, it has two transmembrane segments joining the P-region and there can be up to 8TM segments, like in yeast TOK channel.

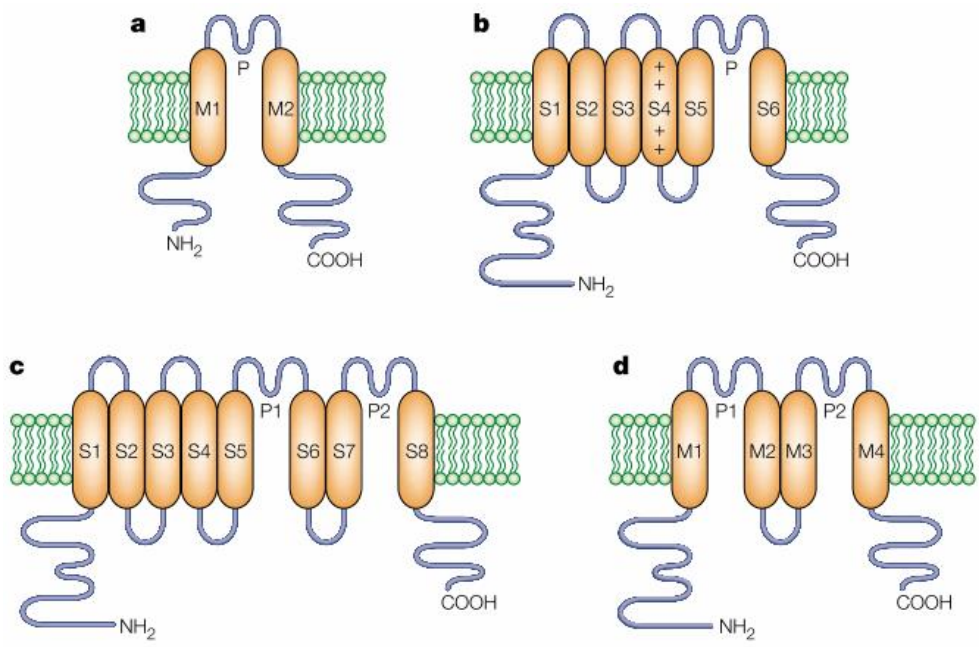

Figure 17: Four classes of potassium channels.

(a) Two-transmembrane potassium (2TM) channel with one P loop joining the transmembrane helices. This structure is present in inwardly rectifying and bacterial potassium channels. (b) 6TM channel with one P loop – most common class in ligand-gated and voltage-gated potassium channels. S4 plays a role in voltage sensing. (c) 8TM channel with two P loops. (d) 4TM channel with two P loops – a structure of two-pore domain potassium channels (K2P) (Choe, 2002).

There are three major classes of potassium channels that are categorised based on their structure and function: (1) voltage-gated (Kv) - 6TM; (2) inwardly rectifying (Kir) - 2TM; and (3) tandem pore domain (K2P) – 4TM channels. As the project is based on two-pore domain potassium (K2P) channels, will go more into detail in understanding the structure and role played by K2P channels.

1.8.2.1 K2P channels

Leak two-pore domain K+ channels (K2P) are generally described as voltage-independent "background" potassium channels (Goldstein *et al.*, 2005; Thomas and Goldstein, 2010). However, Schewe et al. (2016) found that most of the K2P channels, except for TWIK-1, show time dependant voltage activation caused by ion movement into high electric field of an inactive selectivity filter.

K2P channels have a tetrameric structure which is composed of transmembrane segments named M1 to M4, two-pore domains (P1 and P2) forming the wall of the channel pore and two extracellular cap helices (C1 and C2) that are M1-P1 linkers (Renigunta *et al.*, 2015; Zuniga and Zuniga, 2016). Those K2P subunits, unlike other potassium channels having four subunits, assemble as dimers forming a pseudo-tetrameric pore (Schewe et al., 2016).

Human K2P family consists of 15 members that are further divided into six subfamilies according to the structure and function of the channel. These subfamilies are TWIK (tandem of pore domains in a weak inward rectifying K+ channel), TREK (TWIK-related K+ channel), TASK (TWIK-related acid-sensitive K+ channel), TALK (TWIK-related alkaline pH-activated K+ channel), THIK (tandem pore domain halothane-inhibited K+ channel) and TRESK (TWIK-related spinal cord K+ channel) (for detailed review on all K2P channels please refer to Enyedi & Czirják (2010)). The first two-pore K^+ channel reported in the literature was TOK1 (Ketchum *et al.*, 1995). However, TOK1 is composed of eight transmembrane helices and is strongly outwardly rectifying; therefore, it is not included in the K2P family. First K2P family members composed of four transmembrane segments were discovered in 1996 and they were TWIK-1 (Lesage *et al.*, 1996) and TREK-1 (Fink *et al.*, 1996). The last member of the K2P family, TRESK, has only been discovered in 2003 (Sano *et al.*, 2003).

K2P channels are regulated by a variety of physiological mediators that can cause activation (such as acidic pH, arachidonic acid, heat, stretch, calcium) or inhibition (protein kinase A/C, zinc, acidic pH, arachidonic acid) of specific channels (Enyedi and Czirják, 2010). So far, three gating mechanisms have been identified that are present in potassium channels. The first one is called C-type gating, which is utilised by many K2P channels. Pore closure in C-type gating is caused by amino acids present at the narrow selectivity filter that pinch shut in this way closing the channel. The second gating mechanism works by opening/closing of amino acid movement at the intracellular part of the pore (Mathie *et al.*, 2010). There is also N-type inactivation mechanism which can involve the N terminus of principal subunits (alpha – α) or N terminus of associated beta (β) subunit of the channel. The auto-inhibitory peptide binds to N terminus leading to inhibited current flow (Yellen, 2002).

1.8.2.1.1 K2P role in physiology and neuron excitability

K2P channels are found in both animal kingdom and plants (Enyedi and Czirják, 2010; González *et al.*, 2015). K2P channels play a significant role in neuronal excitability by regulating membrane potential and membrane input resistance (Talley *et al.*, 2001). Two-pore domain K^+ channels work by keeping the cells closer to their resting membrane potential. Therefore, if K2P channels are absent, cells become overexcited. This can lead to increased sensitivity to pain and can contribute to migraine occurrence (Lafrenière *et al.*, 2010; Tulleuda *et al.*, 2011; Steinberg *et al.*, 2014; Renigunta *et al.*, 2015).

There is a widespread expression of K2P channels in the CNS (Talley *et al.*, 2001; Aller and Wisden, 2008), with different K2P genes having different expression patterns. Apart from CNS, K2P channels are also found in skeletal muscles (Afzali *et al.*, 2016), heart muscle (Liu and Saint, 2004; Ellinghaus *et al.*, 2005), liver, pancreas, lungs (Girard *et al.*, 2001), kidney, adrenal

glands (Sepulveda *et al.*, 2015) where they function to regulate RMP, ion transport, sense oxygen levels and control hormone secretion.

K2P channel defects were also found to contribute to changes in circadian behaviour. Research done on TASK-3 knock-out (KO) mice showed that animals display behavioural differences compared to wild-type controls (Linden *et al.*, 2007). In this study, TASK-3 KO mice were generated by inactivating the *Task-3* gene. *Task-3* was inactivated by combined homologous and insertional recombination, where exon1 of *Task-3* gene was flanked with loxP sites and neomycin cassette was inserted as a positive selection marker. Multiple inverted exon1 repeats and addition of neomycin caused destruction of *Task-3* gene (more details about the generation of TASK-3 knock-out mouse can be found in (Brickley *et al.*, 2007)). Work by Linden *et al.* (2007) has shown that lack of TASK-3 channel causes a significant increase in locomotor activity during the dark phase, but no differences were observed during the day and mice were found to be significantly heavier. During the motor coordination test, TASK-3 KO mice showed affected ability when walking on a narrow beam (0.8cm) leading to more falls. Knock-out mice showed impaired working memory, as shown by T-maze spontaneous alteration test and they had reduced sensitivity to halothane and isoflurane – inhalation anaesthetics.

Removal of only one of the K2P channels TASK-3 had major impact on locomotor activity. Just like TASK-3, TRESK has a widespread distribution in the brain, therefore it may also have an impact on the behavioural output of an animal. This thesis will assess the role of TRESK in circadian rhythms of mice.

1.8.3 TRESK

1.8.3.1 Expression

TWIK-related spinal cord K+ channel (TRESK) was first detected in the spinal cord (Sano *et al.*, 2003). It is also found in dorsal root and trigmental ganglia, cerebrum, cerebellum, brain stem, as well as in non-nervous tissues, especially in mice (e.g. spleen, testis, thymus, lung, heart) (Dobler *et al.*, 2007; Lafrenière *et al.*, 2010; Enyedi and Czirják, 2015).

A frameshift mutation in TRESK has been associated with migraine (Lafrenière *et al.*, 2010; Lafrenière and Rouleau, 2011), where the activation of trigeminal nociceptors is believed to be responsible for the headache phase of migraine (Weir and Cader, 2011). It is very likely that TRESK contributes to membrane excitability because TRESK KO animals show enhanced dorsal root ganglia excitability (Dobler *et al.*, 2007). Further research on TRESK KO mice has shown that in absence of TRESK mice are hypersensitive to noxious thermal stimuli and have mechanical hypersensitivity that could be linked to neuropathic pain in migraine (Weir *et al.*,

2019). High levels of TRESK mRNA were also detected in mouse retina (Hughes *et al.*, 2017) indicating possible involvement in the photic and non-photic mechanisms of light.

1.8.3.2 Structure

The human TRESK gene is made of 384 amino acids (AA's), it has four transmembrane helices and two-pore forming domains, both, N and C termini are located intracellularly. Between the second and third transmembrane segments, TRESK channels have long, more than 120 AA's, intracellular loop and short (30 AA's) C-terminal tail (Enyedi and Czirják, 2015) (Figure 18).

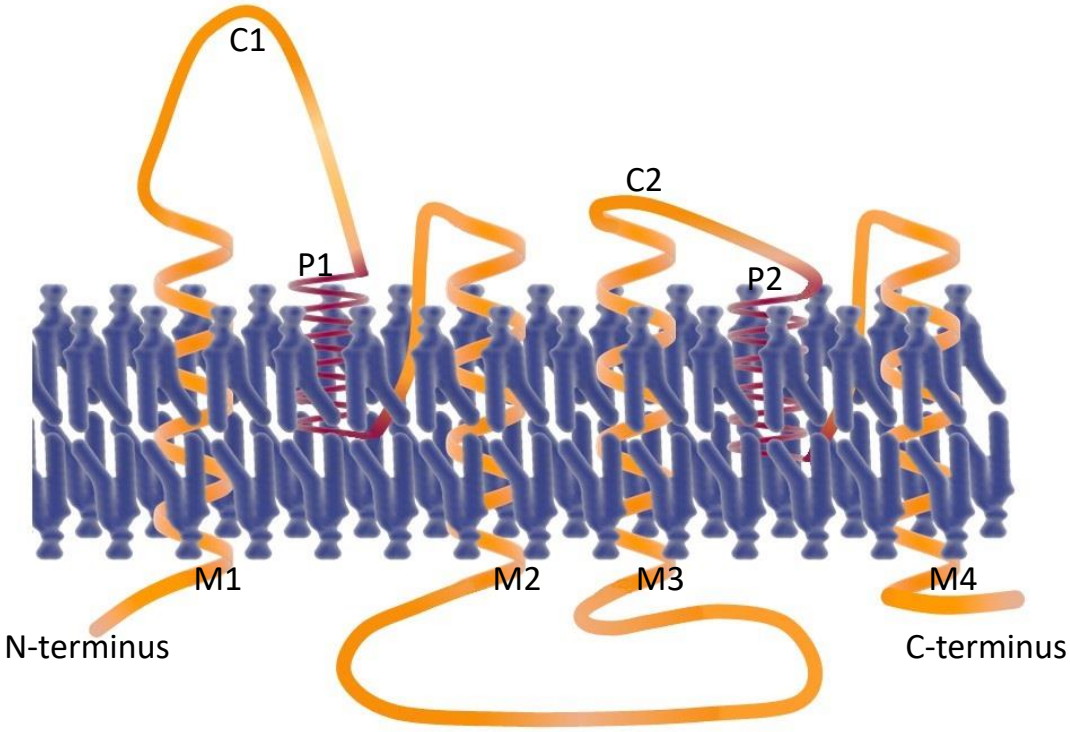

Figure 18: TRESK channel structure.

A schematic representation of TRESK subunit organisation containing four transmembrane domains (orange), two-pore domains (burgundy) and extracellular cap helices (C1 and C2). The long intracellular loop containing more than 120 amino acids is between transmembrane segments M2 and M3 and it is unique to TRESK.

Short C-terminal tail is very unusual when comparing to other K2P channels. In K2P channels like TREK and TASK, it is a site of major regulatory sequences – thermo- and mechanosensitivity, responsible for the effects of volatile anaesthetics. Also, in TASK channels the C-terminal tail has phosphorylation sites for protein kinases A and C, as well as has a binding site for Gq proteins regulating TASK (Enyedi *et al.*, 2012). More important in regulation seems to be a long intracellular loop between 2nd and 3rd transmembrane domains. It contains calcineurin and adaptor protein 14-3-3 binding sites, important for TRESK regulation.

Human and mice *Tresk* genes have only 65% identity; therefore murine channel was considered to be a new member of K2P family, an isoform for human TRESK channel (Kang *et al.*, 2004). However, there is only one *Tresk* gene identified in human and mouse genome databases, so human and mouse *Tresk* genes are orthologues (Keshavaprasad *et al.*, 2005; Dobler *et al.*, 2007).

1.8.3.3 Channel activation and inhibition

TRESK is inhibited by unsaturated free fatty acids, non-specific K+ channel blockers, such as quinidine, extracellular zinc and extreme acidification. Zn^{2+} and acidification only affect mice TRESK channels because of histidine, which in human protein is substituted by tyrosine protecting from pH sensitivity (Keshavaprasad *et al.*, 2005; Dobler *et al.*, 2007). TRESK channel is activated by an increased level of cytoplasmic calcium, which indirectly regulates channel activity (Czirják *et al.*, 2004). Elevated calcium increases the affinity of calcineurin to the channel at the LQLP site, causing phosphatase activation. Intracellular loop of TRESK channel has two serine regulatory sites: Ser-264 that binds protein 14-3-3, as well as the cluster of three adjacent serine residues: Ser-274, Ser-276 and Ser-279 (Czirják and Enyedi, 2010). Calcineurin activated phosphatase dephosphorylates serine regulatory sites leading to detachment of the 14-3-3 protein from Ser-264 activating the channel (Figure 19) (Enyedi and Czirják, 2015). Apart from calcineurin activation, TRESK can be also activated by co-expression of PKC isoforms eta and epsilon. This activation is not mediated by calcineurin phosphatase, as PKC can indirectly dephosphorylate the S264 site by inhibiting the kinase responsible for phosphorylating the channel at the S264 (Pergel *et al.*, 2019).

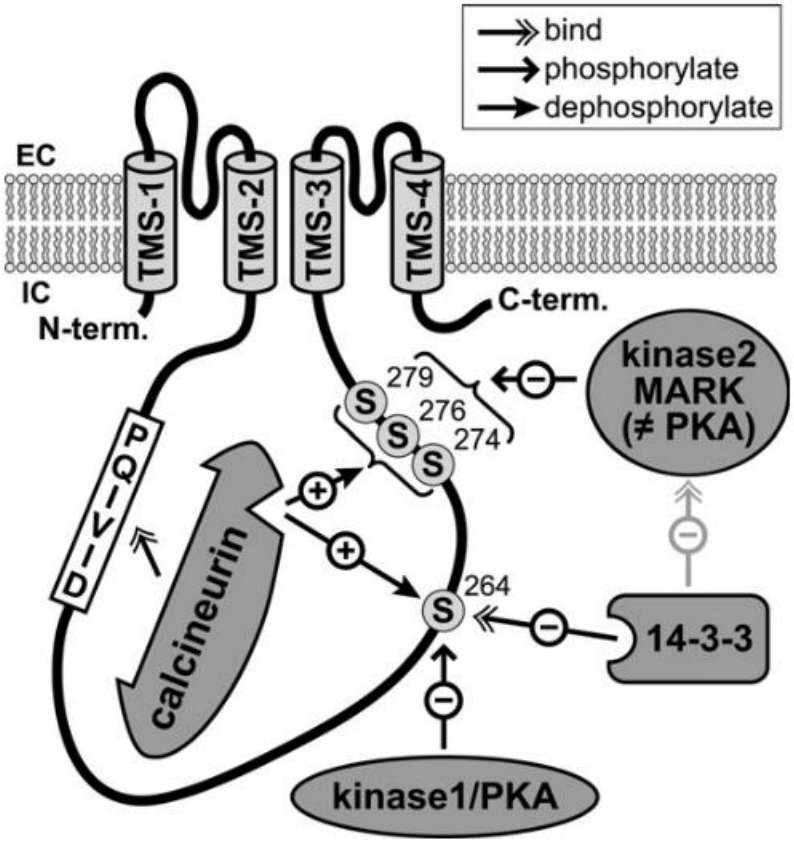

Figure 19: Phosphorylation dependent TRESK regulation.

Kinases 1 and 2 phosphorylate serine cluster and in this way inhibit TRESK current during resting conditions. Microtubule affinity regulating kinases (MARK) may be involved in kinase 2 activity, whereas protein kinase A can replace kinase 1, but not 2. Calcium-calmodulin complex activated calcineurin binds PQIVID motiv in the intracellular loop of TRESK. This leads to dephosphorylation of one or both regulatory domains containing serine and the channel is activated. Adapter 14-3-3 protein can contribute to the channel inhibition by binding to phosphorylated S264 site, or it can directly inhibit kinase 2 (Enyedi *et al.*, 2012).

1.8.3.4 TRESK and calcineurin

In neurons Ca^{2+} regulates a number of processes, such as membrane potentials, secretion and circadian gene expression, all showing circadian oscillations (Colwell, 2000). Intracellular calcium ($[Ca^{2+}]_i$) is known to have endogenously regulated diurnal variation with levels higher at daytime rather than night. This pattern is maintained even under reversed LD cycle, therefore, the pattern of $[Ca^{2+}]_i$ release is light dependant.

Within the intracellular loop, TRESK has a calcineurin binding site. Elevation of cytoplasmic calcium can regulate the membrane potential through TRESK activation. This activation is eliminated by inhibiting calcium/calmodulin dependent protein phosphatase – calcineurin – indicating a direct link between calcium and TRESK activation (Czirják *et al.*, 2004; Czirják and Enyedi, 2010).

1.8.3.5 Effect of anaesthetics

Background K^+ currents present in excitable cells are mediated by K2P channel family. Some of the currents passing by some K2P family members are enhanced by volatile anaesthetics suggesting the mechanism of anaesthesia. TRESK presence not only in the spinal cord but also in the brain, suggests its involvement in anaesthesia. Research done by Liu et al. (2004) and Keshavaprasad et al. (2005) confirms the contribution of volatile anaesthetics (isoflurane, halothane, sevoflurane and desflurane) to enhancement of the currents carried by TRESK. On the other hand, use of intravenous anaesthetics did not produce significant enhancement of the TRESK currents and local anaesthetics (such as bupivacaine and lidocaine) resulted in current inhibition.

The role of anaesthetics is to cause analgesia, anxiolysis, amnesia and to suppress somatic responses to injury (Steinberg *et al.*, 2014). Anaesthetics open TRESK to enhance the currents carried by. Therefore, deficiency of TRESK channels should result in reduced sensitivity to anaesthetics. However, it was found that TRESK gene knock-out (KO) animals are less sensitive only to isoflurane comparing to WT animals (minimum alveolar concentration was increased by 8%) and there was no significant difference in sensitivity to other volatile anaesthetics. This indicates that TRESK is involved in the mechanism of action of anaesthetics, but (1) in KO animals the channel might have been substituted by others, (2) volatile anaesthetics work on multiple targets or (3) TRESK has no significant impact in anaesthetic effect (Chae *et al.*, 2010; Enyedi and Czirják, 2015).

1.8.3.6 Protective mechanism from light and TRESK

Bright light can cause damage to the retina. Short time exposure to extremely bright light can produce immediate thermal injury. Prolonged exposure to bright light results in photochemical damage. It means that retinal cells may undergo chemical changes resulting in cell death (Hunter *et al.*, 2012). One of the natural mechanisms protecting the eyes from too much light is pupillary constriction as it regulates the amount of light reaching the retina. But apart from direct damage to the eyes, bright light exposure is one of the migraine triggers. Migraine is a common recurrent headache affecting three times more females than males (Lafrenière *et al.*, 2010). Interestingly, loss of function TRESK mutation has been linked with migraine. It could be hypothesised that healthy individuals would normally display a light protective mechanism, where they would try to avoid the bright light source or minimise the exposure. If non-functional TRESK individuals would not be able to display these protective behaviours, it could be one of possible reasons why they have increased risk for migraine.

1.9 Circadian regulation of SCN electrical properties

Ion channels are essential to maintain stable membrane potential and to be able to generate action potentials. The molecular clock is not an exception. SCN electrical properties are tightly controlled by a wide range of ion channels that also differ during the day and night, as shown below. One of the unique SCN properties is endogenous generation of action potentials in absence of the synaptic drive. During the daytime, SCN neurons are more depolarised (with the RMP between -50mV and -55mV) compared to other neurons that are not spontaneously active. Some of SCN neurons can even be so depolarised, that they are not able to generate action potentials at all (Belle *et al.*, 2009). For a spontaneous activity to take place, a combination of intrinsic membrane currents are needed: currents providing excitatory drive necessary for spontaneously active neurons, currents translating excitatory drive into regular action potentials pattern and currents silencing firing during the night-time by hyperpolarising the membrane (Allen *et al.*, 2017).

SCN neurons are mostly electrically silent during the subjective night and they fire action potentials near the dawn continuing to generate action potentials throughout the day. This pattern is uniform across both diurnal and nocturnal animals. During the day, SCN neurons are in the depolarised state due to excitatory drive provided by cation currents: persistent Na^+ current, hyperpolarization-activated (I_H) conductance and voltage-sensitive calcium (Ca^{2+}) currents. Opening of hyperpolarisation activated cyclic nucleotide-gated (HCN) ion channels is one more excitatory drive important in pacemaking of the neurons. Opening of HCN channels enables Na^+ entering and K^+ leaving the neurons causing slow membrane excitation. A sustained pharmacological block of HCN channels greatly reduces the frequency of action potentials during the day and diminishes circadian gene expression (Colwell, 2011).

Ca^{2+} channels also are contributors to spontaneous activity in neurons. Measuring the expression of α1 subunits constituting a pore-forming region of the voltage-dependent calcium channels has revealed that L-type channels (α1C) were expressed the most, whereas rhythmic expression pattern was present for P/Q (α1A) and T-type channels (α1G) (Nahm *et al.*, 2005). Based on this study, T-type calcium channels have a peak expression at ZT12. There are studies suggesting T-type calcium channels role in glutamate-induced phase shifts (Kim *et al.*, 2005). The observed expression pattern with peak mRNA at ZT12 would confirm the involvement of T-type calcium channels in light-mediated changes of molecular clock during the night.

Sodium-potassium (Na^+/K^+) pump is crucial for maintaining resting membrane potential in response to the excitatory drive during the day and so pump's activity is also higher during the day (Wang and Huang, 2006). If Na^+/K^+ pump is non-functional, the neural membrane may

depolarise because of disrupted ion flow across the membrane. Generally, for every three Na^+ ions transported out of the cell, two K^+ ions are moved into the cell in this way adding a virtual -1 positive charge for every cycle of ion transport. Disrupting this balance would result in depolarisation because of the charge being in a more positive range than normal.

The RMP of neurons is mainly set by a class of K2P channels (TASK and TREK). They are active over the whole voltage range and are providing 'leak' currents to membranes. They help to maintain negative membrane potential and as a result are responsible for nightly silencing of SCN neurons by maintaining membrane potential in the hyperpolarised state (Allen *et al.*, 2017).

Fast delayed rectifier (FDR) potassium currents generated by Kv3 (voltage-dependent) family of K^+ channels enable SCN neurons to generate regular action potentials by modulating firing frequency. FDR K^+ currents have circadian rhythms and can also be pharmacologically inhibited, resulting in reduced magnitude of the daily rhythm in firing. Generating mice lacking Kcnc1 and Kcnc2 genes coding for the Kv3.1 and Kv3.2 channels showed reduced spontaneous daytime activity, as well as reduced NMDA elicited excitatory responses during the night proving the necessity of FDR K^+ currents for electrical activity and circadian modulation in SCN neurons (Colwell, 2011; Kudo *et al.*, 2011).

Calcium-activated K^+ channels (BK channels) significantly contribute to membrane repolarisation following the action potential in SCN. *Kcnma1* is rhythmically expressed transcript in SCN that encodes pore-forming subunit of BK channels. It was found to be highly expressed during the night, when spontaneous firing rate of neurons is low. Work on *Kcnma1* KO mice proved the importance of BK channels in maintaining low spontaneous firing rate at night and showed, that animals lacking *Kcnma1* have degraded circadian rhythms showing decreased wheel-running activity levels. However, using motion sensors showed that *Kcnma1* KO mice have increased activity compared to WT littermates if they were bred on a C57BL/6J background (Meredith *et al.*, 2006). Also, work done using iberiotoxin, selective inhibitor of BK type I channels, showed that even 40% of afterhyperpolarisation happening after the action potential is due to BK channels (Cloues and Sather, 2003).

1.10 Light evoked regulation in the SCN

The circadian clock is highly synchronised by the light-dark cycle. As a result, circadian clock rhythm can be shifted by changing lighting conditions (photic stimuli). Photic stimuli given during the early subjective night leads to delayed phase shift, whereas animals that receive light pulse during late subjective night result in phase advance, as it was shown in free-running

nocturnal animals (as already seen in Figure 10) (Daan and Pittendrigh, 1976). During delay zone of the phase response curve, light pulse causes induction of both *Per* genes, but only *mPer2* gene expression spreads to the SCN shell. On the other hand, late subjective night light pulse causes elevation of *mPer1* levels causing advancement of behavioural rhythms (Yan *et al.*, 2007).

Light input activates ipRGCs that release glutamate and PACAP as their neurotransmitters. Because SCN is innervated by RHT, as a result of light signalling firing rate is increased and SCN neurons get the Ca^{2+} influx through activation of AMPA and NMDA receptors (ionotropic glutamate receptors) as well as an increase in cAMP levels. Increase in calcium and cAMP activates a cascade of signalling pathways leading to activation of CREB (cAMP response element-binding protein) and CRTC1 (CREB-regulated transcription coactivator 1). They drive transcription of *Per1*, *Per2* and *Sik1* in the nucleus by activating CRE (cAMP response element) (Colwell, 2011; Jagannath *et al.*, 2017). Therefore, following the light pulse during the dark phase, there is an increase in immediate early gene *c-fos* expression within the SCN (Rusak *et al.*, 1990; Best *et al.*, 1999) as well as clock proteins PER1 and PER2 that shift the molecular clock. Production of SIK1 protein acts as a break preventing overproduction of PER1 and PER2. It deactivates CRTC1 by phosphorylation stopping the further transcription of *Per1* and *Per2* genes (Figure 20) (Jagannath *et al.*, 2013).

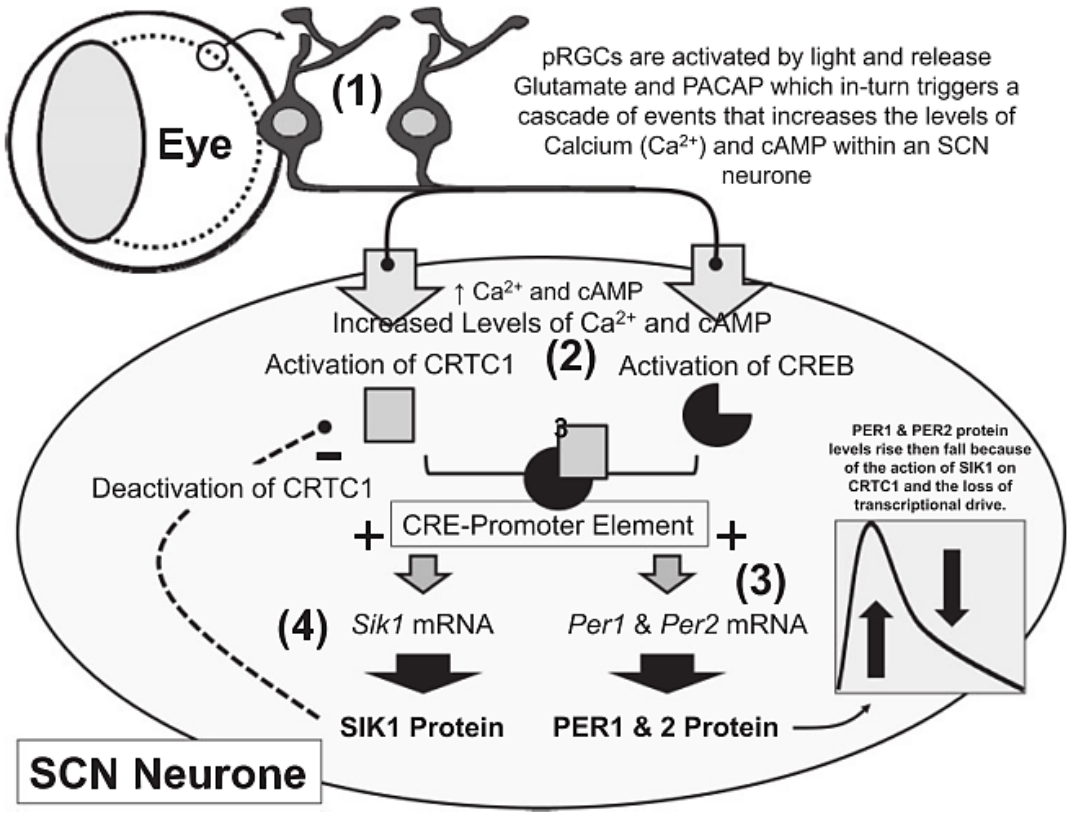

Figure 20: The effect of light on molecular clockwork.

There are four main steps summarising the events happening in SCN neurons after receiving light input. (1) Light detected by intrinsically photosensitive retinal ganglion cells (ipRGCs) triggers the release of neurotransmitters glutamate and PACAP at the ventrolateral side of SCN. This increases intracellular calcium and cAMP. (2) Elevated Ca^{2+} and cAMP activate CREB (cAMP response element binding) as well as CRTC1 (CREB-regulated transcription coactivator 1) proteins. They work together to promote clock gene Per1, Per2 and Sik1 transcription. (3) CRE activation of clock genes leads to increased levels of PER1 and PER2 proteins that shift the molecular clock. (4) SIK1 protein acts as a brake to stop the production of PER1 and PER2 proteins. It phosphorylates CRTC1 in this way inactivating it; therefore, transcription stops (Jagannath et al., 2013, 2017).

1.11 SCN efferent pathways

The main target of neurons emerging from SCN and the important relay for circadian timing system is the subparaventricular zone of the hypothalamus (SPZ) (Vujovic *et al.*, 2015). Here the circadian body temperature, sleep and locomotor activity rhythms are controlled, as it was discovered by performing ibotenic acid lesions in SPZ (Lu *et al.*, 2001). Using injections of retrograde tracers enabled to see that SPZ is innervated from different regions of the circadian pacemaker. Neurons deriving from the SCN shell innervate medial part of SPZ and lateral SPZ receives input from the SCN core as well as direct retinal input through RHT (Moga and Moore, 1997; Leak and Moore, 2001).

Some of the SCN output is also received by the paraventricular nucleus of hypothalamus (PVN). Dorsal PVN neurons regulate melatonin secretion at night by projecting to sympathetic preganglionic column located in the spinal cord. Medial parvicellular PVN neurons secrete corticotrophin releasing hormone into the median eminence in this way regulating secretion of adrenal corticosteroids during the day. However, removal of the PVN had no major effect on circadian regulation of sleep or body temperature indicating that it is only a target of circadian pacemaker and has no influence on circadian entrainment itself (Lu *et al.*, 2001).

The SCN projects to other areas of the brain that have an effect on circadian activity. Therefore, the behavioural changes arising because of induced genetic modifications of specific genes of interest may not be directly linked to SCN, but to the structures linked to it.

1.12 Light mediated behavioural outputs

1.12.1 Seasonal light adaptation

Throughout the year, parts of the world that are away from the equator experience drastic light-dark cycle changes, with shifts in the 24 hours light-dark ratio. Therefore, organisms must be able to adapt to environmental seasonal changes. This requires SCN plasticity. Changes to day length may lead to altered locomotor activity, reproduction and depression (LeGates *et al.*, 2014). SCN has subsets of clocks forming phase clusters that are approximately located in dorsal and ventral regions (Foley *et al.*, 2011). By using PER2::LUC mice it was found that there is a phase gap in between dorsal and ventral SCN regions, with a much larger range in animals exposed to longer periods of light (Evans *et al.*, 2013). Myung *et al.* (2015) identified intracellular chloride to be responsible for SCN coupling as a result of changes in day length. Modulation of intracellular chloride through NKCC1 and KCC2 transporters adjusts the strength and the polarity of $GABA_A$ mediated synaptic input. Increased day length changes the expression patterns of Cl^- transporters by enhancing NKCC1 expression in comparison to KCC2 resulting in more excitatory GABA synaptic input. As a result of excitatory GABA response in the dorsal SCN the period is shortened and synchronising signal from ventral SCN is shortened causing increased phase gap. Therefore, it was suggested that the period lengthening is mediated by GABA.

1.12.2 Jet-lag

Travelling across different time zones leads to disrupted sleep and imbalanced circadian rhythm, what is known as jet lag. The bigger shift in time is experienced, the harder it is for the body to re-adapt to the new light-dark cycle. However, not only sleep is disrupted for those

travelling across different time zones, hormonal secretion becomes imbalanced as well. General malaise, gastrointestinal disturbance might also occur (Sack, 2009).

Frequent travelling and shift work are associated with colorectal, prostate cancers, coronary heart disease and even increased mortality rate (Davidson *et al.*, 2006, 2009). It was found that due to chronic shift lag, cytolytic natural killer (NK) cells' activity is almost completely suppressed leading to increased tumour prevalence in lungs (Logan *et al.*, 2012). Chronic phase advance experiments have also shown that even after two weeks in DD after a set of repeated phase advances, molecular clock mechanism of lung tissue was significantly more advanced compared to skeletal muscle tissue molecular clock. This indicates that lung tissue did not recover from chronically shifting LD cycle (Wolff *et al.*, 2013). Therefore, it might be possible that inability for lungs to synchronise to changing rhythm makes them more susceptible to cancer, which could be mediated by suppressed NK cells activity.

Jet-lag symptoms arise as a result of the internal circadian clock and external solar time misalignment. Melatonin and cortisol are hormones highly influencing sleep/alertness behaviour. Melatonin is actively secreted in the pineal gland during the night, making an individual sleepy. However, this hormone is not associated with sleep in nocturnal animals, because its secretion patterns are the same as in diurnal species (Sack, 2009).

After changes in the solar cycle experienced following transmeridian travel, inner body clock still works in the same rhythm as before the changes and several days are needed for the clock to re-entrain (Figure 21). When travelling across different time zones, the light onset occurring at a different time of the day triggers altered clock gene expression. For example, during 6-hour advance, instead of light onset being at ZT0, it starts at ZT18. Light acutely increases *mPer1* and *mPer2* levels, especially on day 1 during the first few hours of illumination. *mPer1* and *mPer2* expression normalise on day 3, whereas *mCry1* expression is normalised only at around day 8 (Reddy *et al.*, 2002). However, clock genes must re-synchronise not only in SCN, but also in peripheral tissues. Research by Davidson et al. (2009) showed that SCN needs at least eight days to re-establish internal synchrony, whereas thymus, lung, spleen and oesophagus complete the resynchronisation on day 5.

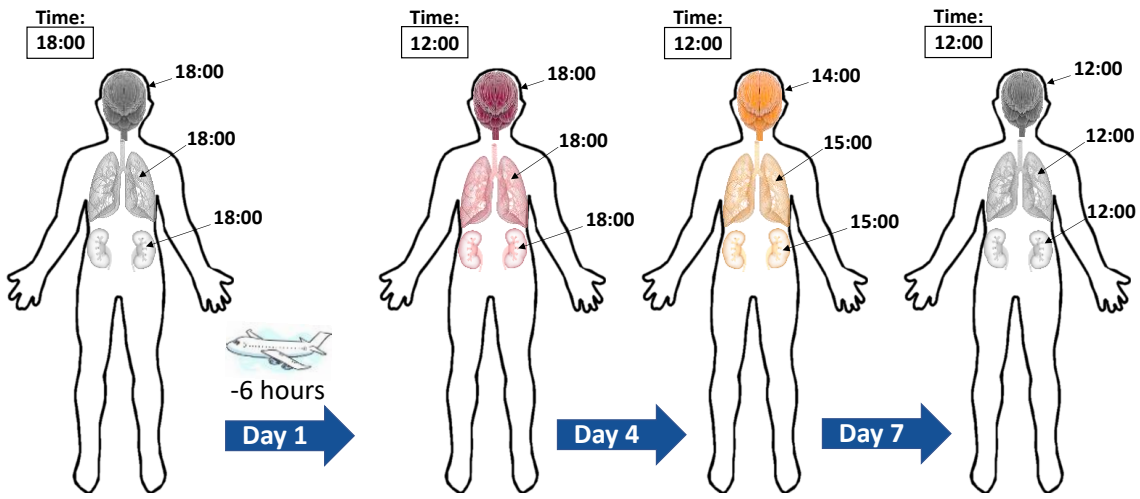

Figure 21: Schematic representation of jet-lag.

When travelling across time zones, our molecular clock needs to re-synchronise to the changed external timing. During the first few days in a new time zone, the clock is misaligned – it is still synchronised to the previous timings that were present before travelling. When entraining to new time, SCN is the first to adapt and then it further synchronises peripheral clocks. That is why on day 4, for example, SCN is more advanced comparing to peripheral clocks in lungs and kidney. To shift by one hour, it takes approximately one day. Therefore, when experiencing 6-hour transmeridian travel, the body should re-entrain to the new timing in under a week. (Adapted from Hugh Piggins talk in Oxford "Neurons, networks and circadian rhythms").

1.12.3 Masking

Another behavioural response to light is masking. Masking is an acute physiological response to external zeitgeber without circadian pacemaker involvement. It results in increased or decreased locomotor activity depending on the nature of the animal's activity (diurnal or nocturnal). Diurnal animals were found to start and finish their activity exactly with the lights on and off, even when the length of the day was altered (4, 6, 8, 10 hours of light during 24-hour day) (Aschoff, 1960). In contrast, nocturnal animals suppress their locomotor activity during the lights-on period and start their activity as soon as the lights are off. This is known as positive and negative masking (Aschoff and von Goetz, 1988).

Immediate melatonin reduction as a result of light pulse at night-time results in inhibited locomotor activity giving a direct masking response (Redlin, 2001). Melatonin is a hormone mainly produced by the pineal gland, with some of it also produced by the retina. It is secreted during the night-time whether the species are diurnal or nocturnal and its release is controlled by the SCN. A light pulse at night triggers glutamate release at the RHT synapses, suppressing melatonin expression in the SCN. Glutamate receptor NMDA inhibition by antagonist MK-801

was found to be capable of inhibiting decline in pineal melatonin (Colwell *et al.*, 1991) indicating that glutamate and its receptors are involved in melatonin reduction and therefore might be major players in masking.

Many strains of inbred mice, including C57BL/6J, make very little or no melatonin. During the melatonin synthesis, with the help of enzymes serotonin is converted to melatonin. Serotonin N-acetyltransferase is the penultimate enzyme in the melatonin synthesis pathway, but this enzyme is absent in C57BL/6J mouse strain (Roseboom *et al.*, 1998). Despite this, light can still induce masking responses. The retina is very important in the mechanism of masking, and research has shown that in absence of rods and cones, animals can still show masking behaviour that is driven by ipRGCs (Mrosovsky and Hattar, 2003; Mrosovsky and Thompson, 2008). Work on intact retinae has revealed that not only melanopsin containing ipRGCs, but also cones play a role in masking ensuring a masking response during a dynamic range of wavelengths (Thompson *et al.*, 2008). Retinal ganglion cells project to about 30 retinorecipient brain regions, including SCN, IGL, olivary pretectal nucleus, dorsal lateral geniculate nucleus and superior colliculus. However, lesions of IGL, visual cortex, retinorecipient pretectum, tectum dorsal lateral geniculate or ventral lateral geniculate did not abolish the mechanism of masking (Morin, 2013b). A further research has proposed that SCN is the structure responsible for the control of masking.

1.13 Ageing of the molecular clock

Ageing affects us all leading to functional deterioration of organs and brain systems. There are several theories proposing possible changes that happen in cells leading to ageing. DNA damage and repair theory suggest that genomic instability and ageing is a result of unrepaired DNA damage. Another theory states that accumulation of mitochondrial DNA damage causes physiological dysfunctions and diseases through the release of free radicals. The third one is a telomere theory of ageing. Telomeres play an important role preventing the chromosome ends from being recognised as double strand breaks. Telomeres shorten with each round of cell division and this leads to induced DNA damage response. Apart from these theories of ageing, multiple other factors can contribute to ageing. Cellular senescence, stem-cell depletion, epigenetic changes, impaired protein homeostasis and altered intercellular communication are all involved in the ageing process (Figure 22) (López-Otín *et al.*, 2013; Maynard *et al.*, 2015).

Figure 22: The hallmarks of ageing.

The following nine factors: mitochondrial dysfunction, cellular senescence, stem cell exhaustion, altered intercellular communication, genomic instability, telomere attrition, epigenetic alterations, loss of proteostasis and deregulated nutrient sensing, are suggested to be the causes of ageing (López-Otín *et al.*, 2013).

The SCN with age exhibits a decrease in amplitude of SCN electrical activity and the expression levels of neurotransmitters, such as VIP, GRP and vasopressin, is reduced. These age-related molecular clock changes can lead to sleep fragmentation affecting the general wellbeing. Abnormal circadian clock functions have also been linked to the severity of neurodegenerative and sleep disorders (Kondratova and Kondratov, 2012; Meijer *et al.*, 2012). Interestingly, stabilizing circadian rhythms by introducing regular feeding patterns has shown to improve daily rest, activity and metabolic rhythms in mouse model of Huntington's disease (Maywood *et al.*, 2010). Farajnia *et al.* (2012) have shown that aged mice have desynchronised electrical activity. Extracellular brain recordings of aged mice showed a spread of activity throughout 24-hours, whereas neurons in the SCN of young animals had synchronised electrical rhythmicity, with peaks of activity between CT 0-12. Also, aged mice had significantly more depolarised

neurons at night, compared to the resting membrane potential of young animals. One of the many changes associated with ageing is the decline in binding densities and functions of NMDA receptor, with NR2B subunit affected the most (Magnusson, 2012; Biello *et al.*, 2018). As already discussed in previous chapters, NMDA plays an important role in glutamate signalling in SCN neurons resulting in intracellular calcium increase that helps to facilitate behaviour responses to the environment. With changes in NMDA or its subunits during ageing, the behavioural responses to light could be altered.

It was already suggested that K2P channels are contributing to the nightly hyperpolarisation of the SCN neurons (Allen *et al.*, 2017). Therefore, absence of one or more leak potassium channels could change the electrical properties of the SCN by making SCN neurons more depolarised. Maintaining SCN neurons at a more depolarised state since birth, could lead to the behavioural changes in aged mice that could be observed using locomotor activity recordings.

1.14 Transgenic models in research

Gene editing is commonly used to test the effects or certain genes affecting individual cells or the entire organism. This can involve insertion, deletion or replacement of a DNA segment.

The genome can be edited using engineered endonucleases that can cut DNA at specific locations. One of the most commonly used endonucleases is CRISPR-Cas9 (Clustered Regularly Interspaced Short Palindromic Repeat). CRISPR-Cas9 works by transfecting the cell with Cas9 endonuclease protein together with specially designed guide RNA that eventually leads to gene insertion or deletion. Another common gene editing method is viral transfection using recombinant adeno-associated virus (rAAV). It is a very efficient method and is non-pathogenic, therefore it can be used *in vivo*. Cre recombinase can also be used for gene editing. Using Cre-loxP method, adenovirus expressing Cre recombinase is injected in the region of interest. There it catalyses recombination between two Cre-specific loxP sites that are on both ends of the gene of interest (Sauer and Henderson, 1988).

A lot of research is undertaken using different cell lines. This is cost-effective, easy to use and cells can be easily genetically engineered to meet the researcher's needs. However, very often these cell lines are already genetically manipulated and constant passaging of cells can further induce genotypic and phenotypic changes affecting the reproducibility (Kaur and Dufour, 2012). Stem cell research has an increasing use in the research community with induced pluripotent stem cells (iPSCs) gaining popularity. Even though stem cells can be used for

modelling disease processes, they still do not provide the ability to see how a certain gene would affect the entire organism. This is where animal research comes in.

In the UK, animal research is tightly controlled by the Home Office, with very tight regulations present in other countries too. Mice are commonly used animal model as their DNA protein-coding regions have 85% similarity to humans. Moreover, mice have relatively quick reproduction rate with gestation lasting on average 20 days and weaning age being 21 days. To make genetically modified mice, the genome can be edited at the embryo stage and this would cause genetic changes in the entire organism. Alternatively, already mentioned Cre-loxP method, that would only target the area of interest, can be used. For example, injection of rAAV construct carrying Cre recombinase through the cannula into the brain would result in a genetic modification in targeted neurons.

1.14.1 TRESK KO animals

Chae et al. (2010) found that TRESK KO animals have increased thermal nociception. Increased perception of pain was also observed after TRESK channel blockage and silencing (Tulleuda *et al.*, 2011). Tulleuda et al. (2011) found that during neuropathic pain TRESK channel is downregulated contributing to neuronal hyperexcitability induced by neuronal injury, whereas animals lacking TRESK channels show activation of sensory neurons and nociceptive fibres and have behavioural evidence of pain. Work on DRG neurons using TRESK functional KO mice has shown that the role of TRESK is to dampen cellular excitability. Also, knocking down the channel reduced the duration of action potentials and caused higher amplitudes of after-hyperpolarisation (Dobler *et al.*, 2007).

Work by Weir *et al.* (2019) has tested the involvement of TRESK in somatosensory processing and they showed *Tresk* mRNA expression in the trigeminal ganglion. Multiple sensorimotor tests (such as thermal sensitivity, innocuous touch and black tape test) showed that TRESK KO mice are more sensitive to the sensory stimuli compared to WT controls. Furthermore, TRESK KO mice spent significantly more time in the dark during the 5 min light/dark box testing and they crossed more squares during the open field test (no significant difference).

Mice used in this project were created by replacing *Tresk* gene (*Kcnk18*) with LacZ-neomycin cassette resulting in TRESK ablation in the entire organism (Weir *et al.*, 2019). By focusing on circadian examination of TRESK KO mice, we will be able to see what role TRESK potassium channel plays in circadian rhythms of the body.

1.15 Project background and aims

As discussed earlier, from the published literature we already know that TRESK is activated by $G\alpha_q$ protein with calcium playing a major role in TRESK function. Work by Laurence Brown has shown that TRESK is highly enriched in SCN as well as in the whole brain (unpublished data). Given the importance of TRESK in regulation of cells excitability, this led us to believe that knocking down TRESK K2P channel would have a significant impact on circadian rhythms.

In this thesis, I will:

- Assess TRESK expression in the SCN;
- Investigate the effects of TRESK K2P channel on:
    - the function of the retina,
    - diurnal as well as circadian locomotor activity,
    - light-induced stress conditions, such as jet-lag and activity compression,
    - molecular changes within the clock,
    - light induced phase shifting effects,
    - the role of K2P channels in ageing.

The aim of this work is to understand the role played by TRESK K2P channels in the suprachiasmatic nucleus.

2 Methods

2.1 Subjects

All mice were bred on a C57BL/6J (Charles River) background from heterozygous parents generating TRESK knock-out and wild type littermate controls. Male mice were housed individually in polypropylene cages with food and water available *ad libitum*.

All experimental procedures were carried out under the Home Office (UK) licence in accordance with Animals (Scientific Procedures) Act (1986) following ethics approval from the University of Kent.

TRESK (GenBank accession number NM332396, Ensembl identification number ENSMUSG40901) knock-out mice were obtained from the KOMP repository. The VelociGene targeting system ablates KCNK18 by replacing the majority of the coding region with a LacZ-neomycin cassette. Knockout mice were initially crossed with wild-type C57BL/6J (Harlan, United Kingdom) (Weir *et al.*, 2019).

2.1.1 Genotyping

2.1.1.1 DNA extraction

Pups born from heterozygous parents had an ear punch taken after the weaning. Tissues placed in sterile Eppendorf tubes were stored in -20°C until the processing. For DNA extraction 100µL DirectPCR (Ear) tissue digest solution (Viagen Biotech, Bioquote, UK) with 1µL Proteinase K (Sigma) was used. Ear notches were fully submerged into the solution and Eppendorf tubes were left overnight at 55^{o}C in the thermoblock. The next day tissue digest was vortexed, heated to 85°C for 45min to denature the Proteinase K and kept in the fridge for up to a week or in -20^{o}C.

2.1.1.2 PCR

Qualitative end-point polymerase chain reaction (PCR) was used for the gene of interest amplification. Two pairs of primers were used for TRESK KO mice: TRESK product forward and reverse primers giving 433bp WT band and Neomycin product forward and reverse primers indicating TRESK KO mice, giving a 492bp band.

Primers used:

TRESK Product:

- F: 5’- ACAGGCAGGGTGATAAGGTG -3’
- R: 5’-GCATGGCTGAGTGATTTCCT-3’

Neomycin Product:

- F: 5’-AGGATCTCCTGTCATCTCACCTTGCTCCTG-3’
- R: 5’-AAGAACTCGTCAAGAAGGCGATAGAAGGCG-3

PCR reaction mix was done using GoTaq® G2 Green Master Mix (Promega, UK) with 2µL of supernatant containing genomic DNA added to the reaction. PCR reactions were heated by thermal cycler at 95°C for 5 minutes, followed by 35 cycles of 95°C for 60 s, 60°C for 60 s, 72°C for 60 s with a final step at 72°C for 5 minutes.

2.1.1.3 Gel electrophoresis

PCR DNA products were separated using 1.5% agarose gel (Sigma, UK) with 10µL of SYBR™ Safe DNA Gel Stain (Thermofisher) prepared in a 1 x TAE (Tris-acetate-EDTA) running buffer. Samples were run for 1 hour 45 minutes at 90V alongside a DNA reference ladder (ThermoScientific, UK).

Electrophoresis gel was removed from the running buffer and photographed under UV illumination.

2.2 RNAscope staining

2.2.1 Brain preparation and slicing

Brains from WT male mice were collected at ZT11.5 and ZT14, washed in PBS and fixed for 24 hours in 4% Formaldehyde solution at 4°C. Brains were cryopreserved by dehydrating them in 15mL falcon tubes containing 10%, 20% and 30% sucrose solutions (for about 24-hours at each sucrose concentration, kept at 4°C). The dehydrated brain was embedded in optimal cutting temperature compound (OCT) media and kept at -80°C.

Coronal 14 µm thick brain slices were cut using a cryostat and slices containing SCN were mounted on SuperFrost Plus adhesion slides. Slides were numbered in order of collection and stored at -20°C.

2.2.2 Staining for SCN

Several slides were randomly selected based in order of collection and were stained with DAPI to check which sections contained the SCN. Staining coronal brain sections every 10-15 slides helped to identify the range where SCN is present.

Coronal brain slices were first lysed using 0.1% and 0.3% Triton X-100 solutions, with 5 min and 20 min incubations, respectively. DNA of lysed cells was stained with DAPI with 15 min incubation in the dark, followed by a wash with PBS and distilled water. Slides with stained tissue were mounted using a coverslip and ProLong™ Gold Antifade Mountant.

As SCN contains densely packed cells, the structure can be easily identified by examining stained nuclei. DAPI stained coronal sections were checked under a fluorescent microscope using DAPI filter. This allowed to know which of the remaining unstained slides should contain SCN.

2.2.3 RNAscope 2.5HD Red

Only slides containing SCN were selected for RNA scope staining. Staining protocol was supplied by the manufacturer (RNAscope® 2.5 HD Detection Reagent – RED User Manual, PART 2, Document Number 322360-USM). The counterstaining of slices with Hematoxylin was excluded and pretreatment steps done before starting the manufacturer protocol are described below.

Slides were removed from -20°C and left at room temperature to acclimatise. Slides were washed with PBS and baked at 60°C for 45 min to prevent slices from detaching. Hydrogen peroxide was applied on each slice for 1 minute followed by mili-q water wash. Slices were then washed with 100% ethanol for 1 minute and baked at 60°C for 5 minutes. After drawing the barrier with Immedge™ hydrophobic barrier pen, slices were treated with Protease Plus and incubated for 15 minutes at 40°C in the hybridisation oven. Final preparation step was to wash the slices with mili-q water.

TRESK probe was used for *Tresk* mRNA staining and positive as well as negative probes were used as controls. Probes for *Tresk* mRNA were provided by Zameel Cader's group, University of Oxford.

After the signal detection step, slices were additionally stained with VIP and DAPI (all of the steps were done in dim light, incubations were in the dark). The subsequent steps were done for staining: RNAscope processed slices were washed in 0.1% Triton X-100 and then blocked for 1 hour in 0.3% Triton X-100 containing 2% normal goat serum (NGS). Anti-VIP antibody

(ab43841) was diluted to 1:20 with 0.3% Triton X-100 containing 2% NGS. The antibody was incubated with the slices for 48 hours at 4°C followed by four 0.1% Triton X-100 washes. Secondary antibody (Goat Anti-Rabbit Alexa Fluor 488) was diluted to 1:600 using 0.3% Triton X-100 and slices with secondary antibody were incubated for 2 hours at room temperature. After incubation slices were washed with PBS, incubated with DAPI for 10 minutes, washed again with PBS and water and mounted using ProLong™ Gold Antifade Mountant

2.2.4 Imaging

Stained slides were imaged using Zeiss 780 inverted confocal microscope. The following microscope settings were used:

- Objective: LD LCI Plan-Apochromat 25x/0.8 Imm Korr DIC M27;
- Channels: 3, 12-bit;
- Image size: x: 600.45 µm, y: 598.79 µm (for TASK-3), x: 603.64 µm, y: 603.64 µm (for TRESK);
- Pinhole: Track 1 Ch1: 38 µm; Track 2 ChS1: 36 µm; Track3 ChS1: 38 µm
- Filters: Track 1 Ch1: 410 – 488 (DAPI); Track 2 ChS1: 562 – 615 (RNAscope RED stain); Track3 ChS1: 490 – 544 (AVP);
- Lasers: Track 1 405 nm: 2.0%; Track 2 561 nm: 2.0%; Track 3 488 nm: 0.7000%;
- Rectangular grid tile scan with 15% overlap and 2x zoom,

2.3 Clock gene and *Tresk* expression in SCN

2.3.1 Tissue retrieval for 24-hour clock gene expression

Age-matched male mice were sacrificed by cervical dislocation at ZT 2, 6, 10, 14, 18, 22 (3 mice per time point). During ZT 2-10 brains were removed under the room light, whereas during ZT 14-22 brains were removed under dim red light. To prevent retinal signalling to the SCN, eyes were immediately removed from animals sacrificed during ZT 14-22. 1 mm coronal brain slices were made using brain matrix and SCN was dissected under the stereomicroscope. Dissected SCNs were immediately submerged in RNAlater (Sigma, UK), frozen on dry ice and then kept at -80°C.

2.3.2 RNA isolation and cDNA synthesis

RNA was isolated from tissue extracts using RNeasy Mini Kit (QIAGEN, UK). RNA concentration was measured using Qubit RNA HS Assay Kit (ThermoFisher) and RNA was reverse transcribed

by Nanoscript reverse transcription kit (Primerdesign, UK) with final working cDNA concentration of 1 ng/µL.

2.3.3 Gene expression by RT-qPCR

20 µL reactions were prepared in triplicate in 96-well white plates (Alpha Laboratories, UK) consisting of 10 µL iTaq™ Universal SYBR® Green Supermix (BioRad), 1 µL 20x TaqMan gene expression assay (Table 1), 6µL Rnase-free water and 3 µL cDNA (For TRESK and TASK-3 expression 7 µL of cDNA were used).

Table 1: 20x TaqMan gene expression assays.

Assay ID:	Gene name:
Mm00501813_m1	Per1
Mm00478099_m1	Per2
Mm00455950_m1	Clock
Mm02014295_s1	Kcnk9
Mm01702237_m1	Kcnk18
Mm02619580_g1	Beta-actin

Reactions were run using Applied Biosystems 7500 fast Real-Time PCR Systems.

Protocol: holding stage (50°C for 20 sec), pre-incubation (95°C for 10 min), amplification (40 cycles x 95°C for 15 sec and 60°C for 60 sec).

2.3.4 Data analysis

After the completed thermocycling protocol, C_t (cycle threshold) values were obtained from the Applied Biosystems 7500 software. Relative expression was calculated using $2^{-\Delta Ct}$, where ΔC_t is C_t (gene of interest) - C_t (reference gene – beta-actin) (Schmittgen and Livak, 2008). Linear detrending and normalisation to mean of the $2^{-\Delta Ct}$ values was done using BioDare2 online tool. Graphs were plotted using GraphPad Prism 7.

2.4 PER2::Luc -TRESK KO bioluminescence recordings

PER2 luciferase mice were crossed with TRESK KO mice and a new line was generated containing PER::Luc and with knocked down TRESK channel.

For bioluminescence recordings, organotypic SCN cultures were used. Age-matched animals were sacrificed at the same time of the day (ZT4.5-6.5) over the two days with equal distribution of TRESK KO and WT mice for each day.

2.4.1 Preparation of solutions

NMDG-HEPES Recovery solution (Table 2) used for slicing was prepared on the day of the experiment and used over two days. The prepared solution was filter sterilised in sterile laminar flow hood and bubbled with carbogen gas mixture (95% Oxygen: 5% Carbon dioxide) before use.

Recording media stock (Table 3) solution was used from refrigerated stock.

Table 2: A list of ingredients and needed concentrations to make the NMDG-HEPES Recovery solution.

NMDG-HEPES Recovery Solution			
Can be used for mice between 5 weeks to 1 year old.			
	mM	**MW**	**g/L**
NMDG	93	195.2	**18.16**
KCl	2.5	74.6	**0.19**
NaH_2PO_4	1.2	138.0	**0.17**
$NaHCO_3$	30	84.0	**2.52**
HEPES	20	238.3	**4.77**
Glucose solution	25	180.2	**10 mL**
sodium ascorbate	5	198.0	**0.99**
Thiourea	2	76.1	**0.15**
sodium pyruvate	3	110.0	**0.33**
$MgSO_4.7H_2O$ (2M stock)	10	246.5	**5 mL**
$CaCl_2.2H_2O$ (2M stock)	0.5	147.0	**250uL**
HCl (see note) (10M stock)	93		
Adjust pH to~7.35 with HCl (6-8mL needed for 1L)			

Table 3: Ingredients and their volumes for making the recording media.

Recording media	
	Quantity
DMEM Powder	**1 bottle**
Mili-Q water	**1L**
Glucose solution	**9.5mL**
HEPES (1M)	**10mL**
NaHCO3 (7.5% solution)	**4.7mL**
Pen Strep	**2.5mL**
Glutamax (1x)	**10mL**
Adjust pH to~7.3 with HCl	

Recovery media solution was prepared fresh on the by mixing recording media with 2.5 mM AP-V (DL-2-Amino-5-phosphonopentanoic acid) and 100 nM MK-801 (Dizocilpine) – both NMDA receptor antagonists inhibiting electrical activity in neurons. For 12 SCN slices, 6 mL of recording media with 150 µL AP-V and 6 µL MK-801 were mixed (500 µL/slice). Recovery media was prepared on the day at kept at 37°C.

Recording media was prepared by mixing recording media with 1/50 B27 (supports the growth and viability of neurons), 400M Luciferin (Substrate for firefly luciferase) and 1/20 FBS (Foetal

Bovine Serum – a mixture of biomolecules enhancing growth). For 12 SCN slices 6 mL of recording media, 120 µL B27, 300 µL FBS and 24 µL Luciferin were used (500 µL/slice). Recording media was prepared on the day and kept at 37°C covered with foil to protect from light.

2.4.2 Slicing

Animals were killed by cervical dislocation. Cerebellum was cut on the coronal plane and brain glued to the mould (Figure 23).

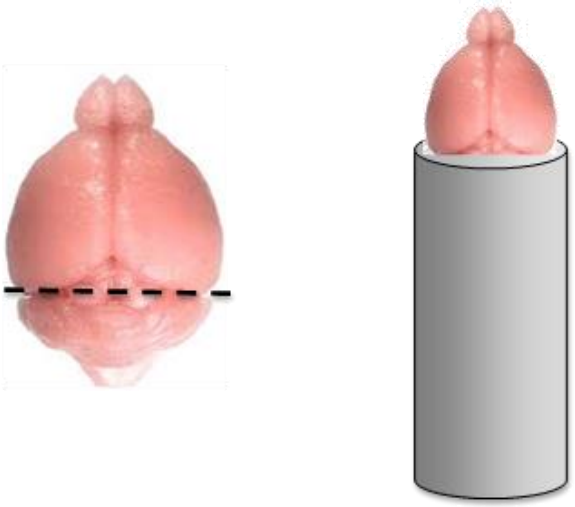

Figure 23: Brain mounting for sectioning.

Mould was filled with 3% Low Melt Agar and chilled clamp was placed over metal tubing of the mould to rapidly cool and solidify the agar.

Brain was sliced in compresotome filled with NMDG-HEPES Recovery solution and bubbled with carbogen. 250 µm coronal slices were cut and slices of interest removed to the 12 well plate with fresh NMDG-HEPES Recovery solution. Maximum 3 animals at a time were used to prevent brain slices from degradation and to ensure similar phase of the molecular clock.

2-3 slices from animal contained SCN which was dissected using needles.

2.4.3 Recovery and recording

In sterile laminar flow hood, 500 µL of recovery media for each SCN slice was placed in 24 well plate. Millipore membrane was inserted into well containing recovery media and 1 SCN section per membrane was placed in the middle (NMDG solution removed from Millipore membranes using pipettes). Slices were incubated at 37°C oven for 1 hour.

For bioluminescence recordings, 500 µL of recording media was added into white 24 well plate. Millipore membranes with SCN slices were transferred to the recording media, sealed with clear film and placed into 37°C incubator for an hour, or the next day if more SCN slices had to be added.

Prepared recording plate was then placed into TriStar^2 S LB 942 Berthold microplate reader with 100 sec of recording time every hour.

SCN slices were recorded for four days and the first 15 hours of recording were excluded from the analysis.

2.4.4 Data analysis

MultiCycle software by ActiMetrics was used for data analysis (period calculation, bioluminescence normalisation) and graphs plotted using GraphPad Prism 7 with error bars representing SEM. Student's t-test or two-way ANOVA with either Tukey's or Bonferroni's multiple comparison tests were used for statistical analysis.

2.5 Pupillometry

12:12 LD entrained animals were dark-adapted in the room with infrared illumination for 1 hour before the pupillary measurements. Animals were hand restrained and the irradiant light provided by the xenon arc lamp (OptoSource High Intensity Arc, Cairn Research) was directed straight to the eye. Pupil recordings of the contralateral eye were done using CCD camera (Best Scientific, Swindon) capturing an image of the eye every 0.3 sec.

480nm blue light filter was used, providing 0.15 mW light intensity. All pupillary measurements were done in between ZT 4-6.

Normalised pupil area was calculated by dividing fully constricted pupil areas (images captured after light exposure) by fully dilated pupil areas (images captured before light exposure) for each animal during all irradiances by using ImageJ software (NIH, USA). Data were plotted using GraphPad Prism 7 with error bars representing standard error of the mean.

2.5.1 Single-pulse pupillometry

Pupillary images were taken for 3 sec in the dark following 60 sec of image recording under 480nm irradiant light (Figure 24). Light intensity was reduced by one log unit using neutral density (ND) filters 0 ND – 6 ND (irradiance Log: 8.6 - 14.6 photons/cm^2/sec).

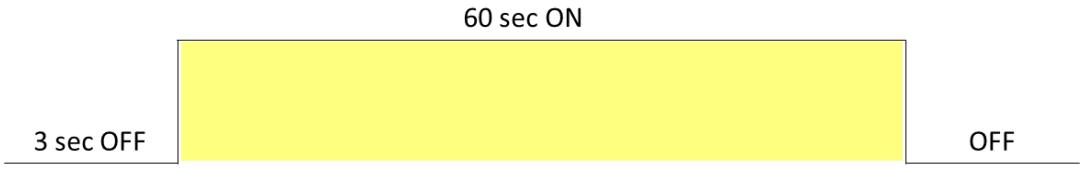

Figure 24: Shutter programming for lights ON/OFF during single pulse pupillometry.

Images were taken for 3 seconds in the dark to get the baseline of dilated dark-adapted pupil followed by 60 seconds of imaging in the 480nm light. Neutral density filters were used to reduce light intensity by one log unit allowing to plot irradiance response curve.

Photon irradiance was calculated using equation (Table 4):

$$Irradiance = \frac{P}{h \times \frac{c}{\lambda}} = \frac{P \times \lambda}{h \times c}$$

where:

- P – light intensity measured in Watts
- h – Planck's constant (6.626 x 10^{-34} Ws^2)
- c – the speed of light (3 x 10^{17} nm/s)
- λ – light wavelength in nm

The equation can be further simplified giving:

$$Irradiance\ (\text{photons/cm}^2\text{/sec}) = P \times \lambda \times 5.03 \times 10^{15}$$

Table 4: Irradiance conversion from Watts to photons/cm^2/s.

Irradiance (480nm)			
	Watts	**photons/cm^2/s**	**Log (photons/cm^2/s)**
0ND	1.50 x 10^{-4}	3.62 x 10^{14}	14.559
1ND	1.50 x 10^{-5}	3.62 x 10^{13}	13.559
2ND	1.50 x 10^{-6}	3.62 x 10^{12}	12.559
3ND	1.50 x 10^{-7}	3.62 x 10^{11}	11.559
4ND	1.50 x 10^{-8}	3.62 x 10^{10}	10.559
5ND	1.50 x 10^{-9}	3.62 x 10^{9}	9.559
6ND	1.50 x 10^{-10}	3.62 x 10^{8}	8.559

For the rate of pupillary constriction during the 63-second interval (3 sec light off and 60 sec light on) pupil images were analysed every 0.9 sec (every third image), except between 2.7 sec and 5.4 sec, when measurements were taken every 0.3 sec because of high constriction rate as the light turned on. Pupil area for each measurement was normalised to the fully dilated pupil area.

For the irradiance response curve (IRS) data non-linear regression curve (irradiance log Vs normalised response) was fitted for statistical analysis.

2.5.2 Two-pulse paradigm

Pupillary images were taken for 3 sec in the dark following 10 sec lights ON, 10 sec OFF, 10 sec ON (Figure 25) of image recording under 480nm irradiant light. Light intensity was reduced by one log unit using neutral density (ND) filters 0ND – 2ND (irradiance Log: 8.6 - 12.6 photons/cm2/sec). The rate of pupillary constriction was analysed every 0.9 sec (every third image). Pupil area for each measurement was normalised to the fully dilated pupil area measured during the first 3 sec of recording.

Figure 25: Shutter programming for lights ON/OFF during double pulse pupillometry.

Pupil images were taken for 3 seconds in the dark to get the baseline of dilated dark-adapted pupil. This was followed by 10 seconds of imaging in the light, then again 10 seconds in the dark, for the analysis of the rate of pupil resetting. After the second set of recording in the dark, 10 seconds of imaging in light was repeated again.

2.5.3 Data analysis

Pupil area was calculated from obtained images using the ImageJ software (version v1.52p). To better visualise the pupil area, brightness and contrast were adjusted. By using the ellipse option, area of the pupil was selected and ImageJ calculated the area (Figure 26). These area values were used for plotting irradiance response curve and pupil constriction rate.

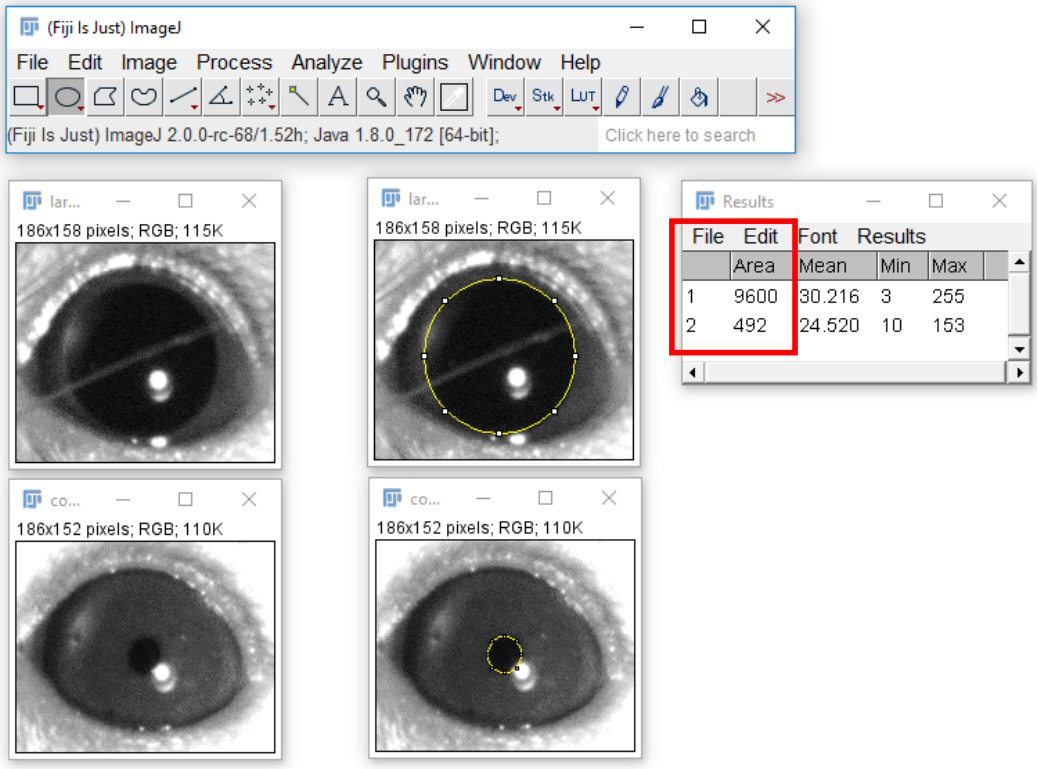

Figure 26: Data analysis for pupillometry.

Using ImageJ software ellipse was used to highlight the pupil area. Software can measure the area, in this example giving the value of 9600 in the dilated pupil. Constricted pupil area in this example is 492, therefore the normalised pupil area would be 492/9600=0.05.

Single-pulse pupillometry. To plot the irradiance response curve, the most constricted area of the pupil (min) for each animal was divided by the most dilated area (max) obtained during recording in darkness giving a normalised pupil area. This was repeated for all animals for pupil images taken across all irradiances. For the pupil constriction rate, the most dilated pupil area was measured and this value was used for all the images from the same recording. Normalised pupil area was calculated for every image in the first 2.4 seconds of light (9 images at 0.3 second intervals) and then every 0.9 seconds until the end of recording (60 seconds in total).

Two-pulse paradigm. For the pupil constriction rate, the most dilated pupil area was measured and the value was used for all the images from the same recording. Four pupil measurements were done for the first 3 seconds of the dark (every 0.9 seconds) followed by pupil area measurement every 0.3 seconds in the first second of a light pulse with subsequent measurements every 0.9 seconds until the end of recording.

All data were processed in the Microsoft Excel and graphs were plotted using GraphPad Prism 7 with error bars representing standard error of the mean. Two-way ANOVA with Bonferroni's multiple comparisons test was done for statistical significance analysis.

2.6 Behavioural recordings

2.6.1 12:12 light-dark cycle

All the behaviour recordings were done in the Charles River Laboratories (Kent) using infrared sensors (LuNAR™ PIR 360°, Risco Group) or 8 cm internal diameter cardboard running wheels (will be indicated in the data) and the data were collected using The Chronobiology Kit (Stanford Software systems). Activity counts per minute were recorded and data were saved to the computer every hour.

The light was administered using LED strips fitted above each row of cages providing equal irradiance to all animals. LD cycle was controlled by the programmed timer and light intensity was adjusted by using neutral density filters.

Animal numbers for the 400 lux light-dark cycle housing: n=5 (WT), n=9 (TRESK KO). During 2000 lux light-dark cycle housing animal numbers were: n=5 (WT), n=15 (TRESK KO). During 400 lux running wheel activity recordings 6 TRESK KO and 6 WT mice where used and their behaviour was compared to IR recordings of 8 TRESK KO and 7 WT (running wheel mice numbers were lower because of faulty running wheels that did not record the behaviour).

2.6.1.1 Data analysis

2.6.1.1.1 24-hour activity profile

24-hour LD activity profile was prepared by extracting data into Microsoft Excel in 30min bins over 9-10 days of activity recording (days, when cages were cleaned, were excluded). Mean 24-hour activity for each animal was calculated and plotted data represents SEM between experimental animals. Data were plotted using GraphPad Prism 7 and statistical significance was assessed using two-way ANOVA with Bonferroni's multiple comparisons test.

2.6.1.1.2 The phase angle of entrainment and alpha duration

Actograms were opened using The Chronobiology Kit Analysis tool (representative simplified actogram shown in Figure 27). For phase angle of entrainment, Actogram Phase Ruler available in the Chronobiology Kit Analysis software was used to measure the time difference (in minutes) between activity onset and the lights off. Activity starting after the lights off was plotted as a negative value (delayed activity onset). For the alpha duration, activity onset and offset were estimated by an eye fit and activity duration was measured using Actogram Phase Ruler. During the eye fit alpha measurement, actogram was visually assessed to determine activity onset and offset and that duration was used as alpha duration. Data is based on 7-10 days of activity and error bars show SEM.

Data were plotted using GraphPad Prism 7 and statistical significance was assessed using Student's t-test.

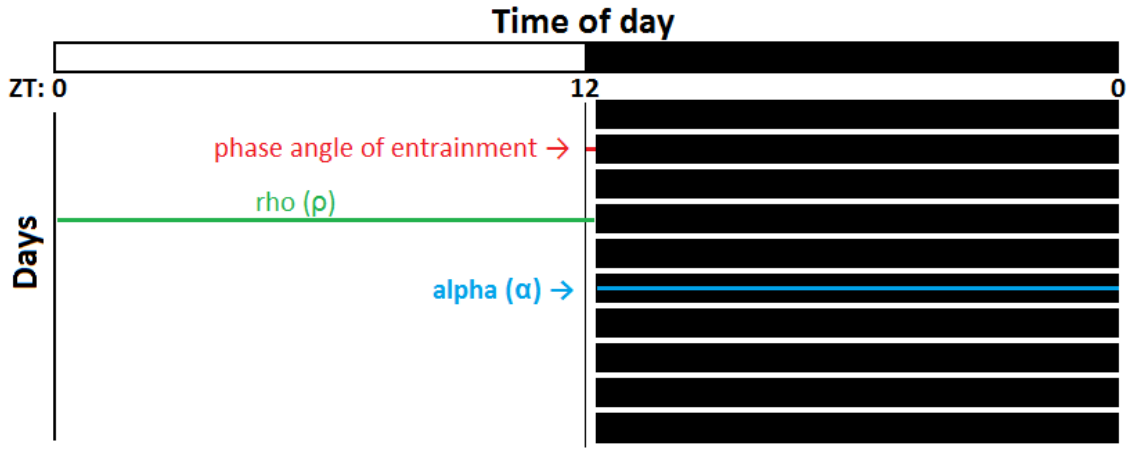

Figure 27: A representative actogram indicating which part of it is used for measuring phase angle of entrainment, rho and alpha periods.

The bar on the top represents the light-dark cycle, whereas horizontal black bars represent different days. The phase angle of entrainment (in red) is the time difference between lights off and activity onset. Alpha (in blue) is activity during the dark phase, whereas rho (in green) is light phase activity measured until activity onset.

2.6.1.1.3 Infrared beam breaks: daily mean activity, alpha and rho periods

Daily infrared beam breaks were calculated by extracting 9-11 days data in 10min bins for 24 hours from ZT2 (animals were still active for some time after the lights turned off; therefore first 2 hours were included into previous day calculations). Mean daily activity was calculated for each animal and plotted using grouped means for both experimental groups.

The onset of alpha activity was counted after there were 5, 10 and 15 (or similar) consecutive IR beam breaks around the ZT12 with no periods of inactivity longer than 30min shortly after that. Alpha offset was at the point where the activity was visibly reduced, with many gaps of inactivity present and the last activity bin not less than 10 IR beam breaks followed by a prolonged period of inactivity (most commonly in between ZT 22-23). Alpha IR beam breaks were calculated by summing all activity from the determined onset to offset. Rho activity was calculated by subtracting alpha values from daily IR beam breaks.

The percentage of alpha/day and rho/day was calculated using the equation:

$$\frac{rho(alpha)\ IR\ beam\ breaks}{daily\ IR\ beam\ breaks} \times 100$$

Night activity per hour was calculated by dividing alpha activity by alpha duration.

Data were plotted using GraphPad Prism 7 and statistical significance was assessed using Student's t-test.

2.6.1.1.4 Activity rhythm amplitude

The amplitude of circadian rhythmicity was measured using Chi-Square Periodogram (Q_P) available in the Chronobiology Kit Analysis tool. When analysing circadian rhythmicity, the Chi-Square Periodogram analysis reflects the variation in period, amplitude, mean level, wave form and phase. The analysis for Chi-Square amplitude is derived from the formula for Q_P (Refinetti, 2004):

$$Q_P = \frac{KN\sum_{h=1}^{P}(M_h - M)^2}{\sum_{i-1}^{N}(Xi - M)^2},$$

Where the data set has *N* values (X_i for i = 1 to *N*) which can be broken down into *K* blocks of period *P*. M_h is the mean of *K* values under each time unit of the period length, *M* is the mean of all *N* values. The amplitude of circadian rhythmicity would show how periodic the data is – the higher the Q_P value, the stronger the rhythmicity in the circadian data set.

Low period was set as 14 hours and high period was set as 36 hours. 20 days of activity recording were used for data analysis. Data were plotted using GraphPad Prism 7 and statistical significance was assessed using Tukey's multiple comparisons test.

2.6.2 Free-running animals (DD)

5 TRESK KO and 5 WT animals were kept in complete darkness to free run. Once the free-running period was established, data were extracted in 10 min bins for daily IR beam breaks or in 30 min bins for 22-hour behaviour profile.

2.6.2.1 Data analysis

When free-running, mice have a period that is shorter than 24 hours. To avoid overlap of the data when plotting 24-hour behaviour profile, 22-hour behaviour profile was plotted instead. For 22-hour DD activity profile activity onset was determined based on actograms and that was set as CT12. From CT 12, -11/+11 hours of activity data were used to plot the 22-hour profile. Behaviour measurements were done after previously housing animals in 2000 lux or 400 lux light.

Tau was measured by subtracting the mean daily advance from 24-hours. For example, if over 10 days mouse has advanced the behaviour by 100 min, the advance is 10 min/day, which means that internal period is 23 hr 50 min.

Data were plotted using GraphPad Prism 7 and statistical significance was assessed using either Student's t-test or two-way ANOVA with Bonferroni's or Tukey's multiple comparisons tests.

2.7 Increasing photoperiod

9 TRESK KO and 6 WT littermates were housed under IR sensors with 400 lux illumination during the light phase provided by LED strips fitted above the cages. Animals were entrained under 12:12 LD cycle with lights on 6:00-18:00 for 14 days. On day 15 the light-dark cycle was changed to 14:10 LD with lights on 5:00-19:00 (photoperiod was increased by adding 1 hr to the dawn and 1 hr to the dusk) and it was maintained for 7 days. 2 hr increase in photoperiod was performed weekly resulting in 7-day photoperiods of 12:12, 14:10, 16:8, 18:6, 20:4, 22:2 LD with the last photoperiod being in constant light (LL). Days 3-5 after the change in photoperiod were used for the analysis of phase angle of entrainment, alpha period measurements and activity level during the dark phase of the day.

2.7.1 Data analysis

Data were analysed by visually examining actograms and by extracting the individual values to Microsoft Excel. For the dark period activity, all infrared beam breaks that happened in the dark phase only were added up. Alpha duration and phase angle of entrainment were calculated using the Actogram Phase Ruler available at the Chronobiology Kit Analysis tool.

Data were plotted using GraphPad Prism 7 with error bars representing SEM. Statistical significance was assessed using two-way ANOVA with Bonferroni's multiple comparisons test.

2.8 Constant light (LL) behaviour

To measure the free-running period in constant light conditions, two protocols were used. In the first protocol, mice were housed under increasing photoperiod conditions, where they received 2 hours less dark each week until they were in constant light for two weeks.

In the second protocol, mice were entrained to LD 12:12 and then released in constant light. During the first week, animals were allowed to develop free-running rhythm and behaviour recording for the next two weeks was used for the data analysis.

2.8.1 Data analysis

Data from 7 days of constant light was extracted in 5-minute bins. Period data were measured using BioDare2 online tool, where the FFT-NLLS (The Fast Fourier Transform Non-linear Least

Squares) fit method was used for period analysis. This method is based on curve fitting and is aimed at analysing free-running circadian behaviour. No data detrending was used and period range was chosen as 18-34 hours. Data obtained from BioDare2 online tool was extracted in Microsoft Excel format and a visual graph of periods was saved from the website.

2.9 Negative masking

2.9.1 Masking behaviour during 12:12 LD cycle with additional ZT14-16 light

5 TRESK KO and 5 WT mice were housed under 12hr light 12hr dark cycle for two weeks with locomotor activity recorded using IR sensors. After baseline recordings, 2 hours of light at ZT14-16 was added to the original cycle and behaviour was recorded for two weeks.

2.9.1.1 Data analysis

Locomotor activity data were extracted in 10 min bouts for daily and alpha period and masking behaviour, whereas the 24-hour profile was plotted using data extracted in 30min bouts. 9 days of baseline activity and 10 days of masking were used in data analysis.

Alpha activity onset was counted after there were 5, 10 and 15 (or similar) consecutive IR beam breaks around the ZT12 with no periods of inactivity longer than 30min shortly after that. Alpha offset was at the point where activity was visibly reduced, with many gaps of inactivity present and the last activity bin not less than 10 IR beam breaks followed by a prolonged period of inactivity (most commonly in between ZT 22-23). Alpha IR beam breaks were calculated by adding up all activity from the determined onset to offset.

The percentage of alpha a day calculated using the equation:

$$\frac{\text{alpha } IR \text{ beam breaks}}{daily\ IR\ beam\ breaks} \times 100$$

The IR beam breaks during ZT14-16 period was calculated by adding up all the activity during baseline and comparing it to the light pulse activity during masking. The percentage of IR beam breaks during ZT14-16 period was calculated using the equation above, where instead of alpha activity, ZT14-16 activity was used.

Data were plotted using GraphPad Prism 7 with error bars representing SEM. Statistical significance was assessed using two-way ANOVA with Bonferroni's multiple comparisons test.

2.9.2 Randomised masking

7 TRESK KO and 7 WT mice were housed under 12:12 LD cycle with locomotor activity recorded using IR sensors. To measure acute masking response, an additional 2 hours of light were given during the circadian night: Day 1 ZT18-20, day 3 ZT16-18, day 5 ZT14-16. One day before the light pulse was used as a baseline for the time interval of interest

2.9.2.1 Data Analysis

Data for each time interval (ZT14-16, ZT16-18 or ZT18-20) was extracted in 1min bins and mean of three recordings for each animal and for each time slot was used to prepare the final data set for all mice.

Data were plotted using GraphPad Prism 7 with error bars representing SEM. Statistical significance was assessed using two-way ANOVA with Tukey's multiple comparisons test.

2.10 Phase resetting by brief light pulses - Aschoff type I and Aschoff type II protocols

Aschoff type I: 12:12 LD entrained animals (10 TRESK KO, 4 WT, except during 400 lux light pulse, where 7 TRESK KO and 6 WT mice were used) having 2000 lux illuminance provided by LED lighting during the light period, were placed in darkness and allowed to free run for a minimum of 7 days. Time of activity onset was determined by analysing actograms a day before the light pulse was given. 5-minute light pulses of different light intensities were given at CT14. 2000 lux, 700 lux, 70 lux, 10 lux light was used (white LED lights) and moving animals to other room with no light pulse given was used as control. Mice were kept in their home cages for the duration of a light pulse.

Aschoff type II: 5 TRESK KO and 5 WT mice were entrained to 12:12 LD cycle with 400 lux illumination during the light period. After stable entrainment, for at least seven days all mice received a 5min 2000 lux / 400 lux or 100 lux light pulse at ZT14. Light pulse was administered using LED strips fitted above the cages and by changing their intensity with neutral density film and/or changing the angle of the light direction from the LED strip. After the light pulse mice were left to free-run in constant darkness for 9-10 days. Cages were not cleaned two days before the light pulse and throughout the free-running phase.

2.10.1 Data analysis

Linear regression lines were eye-fitted on actograms through activity onsets pre and post pulse. Activity data from days 3-9 after the pulse and six days before the pulse were used to analyse the phase shift (data from 2 days after the light pulse was excluded as the SCN is still in the transition state). Distance between two regression lines was measured on the 1st day after the pulse. Eye-fit was assessed independently by another member of the lab.

Statistical analysis and graphs were done using GraphPad Prism 7 with error bars representing SEM. Two-way ANOVA with Bonferroni's multiple comparisons test was used for statistical analysis.

2.11 Light pulse induced clock gene changes

Male mice were housed under 350 lux light in a light-tight chamber (LTC) for three weeks with lights on 23:00-11:00.

One day before tissue collection lights were turned off and animals stayed in constant dark. On the day of experiment control animals were removed and experimental animals received 30 min 350 lux light pulse at CT14. 1-hour after the end of light pulse (CT 15.5) the SCNs were removed from experimental and control (no light pulse) by slicing brain using 1mm coronal brain matrix and dissecting SCN with needles under the stereomicroscope. All work was done under dim red light.

Dissected SCNs were immediately submerged in RNAlater (Sigma, UK), frozen on dry ice and then kept at -80°C.

Animals: controls - 5 WT, 3 TRESK KO; light pulse - 6 WT, 3 TRESK KO.

2.11.1 RNA isolation and cDNA synthesis

RNA was isolated from tissue extracts using RNeasy Mini Kit (QIAGEN, UK). The RNA concentration was measured using Qubit RNA HS Assay Kit (ThermoFisher) and RNA was reverse transcribed by Nanoscript reverse transcription kit (Primerdesign, UK) with the final working cDNA concentration of 1 ng/µL.

2.11.2 Gene expression by RT-qPCR

20 µL reactions were prepared in triplicate in 96-well white plates (Alpha Laboratories, UK) consisting of 10 µL PrecisionPLUS qPCR Master Mix with SYBR green (Primerdesign, UK), 6.2 µL nuclease-free water, 0.9 µL 10 µM of each forward and reverse primers and 2 µL cDNA. For

non-template controls, all the steps were done just like for the brain samples, but instead of RNA, nuclease-free water was added.

Primers:

- Beta-actin

F: 5'ACCAACTGGGACGATATGGAGAAGA-3'

R: 5'CGCACGATTTCCCTCTCAGC-3'

- cFos

F: 5'ATCGGCAGAAGGGGAAAGTAG-3'

R: 5'GCAACGCAGACTTCTCATCTTCAAG-3'

- Per1 (500nM)

F: 5'AGTTCCTGACCAAGCCTCGTTAG-3'

R: 5'CCTGCCCTCTGCTTGTCATC-3'

- Per2 (500nM)

F: 5'GTCCACCTCCCTGCAGACAA-3'

R: 5'TCATTAGCCTTCACCTGCTTCAC-3'

Reactions were run using Applied Biosystems 7500 fast Real-Time PCR Systems.

Protocol: Pre-incubation (95°C for 2 min); Amplification (40 cycles x 95°C for 15 sec, 60°C for 60 sec); Melting curve (continuous: 95°C for 15 sec, 60°C for 60 sec, 95°C for 30 sec, 60°C for 15 sec).

2.11.3 Data analysis

Relative expression was calculated using $2^{-\Delta Ct}$, where ΔC_t is C_t (gene of interest - GOI) - C_t (reference gene – beta-actin).

Fold change following a light pulse was calculated using the following steps:

1. ΔC_t: threshold cycle (C_t) of GOI in each sample was normalised to reference C_t value giving ΔC_t value [C_t (GOI) – C_t (reference gene)].
2. $\Delta\Delta C_t$: WT sham (no light pulse given at ZT14) was used as a baseline value to which ΔCt values of samples obtained from animals that received light pulse were compared providing $\Delta\Delta C_t$ [ΔCt (sample) - ΔCt (WT sham)].
3. Fold change: $2^{-\Delta\Delta Ct}$ ($\Delta\Delta C_t$ for WT sham is 0, so 2^0 is 1)

All graphs were plotted using GraphPad Prism 7 with two-way ANOVA and Bonferroni's multiple comparisons test used for statistical analysis.

2.12 6-hour phase advance (jet-lag)

8 TRESK KO and 4 WT (2000 lux housing); 5 TRESK KO and 5 WT (400 lux housing) animals were entrained to 12:12 LD cycle with lights on 6:00-18:00 for a minimum of 7 days. Illuminance was provided by LED lighting during the light period. LED strips were fitted above each row of cages providing equal irradiance to all animals. LD cycle was controlled by the programmed timer.

On the day of 6-hour phase advance animals had a "short day" with lights on 6:00-12:00. After the advance, the lights were on 00:00-12:00.

2.12.1 Data analysis

Once the phase advance was complete, regression lines were eye-fitted through activity onsets (7 days before phase advance (red), 7 days after the phase advance was complete (blue) and activity onsets were measured as a distance between red line (activity onset before phase advance) and actual activity onset (green regression line is a schematic indication of the activity onset) (Figure 28). Phase shift was complete once the activity onset reached the regression line marking activity onset of the entrained animals.

Significance of the results was evaluated by using two-way ANOVA with Bonferroni's multiple comparisons test using GraphPad Prism 7 with error bars representing SEM.

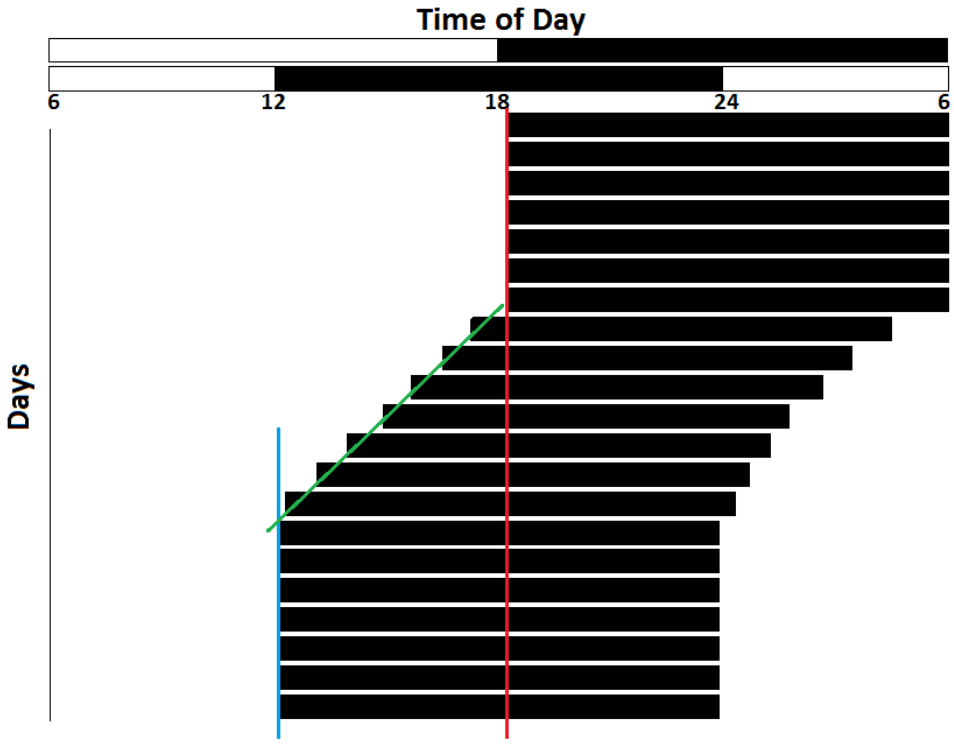

Figure 28: Schematic actogram representing 6-hour phase advance (jet-lag) experiment.

Bar on the top represents the initial light-dark cycle (lights on 6:00 – 18:00), the bar underneath represents light-dark cycle after 6-hour advance (lights on 00:00-12:00), whereas horizontal black bars represent different days. Regression lines were fitted to measure the phase shift. Red line indicates activity onset before the phase advance, blue – activity onset after the phase advance and green line is drawn through activity onsets during the phase advance period.

2.12.2 Phase resetting by brief light pulse simulating the first day of jet-lag

Mice (8 TRESK KO and 7 WT) entrained to a 12:12 LD cycle housed under 2000 lux were given a 5 min 2000 lux light pulse (LED light) at ZT18 and were left in darkness to free run.

A second group containing 5 TRESK KO and 5 WT mice were housed under 400 lux light and received a 5 min 400 lux light pulse at ZT 18 (Aschoff type II protocol).

2.12.2.1 Data analysis

Linear regression lines were eye-fitted through the activity onsets pre and post pulse. First three days were not used as animals were allowed to adjust. Activity data from days 4-9 after the pulse and six days before the pulse were used to analyse the phase shift. Distance between two regression lines was measured on the 1st day after the pulse.

Statistical analysis and graphs were done using GraphPad Prism 7 with error bars representing SEM and student's t-test used for statistical analysis.

2.13 mGluR1 antagonist (A-841720) effect on phase shifting

9 TRESK KO and 6 WT mice were entrained to LD 12:12 with 400 lux light intensity during the day. After stable entrainment, mice were left to free-run for a week and time of activity onset was determined by analysing actograms a day before the injections.

A-841730 (Sigma) was dissolved in DMSO, resulting in a 50 mM stock solution. The stock was diluted using saline and the resulting working solution was 100 µM with 0.2% DMSO. Working drug and control (saline with 0.2% DMSO) solutions were prepared on the day of injections, with a dose of 100 µM/kg.

Drug or vehicle was injected at CT13.5 with 5 min 130 lux light pulse 30 min after the injection (CT14). Injections were performed in the dark with dim red light and light pulses were delivered in home cages. Mice were left free-running in constant darkness and phase delay was measured after nine days from the injection. The second set of injections were done after two weeks, with drug injected instead of saline and vice versa.

2.13.1 Data analysis

For phase-shifting measurement, linear regression lines were fitted on actograms through activity onsets pre and post pulse. Activity data from days 3-9 after the pulse and six days before the pulse were used to analyse the phase shift (data from 2 days after the light pulse was excluded as the SCN is still in the transition state). Distance between two regression lines was measured on the 1st day after the pulse.

Statistical analysis and graphs were done using GraphPad Prism 7 with error bars representing SEM. 2-way ANOVA with Bonferroni post hoc test were used for statistical analysis.

2.14 The effect of Forskolin on phase shifting

7 TRESK KO and 7 WT mice were entrained to LD 12:12 with 400 lux light intensity during the day. Mice were randomly placed across three different rows with a mix of controls, WT and TRESK KO animals in each row to reduce variability in the acquired data. After one week of entrained behaviour, 10 mg/kg of forskolin (FK-506, Sigma) was administered intraperitoneally (i.p.) at ZT8. 5 min 400 lux light pulse was given at ZT14 and animals were left to free-run for at least nine days. Injections were done over two rounds. Firstly, 4 WT and 4 TRESK KO received FK-506 and other animals had a vehicle administration, whereas on the second round 3 WT and 3 TRESK KO that previously had vehicle only injection were administered FK-506 and the rest had vehicle administration.

Drug preparation: FK-506 was dissolved in 300 µL of DMSO, resulting in 16.7 µg/µL concentration. The stock was diluted with physiological saline giving 1 µg/µL concentration with final DMSO concertation being 6%. Vehicle solution was physiological saline with 6% DMSO. The other way of preparing the drug was by dissolving FK-506 powder in 100% ethanol and then further diluting the aliquot in the PBS resulting in 20% ethanol with 5 µg/µL of the drug, with controls receiving 20% ethanol injections. In both cases, the drug was prepared on the day of injections and remaining stock was kept at -20°C.

2.14.1 Data analysis

For phase-shifting measurement, linear regression lines were fitted on actograms through activity onsets pre and post pulse. Activity data from days 3-9 after the pulse and six days before the pulse were used to analyse the phase shift (data from 2 days after the light pulse was excluded as the SCN is still in the transition state). Distance between two regression lines was measured on the 1st day after the pulse. Eye-fit was assessed independently by another member of the lab.

Locomotor activity during the dark phase of the day (ZT12-0) was measured by extracting IR beam breaks in 1 min bins. Baseline activity was taken from one day before the injection.

Statistical analysis and graphs were done using GraphPad Prism 7 with error bars representing SEM. 2-way ANOVA with either Tukey's or Bonferroni's post hoc tests were used for statistical analysis.

2.15 Ageing experiments

TASK-3/TRESK KO mice were generated by crossing TASK-3 KO with TRESK KO until homozygous animals were obtained that were further used for breeding of double knockouts. 5 WT, 5 TRESK KO and 5 TASK-3/TRESK KO mice had their locomotor activity recorded using IR sensors.

3 TRESK expression in the SCN and its role in PER2 rhythmicity

3.1 Introduction

Electrical properties of the suprachiasmatic nucleus are tightly regulated by a number of ion channels that differ during the daytime and at night. This allows circadian variation in resting membrane potential: SCN neurons are more depolarised during the day and hyperpolarised at night. K2P channels TASK and TREK are known to be contributing to hyperpolarisation of the resting membrane potential at night (Colwell, 2011). However, so far there is no published literature on TRESK and its role in the SCN or circadian rhythms.

[REDACTED]

3.2 Results

[REDACTED]

3.3 Discussion

[REDACTED]

4 Retinal decoding of light in TRESK KO mice

4.1 Introduction

Intrinsically photosensitive retinal ganglion cells (ipRGCs) containing melanopsin mediate the non-image forming functions of light. This not only aids in SCN entrainment, but it also has projections to the olivary pretectal nucleus (OPN) that is responsible for pupillary light reflex. Pupillary constriction is mediated by parasympathetic stimulation. It involves the OPN receiving direct innervation from the retinohypothalamic tract. The OPN projects to Edinger-Westphal (EW) nucleus innervating the iris sphincter muscle and the ciliary muscle though ciliary ganglion. Pupillary dilation is a sympathetically driven response starting from hypothalamus with the first synapse at the Budge's centre. From there, postsynaptic neurons exit at the superior cervical ganglion and its sympathetic fibres innervate the iris dilator muscle.

Through pupillary reflex measurements, we can assess the function of photoreceptors present in the retina. Rods are the most sensitive photoreceptors that are active at dim light. Cones, on the other hand, are active even under the brightest daylight; therefore, they are responsible for pupillary light reflexes under bright light. In dark adapted rods, excitation of a single rhodopsin molecule yields a detectable signal, whereas cones would only yield a detectable signal after activating 4-10 visual pigments per cell (Korenbrot, 2012). Melanopsin phototransduction has low sensitivity, hence it contributes to encoding high irradiances, with its signalling overlapping with cone inputs (Lall *et al.*, 2010).

Pupillary light reflex (PLR) measured using mice lacking rod and cone photoreceptors has shown that despite the absence of both photoreceptors, bright white light stimulus resulted in rapid and extensive pupillary constriction similar to wildtype mice (Lucas *et al.*, 2001). Irradiance response curve (IRC) shows the pupillary constriction under different irradiances that corresponds to the action of each of the photoreceptors. PLR of rodless and coneless mice plotted after using 506 nm monochromatic light caused an increased slope of the plotted IRC and decreased sensitivity to light. The curve has shifted by 2.5 log units compared to the wildtype IRC and experiment showed a delayed pupil constriction in response to light stimulus. Testing multiple wavelengths confirmed reduced sensitivity in pupillary response as more light was needed to elicit pupillary constriction at all wavelengths. Furthermore, rodless coneless mice were the most sensitive to 479nm wavelength as seen from the action spectra. This wavelength is characteristic of melanopsin absorbance.

Work on melanopsin knockout mice has shown the disruption in PLR. Despite PLR being indistinguishable from wild-type controls under low irradiances and no changes in number, morphology or projections of retinal ganglion cells, at high irradiances pupils were not constricting to the same level as in melanopsin containing animals. Carbachol (a parasympathetic agonist resulting in pupil constriction) application evoked equally strong pupil constriction in melanopsin containing and knockout mice. Therefore, pupil constriction defect in melanopsin knockout mice during high irradiance was not due to intrinsic defect in the iris sphincter muscle (Lucas *et al.*, 2003). These findings suggest that rods, cones and melanopsin complement each other – they work together to provide a full dynamic range of the pupillary light reflex at different wavelengths of light and light intensity.

[REDACTED]

4.2 Results

[REDACTED]

4.3 Discussion

[REDACTED]

5 Diurnal locomotor activity of TRESK KO mice under light-dark cycle and constant dark

5.1 Introduction

Light plays an important role in the entrainment of the molecular clock. The SCN is able to adapt the organism to environmental light-dark cycle resulting in a robust activity rhythm and rest. However, this type of activity is determined by environmental conditions. As a result, displayed behaviour is only a representation of entrainment and is not an intrinsic rhythm. Intrinsic SCN driven activity can be assessed by behaviour recordings in free-running animals housed in constant dark. This would allow to assess the internal circadian rhythmicity and to measure the internal period length (*tau*).

When entrained, animals are fully adapted to the environment. This is achieved through factors like light information, social interactions and food availability. For example, mice living in the wild always have to adapt to the environmental light conditions that change throughout the year. Apart from light, their entrainment is highly dependent on non-photic stimulants, such as availability of food or presence of predators. Work with mice in laboratory settings allows us to accurately assess their photoentrainment. In a controlled laboratory environment, mice have constant access to food and there is no danger of predators, therefore the main variable in their entrainment becomes the environmental light.

Light intensity can have a big impact on the animals' activity. In the outside world light illumination varies from 1 lux at night all the way to 10.000 lux in a bright sunlight illumination, which is very intense and even painful light (imagine looking straight into the sun without sunglasses). Widely accepted light intensity for rodent housing in laboratories is under 400 lux – illumination similar to that of sunrise and sunset on a clear day. Nevertheless, light intensity in the laboratory can be easily controlled based on the experiment needs and questions to be answered.

[REDACTED]

5.2 Results

[REDACTED]

5.3 Discussion

[REDACTED]

6 Effects of light on masking behaviour

6.1 Introduction

Light is the most universal and efficient external entrainment signal (Aschoff, 1999). As a zeitgeber, light can not only entrain circadian rhythm by controlling phase and period, but it can also have "positive" or "negative" effects on the behaviour, which is known as masking (Mrosovsky, 1999). A positive effect of masking would be an increase in activity when the lights are on in diurnal species or activity enhancement by dark in nocturnal animals. In contrast, a negative effect is considered to be activity suppression by darkness in diurnal and light in nocturnal species.

Masking does not affect entrainment of the clock, but it leads to changes of activity by "masking" the behaviour of a pacemaker and this activity change only lasts for the duration of masking signal (Rietveld *et al.*, 1993). This allows an organism to act immediately to the changes in the environment. There are several types of masking, with terms positive and negative masking used the most. Positive masking is the enhancement of activity, such as increased activity by light in diurnal species. Negative masking, on the other hand, leads to suppressed activity, as we see in nocturnal animals receiving light, or diurnal animals in the dark. Despite having an effect on locomotor activity, masking effect is not controlled by the SCN.

All living organisms are adapted to entrain to changing photoperiods. This is annually experienced during the daylength changes in winter and summer. These changes are gradual and the resulting light-dark cycles are not extreme. However, organisms are only able to entrain the clock to a certain extent, with periods adjusted within 23-25 hours. The entrainment range depends on how much the animal can advance and delay its phase, which is assessed by generating a phase response curve (PRC) (Roenneberg *et al.*, 2010). During photoperiods that are too extreme, animals are able to entrain anymore, and their behavioural response is masking – activity suppression in presence of light. Therefore, during seasonal light adaptation experiment, when the night-time is shortened weekly by two hours until animals are free-running in constant light, the mechanism resulting in compressed activity is masking.

Housing nocturnal animals under constant light (LL) results in increased circadian period (*tau,* τ), which is longer than free-running period in constant darkness (Aschoff, 1960). Housing in LL disrupts endogenous circadian rhythms resulting in decreased locomotor activity in nocturnal

animals or even arrhythmic behaviour, where the arrhythmicity arises because of desynchronised individual SCN neurons (Chen *et al.*, 2008).

[REDACTED]

6.2 Results

[REDACTED]

6.3 Discussion

[REDACTED]

7 Phase-shifting light induced behavioural and molecular changes

7.1 Introduction

[REDACTED]

Majority of the protocols covered until now were based on natural daily behaviour, that could often be experienced when living in the wild. Protocols in this chapter will put animals under stress and push their systems to the limits to test their responses to night-time light pulses and sudden changes in photoperiod that are experienced when travelling across different time zones.

Resetting of the circadian clock to different intensity light pulses will be measured using two protocols – Aschoff type I and Aschoff type II. During type I protocol, experimental subjects are entrained to the 12:12 LD cycle and once stable entrainment is reached, they are released to constant darkness to free-run. After a week of free-running governed by endogenous signalling, the phase is determined by measuring activity onset, which corresponds to CT 12 (circadian time). This is a very long and time-consuming protocol because each experimental subject needs to receive a light pulse based on its endogenous period and in most cases, it can differ a lot from other subjects. Moreover, there is a risk of developing increased photosensitivity due to prolonged constant dark housing. When using Aschoff type II protocol light pulses to all subjects are administered simultaneously, because animals are entrained to the 12:12 LD cycle, then they receive a light pulse and are released into constant darkness to free-run. This protocol is more natural compared to type I because exposure to constant dark for prolonged periods is not very common in nature. Aschoff type II protocol eliminates confounding effects of chronic darkness (such as increased photosensitivity) and this protocol is commonly used in animals that have unstable circadian rhythms when kept in constant dark. One of the biggest advantages of using type II protocol is simultaneous administration of light pulse to all experimental subjects. In our experimental setting, it means that mice can stay in their home cages and they are not disturbed by moving, so the results are more accurate.

Clock resetting by light pulse happens by altering *Per1* and *Per2* gene expression as a result of a light pulse. Increases in *Per1* levels are involved in phase advances, whereas *Per2* increases are present during phase delays (Yan and Silver, 2002). The expression of these genes can be quantified to assess the effect of light on the SCN. Here I will present data using both phase-

shifting protocols and will measure clock protein expression following a light pulse, to compare the effects of light on endogenously controlled and entrained molecular clock.

Apart from clock resetting to short light pulses, changes of the environmental light-dark cycle also require resetting of the clock. Molecular clock genes, as explained in the introduction (1.7 The molecular clock) control 24-hour cycle through transcription and translation of the number of proteins. During transmeridian travel, this synchronised molecular control system gets disrupted. It is misaligned with external timings as the molecular clock is still entrained to the time before travelling. For changes to occur and for the central as well as peripheral clocks to get entrained to new light-dark cycles, transcription-translation mechanism of clock genes has to change. It would be ideal that light reaching SCN would immediately entrain the molecular clock through increased production of PER1 and PER2 levels controlling phase shifting. However, SIK1 protein acts as a break preventing overexpression of *Per1* and *Per2* genes (Figure 20). About one hour after the light pulse, SIK1 phosphorylates CRTC1 (cAMP response element-binding protein regulated transcription coactivator 1) this way stopping further *Per1* and *Per2* transcription (Jagannath *et al.*, 2013). This inhibitory mechanism prevents the molecular clock from rapid shifts, with controlled phase shifting of about 1-hour a day. It means that, for example, when crossing six time zones, re-entrainment would take about six days and until full entrainment is reached, the body would experience jet-lag symptoms, such as fatigue and nausea. By simulating jet-lag in our laboratory setting we were able to test the molecular clock resetting mechanism in TRESK KO mice. During 6-hour advance, on the first day of changing light-dark cycle the lights turn on at midnight instead of 6 am. However, SCN is still entrained to the previous light-dark cycle; therefore, midnight is ZT18, not ZT0. This is the time when molecular clock advances in response to a light pulse. The effect of the first day of jet-lag was tested using Aschoff type II protocol, where entrained mice received a light pulse and where left to free-run, so as to measure the effect of light on circadian clock resetting.

7.2 Results

[REDACTED]

7.3 Discussion

[REDACTED]

8 Glutamate receptor mGluR1 and calcineurin inhibition effects on TRESK KO mice

8.1 Introduction

Glutamate is an abundant central nervous system excitatory neurotransmitter and it acts as a major signalling molecule transmitting light information from RHT to SCN. Metabotropic glutamate receptor 1 (mGluR1) is one of the receptors highly involved in glutamate signalling and its activation results in an increase in cytoplasmic calcium. Immunohistochemistry staining of mGluR1 has shown abundant expression in the SCN at the day of birth (P0), with slightly decreased expression in adult SCN (van den Pol, 1994). Knowing that TRESK is also expressed in SCN and that mGluR1 activation causes activation of G protein $G\alpha_q$, a protein leading to enhanced TRESK activity through calcineurin (Mathie, 2007), we wanted to see whether mGluR1 inhibition would affect the phase-shifting and how would it differ in TRESK KO and WT mice.

As a result of glutamate activated intracellular pathways, the levels of $[Ca^{2+}]_i$ rise causing an increase in the affinity of calcineurin to the TRESK channel, followed by TRESK activation (Enyedi and Czirják, 2015). Thus calcium regulates membrane potential by activating TRESK, therefore calcineurin inhibition should result in increased intracellular calcium levels maintaining TRESK in its inactive state. It is already known that apart from TRESK activation, calcineurin also regulates photic responses and rhythm generation mechanism in the SCN. Work by Katz *et al.* (2008) has shown that intracerebroventricular injection of FK-506 decreased the level of phase delay caused by a light pulse and chronic application of the compound disrupted the circadian rhythms.

[REDACTED]

8.2 Results

[REDACTED]

8.3 Discussion

[REDACTED]

9 Effect of potassium channels on circadian behaviour in aged mice

9.1 Introduction

All the behaviour recordings, phase shifting and molecular work discussed so far was obtained using young to middle age mice (up to 1-year-old). But what would happen to circadian rhythms of mice with deficient leak potassium channels as they age?

[REDACTED]

It is widely known that with increasing age there are disruptions in the sleep/wake cycles, rhythmic behaviour amplitude decreases and there is an increase in activity fragmentation (Biello, 2009; Nakamura *et al.*, 2011; Farajnia *et al.*, 2014; Zhao *et al.*, 2019). These age-related changes happen in humans as well as in other mammals. It is believed that these changes are mediated at the level of SCN. Work by Viswanathan and Davis (1995) has shown that implanting foetal SCN into old hamsters with ablated SCN has restored circadian function, where the free-running period of aged animals matched the period of younger hamsters. With time animals that have undergone SCN implantation procedure showed a shortening of the period, which indicates that age of the graft is significantly contributing to the free-running period. Work on aged mice has shown desynchronised electrical activity of the SCN and more depolarised neurons at night (Farajnia *et al.*, 2012). It was already suggested that K2P channels contribute to the nightly hyperpolarisation of SCN neurons (Allen *et al.*, 2017). If SCN abundant K2P channels (such as TRESK and TASK-3) are absent, electrical properties of the molecular clock would change, where the neurons would remain depolarised even at night and this could potentially lead to the behavioural changes in aged mice. This change in electrical properties of SCN neurons could further affect the action of receptors contributing to behavioural changes.

[REDACTED]

9.2 Results

[REDACTED]

9.3 Discussion

Healthy ageing is one of the Industrial Strategy Challenge Fund's focus points. Aged population is constantly increasing, with 1 in 4 people predicted to be aged 65 years and over by 2050, whereas as measured in 2018 the proportion was 1 in 5 (Coates *et al.*, 2019).

At present, our understanding of the core mechanisms that underpin the alterations in output of the circadian clock during ageing is poorly understood. However, it is very important to understand how ageing alters the internal workings of the circadian clock, that life quality of the aged population could be improved.

Using mice for ageing research allows to test the changes during ageing and this can even be performed in longitudinal studies, what would be very difficult in humans. Age of mice used in most of the experiments that are not related to ageing is mostly 3-6 months old. This is equivalent to testing 20-30-year-old humans. Ageing mice until they are 18-24 months old allow researchers to use the data for better understanding the age effects that would be equivalent to 56-69-year-old humans (Figure 29) (Hagan, 2017).

[REDACTED]

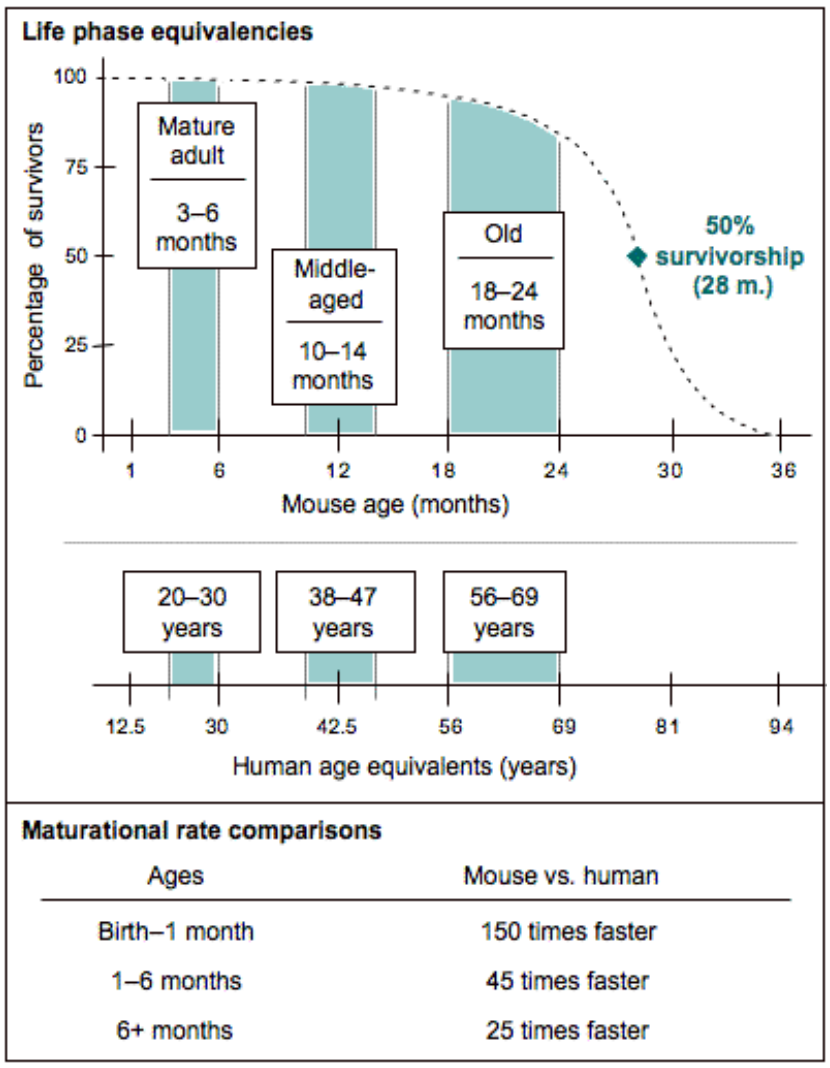

Figure 29: Life phase comparison between mice (C57BL/6J) and humans.

3-6 months old mice widely used in research are equivalent to 20-30-year-old humans. Ageing mice to middle age (10-14 months) and old (18-24 months) allow us to measure the effects of ageing that would be equivalent to 38-47-year old and 56-69-year-old humans (Hagan, 2017).

[REDACTED]

10 Overall discussion

In this thesis, I wanted to investigate the role that TRESK K2P channels play in circadian rhythms. A range of techniques was used to measure the circadian properties and responses of TRESK KO mice to light and we found that TRESK plays an important role in the function of suprachiasmatic nucleus.

[REDACTED]

11 Future work

[REDACTED]

12 References

Abrahamson, E. E. and Moore, R. Y. (2001) 'Suprachiasmatic nucleus in the mouse: Retinal innervation, intrinsic organization and efferent projections', *Brain Research*, 916(1–2), pp. 172–191.

Afzali, M., Ruck, T., Herrmann, A., Iking, J., Sommer, C., Kleinschnitz, C., Preuße, C., Stenzel, W., Budde, T., Wiendl, H., Bittner, S. and Meuth, S. (2016) 'The potassium channels TASK2 and TREK1 regulate functional differentiation of murine skeletal muscle cells.', *American Journal of Physiology - Cell Physiology*, pp. 583–595.

Albers, E. H., Walton, J. C., Gamble, K. L., McNeill, J. K. and Hummer, D. L. (2016) 'The Dynamics of GABA Signaling: Revelations from the Circadian Pacemaker in the Suprachiasmatic Nucleus', *Frontiers in Neuroendocrinology*. Elsevier Inc., 44, pp. 35–82.

Allen, C. N., Nitabach, M. N. and Colwell, C. S. (2017) 'Membrane Currents, Gene Expression, and Circadian Clocks', *Cold Spring Harbor Perspectives in Biology*, 9(5), pp. 1–16.

Allen, N. J. and Barres, B. A. (2009) 'Glia — more than just brain glue', *Nature Neuroscience*, 457(7230), pp. 675–677.

Aller, M. I. and Wisden, W. (2008) 'Changes in expression of some two-pore domain potassium channel genes (KCNK) in selected brain regions of developing mice', *Neuroscience*, 151(4), pp. 1154–1172.

Altimus, C. M., Güler, A. D., Alam, N. M., Arman, A. C., Prusky, G. T., Sampath, A. P. and Hattar, S. S. (2010) 'Rod photoreceptors drive circadian photoentrainment across a wide range of light intensities.', *Nature neuroscience*, 13(9), pp. 1107–12.

Antle, M. C. and Silver, R. (2005) 'Orchestrating time: Arrangements of the brain circadian clock', *Trends in Neurosciences*, 28(3), pp. 145–151.

Armstrong, C. M. (1974) 'Ionic pores, gates, and gating currents', *Quarterly Reviews of Biophysics*, 7(2), p. 179.

Armstrong, C. M. and Hille, B. (1972) 'The Inner Quaternary Ammonium Ion Receptor in Potassium Channels of the Node of Ranvier', *The Journal of General Physiology*, 59(4), pp. 388–400.

Aschoff, J. (1960) 'Exogenous and endogenous components in circadian rhythms.', *Cold Spring Harbor symposia on quantitative biology*, 25, pp. 11–28.

Aschoff, J. (1999) ‘Masking and parametric effects of high-frequency light-dark cycles.’, *The Japanese journal of physiology*, 49(1), pp. 11–18.

Aschoff, J. and von Goetz, C. (1988) ‘Masking of circadian activity rhythms in hamsters by darkness’, *Journal of Comparative Physiology A*, 162(4), pp. 559–562.

Barel, O., Shalev, S. A., Ofir, R., Cohen, A., Zlotogora, J., Shorer, Z., Mazor, G., Finer, G., Khateeb, S., Zilberberg, N. and Birk, O. S. (2008) ‘Maternally Inherited Birk Barel Mental Retardation Dysmorphism Syndrome Caused by a Mutation in the Genomically Imprinted Potassium Channel KCNK9’, *American Journal of Human Genetics*, 83(2), pp. 193–199.

Bargiello, T. A. and Young, M. W. (1984) ‘Molecular-Genetics of a Biological Clock in Drosophila’, *Proceedings of the National Academy of Sciences of the United States of America-Biological Sciences*, 81(7), pp. 2142–2146.

Belle, M. D. C., Diekman, C. O., Forger, D. B. and Piggins, H. D. (2009) ‘Daily Electrical Silencing in the Mammalian Circadian Clock’, *Science*, 326(5950), pp. 281–284.

Benke, T. A., Luthi, A., Isaac, J. T. R. and Collingridge, G. L. (1998) ‘Modulation of AMPA receptor unitary conductance by synaptic activity’, *Nature*, 393(6687), p. 793.

Best, J. D., Maywood, E. S., Smith, K. L. and Hastings, M. H. (1999) ‘Rapid resetting of the mammalian circadian clock.’, *The Journal of neuroscience : the official journal of the Society for Neuroscience*, 19(2), pp. 828–835.

Biello, S. M. (2009) ‘Circadian clock resetting in the mouse changes with age’, *Age*, 31(4), pp. 293–303.

Biello, S. M., Bonsall, D. R., Atkinson, L. A., Molyneux, P. C., Harrington, M. E. and Lall, G. S. (2018) ‘Alterations in glutamatergic signaling contribute to the decline of circadian photoentrainment in aged mice’, *Neurobiology of Aging*. Elsevier Inc, 66, pp. 75–84.

Biello, S. M., Golombek, D. A. and Harrington, M. E. (1997) ‘Neuropeptide Y and glutamate block each other’s phase shifts in the suprachiasmatic nucleus in vitro’, *Neuroscience*, 77(4), pp. 1049–1057.

Brancaccio, M., Edwards, M. D., Patton, A. P., Smyllie, N. J., Chesham, J. E., Maywood, E. S. and Hastings, M. H. (2019) ‘Cell-autonomous clock of astrocytes drives circadian behavior in mammals - Supplementary info’, *Science*, 363(6423), pp. 187–192.

Brancaccio, M., Patton, A. P., Chesham, J. E., Maywood, E. S. and Hastings, M. H. (2017) ‘Astrocytes Control Circadian Timekeeping in the Suprachiasmatic Nucleus via Glutamatergic

Signaling', *Neuron*. Elsevier Inc., 93(6), p. 1420–1435.e5.

Brickley, S. G., Aller, M. I., Sandu, C., Veale, E. L., Alder, F. G., Sambi, H., Mathie, A. and Wisden, W. (2007) 'TASK-3 Two-Pore Domain Potassium Channels Enable Sustained High-Frequency Firing in Cerebellar Granule Neurons', *Journal of Neuroscience*, 27(35), pp. 9329–9340.

Brown, T. M. and Piggins, H. D. (2009) 'Spatiotemporal heterogeneity in the electrical activity of suprachiasmatic nuclei neurons and their response to photoperiod', *Journal of Biological Rhythms*, 24(1), pp. 44–54.

Buhr, E. D. and Takahashi, J. S. (2013) 'Molecular Components of the Mammalian Circadian Clock', *In Circadian clocks*, pp. 3–27.

Chae, Y. J., Zhang, J., Au, P., Sabbadini, M., Xie, G.-X. and Yost, C. S. (2010) 'Discrete change in volatile anesthetic sensitivity in mice with inactivated tandem pore potassium ion channel TRESK.', *Anesthesiology*, 113(6), pp. 1326–1337.

Chen, R., Seo, D. -o., Bell, E., von Gall, C. and Lee, C. (2008) 'Strong Resetting of the Mammalian Clock by Constant Light Followed by Constant Darkness', *Journal of Neuroscience*, 28(46), pp. 11839–11847.

Choe, S. (2002) 'Potassium channel structures', *Nature Reviews Neuroscience*, 3(2), pp. 115–121.

Cloues, R. K. and Sather, W. a (2003) 'Afterhyperpolarization regulates firing rate in neurons of the suprachiasmatic nucleus.', *The Journal of neuroscience : the official journal of the Society for Neuroscience*, 23(5), pp. 1593–604.

Coates, S., Tanna, P. and Scott-Allen, E. (2019) *Overview of the UK Population: August 2019*, *Office for National Statistics*.

Colwell, C. S. (2000) 'Circadian modulation of calcium levels in cells in the suprachiasmatic nucleus', *European Journal of Neuroscience*, 12(2), pp. 571–576.

Colwell, C. S. (2011) 'Linking neural activity and molecular oscillations in the SCN.', *Nature reviews. Neuroscience*. Nature Publishing Group, 12(10), pp. 553–69.

Colwell, C. S., Max, M., Hudson, D. and Menaker, M. (1991) 'Excitatory amino acid receptors may mediate the effects of light on the reproductive system of the golden hamster', *Biol.Reprod.*, 44(4), pp. 604–608.

Conquet, F., Franz-Bacon, K., Ferraguti, F., Bordi, F., Reggiani, A., Matarese, V., Daniel, H., Condé, F., Crépel, F., Bashir, Z. I., Davies, C. H. and Collingridge, G. L. (1994) 'Motor deficit and

impairment of synaptic plasticity in mice lacking mGluR1', *Nature*, 372(6503), pp. 237–243.

Contractor, A., Mulle, C. and Swanson, G. T. (2011) 'Kainate receptors coming of age: Milestones of two decades of research', *Trends in Neurosciences*. Elsevier Ltd, 34(3), pp. 154–163.

Contractor, A., Swanson, G. T., Sailer, A., O'Gorman, S. and Heinemann, S. F. (2000) 'Identification of the Kainate Receptor Subunits Underlying Modulation of Excitatory Synaptic Transmission in the CA3 Region of the Hippocampus', *The Journal of Neuroscience*, 20(22), pp. 8269–8278.

Czirják, G. and Enyedi, P. (2010) 'TRESK background K+ channel is inhibited by phosphorylation via two distinct pathways', *Journal of Biological Chemistry*, 285(19), pp. 14549–14557.

Czirják, G., Tóth, Z. E. and Enyedi, P. (2004) 'The Two-pore Domain K+ Channel, TRESK, Is Activated by the Cytoplasmic Calcium Signal through Calcineurin', *Journal of Biological Chemistry*, 279(18), pp. 18550–18558.

Daan, S. and Pittendrigh, C. S. (1976) 'A Functional analysis of circadian pacemakers in nocturnal rodents - II. The variability of phase response curves', *Journal of Comparative Physiology ??? A*, 106(3), pp. 253–266.

Davidson, A. J., Castanon-Cervantes, O., Leise, T. L., Molyneux, P. C. and Harrington, M. E. (2009) 'Visualizing jet lag in the mouse suprachiasmatic nucleus and peripheral circadian timing system', *European Journal of Neuroscience*, 29(1), pp. 171–180.

Davidson, A. J., Sellix, M. T., Daniel, J., Yamazaki, S., Menaker, M. and Block, G. D. (2006) 'Chronic jet-lag increases mortality in aged mice', *Current Biology*, 16(21), pp. 7–10.

DeWoskin, D., Myung, J., Belle, M. D. C., Piggins, H. D., Takumi, T. and Forger, D. B. (2015) 'Distinct roles for GABA across multiple timescales in mammalian circadian timekeeping', *Proceedings of the National Academy of Sciences of the United States of America*, 112(29), pp. E3911–E3919.

Dineley, K. T., Hogan, D., Zhang, W. R. and Taglialatela, G. (2007) 'Acute inhibition of calcineurin restores associative learning and memory in Tg2576 APP transgenic mice', *Neurobiology of Learning and Memory*, 88(2), pp. 217–224.

Ding, J. M., Buchanan, G. F., Tischkau, S. A., Chen, D., Kuriashkina, L., Faiman, L. E., Alster, J. M., McPherson, P. S., Campbell, K. P. and Gillette, M. U. (1998) 'A neuronal ryanodine receptor mediates light-induced phase delays of the circadian clock', *Nature*, 394(6691), pp. 381–384.

Dobler, T., Springauf, A., Tovornik, S., Weber, M., Schmitt, A., Sedlmeier, R., Wischmeyer, E. and Döring, F. (2007) 'TRESK two-pore-domain K+ channels constitute a significant component of background potassium currents in murine dorsal root ganglion neurones.', *The Journal of physiology*, 585(Pt 3), pp. 867–879.

Doyle, D. A., Cabral, M., Pfuetzner, R. A., Kuo, A., Gulbis, J. M., Cohen, S. L., Chait, B. T. and Mackinnon, R. (1998) 'The Structure of the Potassium Channel : Molecular Basis of K+ Conduction and Selectivity', *Science*, 280(April), pp. 69–77.

Ebling, F. J. P. (1996) 'The role of glutamate in the photic regulation of the suprachiasmatic nucleus', *Progress in Neurobiology*, 50(2–3), pp. 109–132.

Ehlen, J. C., Grossman, G. H. and Glass, J. D. (2001) 'In vivo resetting of the hamster circadian clock by 5-HT7 receptors in the suprachiasmatic nucleus', *J. Neurosci.*, 21(14), pp. 5351–5357.

El-Kouhen, O., Lehto, S. G., Pan, J. B., Chang, R., Baker, S. J., Zhong, C., Hollingsworth, P. R., Mikusa, J. P., Cronin, E. a, Chu, K. L., McGaraughty, S. P., Uchic, M. E., Miller, L. N., Rodell, N. M., Patel, M., Bhatia, P., Mezler, M., Kolasa, T., Zheng, G. Z., *et al.* (2006) 'Blockade of mGluR1 receptor results in analgesia and disruption of motor and cognitive performances: effects of A-841720, a novel non-competitive mGluR1 receptor antagonist.', *British journal of pharmacology*, 149(6), pp. 761–74.

Ellinghaus, P., Scheubel, R. J., Dobrev, D., Ravens, U., Holtz, J., Huetter, J., Nielsch, U. and Morawietz, H. (2005) 'Comparing the global mRNA expression profile of human atrial and ventricular myocardium with high-density oligonucleotide arrays.', *The Journal of thoracic and cardiovascular surgery*, 129(6), pp. 1383–90.

Enyedi, P., Braun, G. and Czirják, G. (2012) 'TRESK: The lone ranger of two-pore domain potassium channels', *Molecular and Cellular Endocrinology*, 353(1–2), pp. 75–81.

Enyedi, P. and Czirják, G. (2010) 'Molecular Background of Leak K ƨ Currents : Two-Pore Domain Potassium Channels', *Physiological reviews*, 90(2), pp. 559–605.

Enyedi, P. and Czirják, G. (2015) 'Properties, regulation, pharmacology, and functions of the K2P channel, TRESK', *Pflugers Archiv European Journal of Physiology*, 467(5), pp. 945–958.

Evans, J. A., Leise, T. L., Castanon-Cervantes, O. and Davidson, A. J. (2013) 'Dynamic Interactions Mediated by Nonredundant Signaling Mechanisms Couple Circadian Clock Neurons', *Neuron*. Elsevier Inc., 80(4), pp. 973–983.

Farajnia, S., Deboer, T., Rohling, J. H. T., Meijer, J. H. and Michel, S. (2014) 'Aging of the suprachiasmatic clock', *Neuroscientist*, 20(1), pp. 44–55.

Farajnia, S., Michel, S., Deboer, T., vanderLeest, H. T., Houben, T., Rohling, J. H. T., Ramkisoensing, A., Yasenkov, R. and Meijer, J. H. (2012) 'Evidence for Neuronal Desynchrony in the Aged Suprachiasmatic Nucleus Clock', *Journal of Neuroscience*, 32(17), pp. 5891–5899.

Feher, J. (2016) *Quantitative Human Physiology an introduction*. Second Edi. Amsterdam Academic Press.

Fernandez, D. C., Chang, Y.-T., Hattar, S. S. and Chen, S.-K. (2016) 'Architecture of retinal projections to the central circadian pacemaker', *Proceedings of the National Academy of Sciences*, (23), p. 201523629.

Fink, M., Duprat, F., Lesage, F., Reyes, R., Romey, G., Heurteaux, C. and Lazdunskil, M. (1996) 'Cloning, functional expression and brain localization of a novel unconventional outward rectifier K+ channel', *The EMBO Journal*, 15(24), pp. 6854–6862.

Fletcher, A. (2014) 'Action potential: Generation and propagation', *Anaesthesia and Intensive Care Medicine*. Elsevier, 15(6), pp. 287–291.

Foley, N. C., Tong, T. Y., Foley, D., Lesauter, J., Welsh, D. K. and Silver, R. (2011) 'Characterization of orderly spatiotemporal patterns of clock gene activation in mammalian suprachiasmatic nucleus', *European Journal of Neuroscience*, 33(10), pp. 1851–1865.

Foster, R. G. and Hankins, M. W. (2007) 'Circadian vision', *Current Biology*, 17(17), pp. 746–751.

Freedman, M. S., Lucas, R. J., Soni, B., von Schantz, M., Muñoz, M., David-Gray, Z. and Foster, R. G. (1999) 'Regulation of Mammalian Circadian Behavior by Non-rod, Non-cone, Ocular Photoreceptors', *Science*, 284(5413), pp. 502–504.

Friedman, D. I. and Dye, T. D. Ver (2009) 'Headache Currents Migraine and the Environment', *Headache*, pp. 941–952.

Fukuhara, C., Suzuki, N., Matsumoto, Y., Nakayama, Y., Aoki, K., Tsujimoto, G., Inouye, S. I. and Masuo, Y. (1997) 'Day-night variation of pituitary adenylate cyclase-activating polypeptide (PACAP) level in the rat suprachiasmatic nucleus.', *Neuroscience letters*, 229(1), pp. 49–52.

Galvao, J., Davis, B., Tilley, M., Normando, E., Duchen, M. R. and Cordeiro, M. F. (2014) 'Unexpected low-dose toxicity of the universal solvent DMSO', *FASEB Journal*, 28(3), pp. 1317–1330.

Gardani, M. and Biello, S. M. (2008) 'The effects of photic and nonphotic stimuli in the 5-HT7 receptor knockout mouse', *Neuroscience*, 152(1), pp. 245–253.

Girard, C., Duprat, F., Terrenoire, C., Tinel, N., Fosset, M., Romey, G., Lazdunski, M. and Lesage, F. (2001) 'Genomic and functional characteristics of novel human pancreatic 2P domain K(+) channels.', *Biochemical and biophysical research communications*, 282(1), pp. 249–256.

Goldstein, S. a N., Bayliss, D. a, Kim, D., Lesage, F. and Plant, L. D. (2005) 'International Union of Pharmacology. LV. Nomenclature andmolecular relationships of two-P potassium channels', *Pharmacological Reviews*, 57(4), pp. 527–540.

González, W., Valdebenito, B., Caballero, J., Riadi, G., Riedelsberger, J., Martínez, G., Ramírez, D., Zúñiga, L., Sepúlveda, F. V, Dreyer, I., Janta, M. and Becker, D. (2015) 'K_2p channels in plants and animals.', *Pflügers Archiv : European journal of physiology*, 467(5), pp. 1091–104.

Güler, A. D., Ecker, J. L., Lall, G. S., Haq, S., Altimus, C. M., Liao, W., Barnard, A. R., Cahill, H., Badea, T. C., Zhao, H., Mark, W., Berson, D. M., Lucas, R. J., Yau, K. and Hattar, S. S. (2008) 'Melanopsin cells are the principal conduits for rod/cone input to non-image forming vision', *Nature*, 453(7191), pp. 102–105.

Hagan, C. (2017) *When are mice considered old?*, *https://www.jax.org/news-and-insights/jax-blog/2017/november/when-are-mice-considered-old*.

Hannibal, J. (2002) 'Neurotransmitters of the retino-hypothalamic tract', *Cell and Tissue Research*, 309(1), pp. 73–88.

Harmar, A. J., Arimura, A., Gozes, I., Journot, L., Laburthe, M., Pisegna, J. R., Rawlings, S. R., Robberecht, P., Said, S. I., Sreedharan, S. P., Wank, S. A. and Waschek, J. A. (1998) 'International Union of Pharmacology. XVIII. Nomenclature of receptors for vasoactive intestinal peptide and pituitary adenylate cyclase-activating polypeptide', *Pharmacol.Rev.*, 50(2), pp. 265–270.

Harmar, A. J., Marston, H. M., Shen, S., Spratt, C., West, K. M., Sheward, W. J., Morrison, C. F., Dorin, J. R., Piggins, H. D., Reubi, J. C., Kelly, J. S., Maywood, E. S. and Hastings, M. H. (2002) 'The VPAC2receptor is essential for circadian function in the mouse suprachiasmatic nuclei', *Cell*, 109(4), pp. 497–508.

Harrington, M. E., Hoque, S., Hall, A., Golombek, D. and Biello, S. M. (1999) 'Pituitary adenylate cyclase activating peptide phase shifts circadian rhythms in a manner similar to light.', *The Journal of neuroscience : the official journal of the Society for Neuroscience*, 19(15), pp. 6637–42.

Hartveit, E., Brandstätter, J. H., Enz, R. and Wässle, H. (1995) 'Expression of the mRNA of Seven Metabotropic Glutamate Receptors (mGluR1 to 7) in the Rat Retina. An In Situ Hybridization

Study on Tissue Sections and Isolated Cells', *European Journal of Neuroscience*, 7(7), pp. 1472–1483.

Hastings, M. H., Brancaccio, M. and Maywood, E. S. (2014) 'Circadian pacemaking in cells and circuits of the suprachiasmatic nucleus', *Journal of Neuroendocrinology*, 26(1), pp. 2–10.

Hattar, S. S., Liao, H. W., Takao, M., Berson, D. M. and Yau, K. W. (2002) 'Melanopsin-containing retinal ganglion cells: architecture, projections, and intrinsic photosensitivity', *Science*, 295(5557), pp. 1065–1070.

Hattar, S. S., Lucas, R. J., Mrosovsky, N., Thompson, S., Douglas, R. H., Hankins, M. W., Lem, J., Biel, M., Hofmann, F., Foster, R. G. and Yau, K.-W. (2003) 'Melanopsin and rod-cone photoreceptive systems account for all major accessory visual functions in mice.', *Nature*, 424(6944), pp. 76–81.

Heginbotham, L., Abramson, T. and MacKinnon, R. (1992) 'A functional connection between the pores of distantly related ion channels as revealed by mutant K+channels', *Science*, 258(5085), pp. 1152–1155.

Hille, B. (2001) *Ion Channels of Excitable Membranes*, *Sunderland, MA: Sinauer.*

Hodgkin, A. L. and Huxley, A. F. (1952) 'A quantitative description of membrane current and its application to conduction and excitation in nerve', *The Journal of Physiology*, 117(4), pp. 500–544.

Hodgkin, A. L. and Keynes, R. D. (1955) 'The potassium permeability of a giant nerve fibre', *Journal of Physiology*, 128(1), pp. 61–88.

Hofman, M. a, Fliers, E., Goudsmit, E. and Swaab, D. F. (1988) 'Morphometric analysis of the suprachiasmatic and paraventricular nuclei in the human brain: sex differences and age-dependent changes.', *Journal of anatomy*, 160, pp. 127–143.

Honma, S., Kawamoto, T., Takagi, Y., Fujimoto, K., Sato, F., Noshiro, M., Kato, Y. and Honma, K. I. (2002) 'Dec1 and Dec2 are regulators of the mammalian molecular clock', *Nature*, 419(6909), pp. 841–844.

Horvath, S. and Raj, K. (2018) 'DNA methylation-based biomarkers and the epigenetic clock theory of ageing', *Nature Reviews Genetics*. Springer US, 19(6), pp. 371–384.

Houben, T., Coomans, C. P. and Meijer, J. H. (2014) 'Regulation of circadian and acute activity levels by the murine suprachiasmatic nuclei', *PLoS ONE*, 9(10).

Hughes, S., Foster, R. G., Peirson, S. N. and Hankins, M. W. (2017) 'Expression and localisation

of two-pore domain (K2P) background leak potassium ion channels in the mouse retina', *Scientific Reports*, 7, p. 46085.

Hunter, J. J., Morgan, J. I. W., Merigan, W. H., Sliney, D. H., Sparrow, J. R. and Williams, D. R. (2012) 'The susceptibility of the retina to photochemical damage from visible light', *Progress in Retinal and Eye Research*. Elsevier Ltd, 31(1), pp. 28–42.

Ivell, R., Teerds, K. and Hoffman, G. E. (2014) 'Proper application of antibodies for immunohistochemical detection: Antibody crimes and how to prevent them', *Endocrinology*, 155(3), pp. 676–687.

Jagannath, A., Butler, R., Godinho, S. I. H., Couch, Y., Brown, L. A., Vasudevan, S. R., Flanagan, K. C., Anthony, D., Churchill, G. C., Wood, M. J. A., Steiner, G., Ebeling, M., Hossbach, M., Wettstein, J. G., Duffield, G. E., Gatti, S., Hankins, M. W., Foster, R. G. and Peirson, S. N. (2013) 'The CRTC1-SIK1 pathway regulates entrainment of the circadian clock', *Cell*. Elsevier Inc., 154(5), pp. 1100–1111.

Jagannath, A., Taylor, L., Wakaf, Z., Vasudevan, S. R. and Foster, R. G. (2017) 'The genetics of circadian rhythms, sleep and health', *Human Molecular Genetics*, 26(R2), pp. R128–R138.

Janisse, M. (2013) *Pupillary Dynamics and Behavior*. Springer Science & Business Media.

Kandel, E. R., Schwartz, J. H., Jessell, T. M., Siegelbaum, S. A. and Hudspeth, A. J. (2012) *Principles of Neural Science*. Fifth Edit. McGraw-Hill Publishing.

Kang, D., Mariash, E. and Kim, D. (2004) 'Functional expression of TRESK-2, a new member of the tandem-pore K + channel family', *Journal of Biological Chemistry*, 279(27), pp. 28063–28070.

Katz, M. E., Simonetta, S. H., Ralph, M. R. and Golombek, D. A. (2008) 'Immunosuppressant calcineurin inhibitors phase shift circadian rhythms and inhibit circadian responses to light', *Pharmacology Biochemistry and Behavior*, 90(4), pp. 763–768.

Kaur, G. and Dufour, J. M. (2012) 'Cell lines: Valuable tools or useless artifacts.', *Spermatogenesis*, 2(1), pp. 1–5.

Keenan, W. T., Rupp, A. C., Ross, R. A., Somasundaram, P., Hiriyanna, S., Wu, Z., Badea, T. C., Robinson, P. R., Lowell, B. B. and Hattar, S. S. (2016) 'A visual circuit uses complementary mechanisms to support transient and sustained pupil constriction', *eLife*, 5, p. e15392.

Kefalov, V. J. (2012) 'Rod and cone visual pigments and phototransduction through pharmacological, genetic, and physiological approaches', *Journal of Biological Chemistry*,

287(3), pp. 1635–1641.

Keshavaprasad, B., Liu, C., Au, J. D., Kindler, C. H., Cotten, J. F. and Yost, C. S. (2005) 'Species-spicific differences in response to anesthetics and other modulators by the K2P channel TRESK', *Anesthesia and Analgesia*, 101(4), pp. 1042–1049.

Ketchum, K. A., Joiner, W. J., Sellers, A. J., Kaczmarek, L. K. and Goldstein, S. A. (1995) 'A new family of outwardly rectifying potassium channel proteins with two pore domains in tandem.', *Nature*, 376(6542), pp. 690–695.

Kew, J. N. and Kemp, J. A. (2005) 'Ionotropic and metabotropic glutamate receptor structure and pharmacology', *Psychopharmacology (Berl)*, 179(0033–3158 (Print)), pp. 4–29.

Kim, D. Y., Choi, H. J., Kim, J. S., Kim, Y. S., Jeong, D. U., Shin, H. C., Kim, M. J., Han, H. C., Hong, S. K. and Kim, Y. I. (2005) 'Voltage-gated calcium channels play crucial roles in the glutamate-induced phase shifts of the rat suprachiasmatic circadian clock', *European Journal of Neuroscience*, 21(5), pp. 1215–1222.

Klooster, J., Vrensen, G. F. J. M. and van der Want, J. J. L. (1995) 'Efferent synaptic organization of the olivary pretectal nucleus in the albino rat. An ultrastructural tracing study', *Brain Research*, 688(1–2), pp. 47–55.

Kolb, H. (2003) 'How the retina works', *American Scientist*, 91(1), pp. 28–35.

Kondratova, A. A. and Kondratov, R. V. (2012) 'The circadian clock and pathology of the ageing brain', *Nature Reviews Neuroscience*, 13(5), pp. 325–335.

Konopka, R. J. and Benzer, S. (1971) 'Clock mutants of Drosophila melanogaster.', *Proceedings of the National Academy of Sciences of the United States of America*, 68(9), pp. 2112–6.

Korenbrot, J. I. (2012) 'Speed, sensitivity, and stability of the light response in rod and cone photoreceptors: Facts and models', *Progress in Retinal and Eye Research*. Elsevier Ltd, 31(5), pp. 442–466.

Kudo, T., Loh, D. H., Kuljis, D., Constance, C. and Colwell, C. S. (2011) 'Fast delayed rectifier potassium current: critical for input and output of the circadian system.', *The Journal of Neuroscience*, 31(8), pp. 2746–55.

Lafrenière, R. G., Cader, Z. M., Poulin, J. F., Andres-Enguix, I., Simoneau, M., Gupta, N., Boisvert, K., Lafrenière, F., McLaughlan, S., Dubé, M. P., Marcinkiewicz, M. M., Ramagopalan, S., Ansorge, O., Brais, B., Sequeiros, J., Pereira-Monteiro, J. M., Griffiths, L. R., Tucker, S. J., Ebers, G., *et al.* (2010) 'A dominant-negative mutation in the TRESK potassium channel is

linked to familial migraine with aura', *Nature Medicine*. Nature Publishing Group, 16(10), pp. 1157–1160.

Lafrenière, R. G. and Rouleau, G. A. (2011) 'Migraine: Role of the TRESK two-pore potassium channel', *International Journal of Biochemistry and Cell Biology*, 43(11), pp. 1533–1536.

Lall, G. S., Atkinson, L. A., Corlett, S. A., Broadbridge, P. J. and Bonsall, D. R. (2012) 'Circadian entrainment and its role in depression: A mechanistic review', *Journal of Neural Transmission*, 119(10), pp. 1085–1096.

Lall, G. S. and Biello, S. M. (2002) 'Attenuation of phase shifts to light by activity or neuropeptide Y: A time course study', *Brain Research*, 957(1), pp. 109–116.

Lall, G. S. and Biello, S. M. (2003) 'Neuropeptide Y, GABA and circadian phase shifts to photic stimuli', *Neuroscience*, 120(4), pp. 915–921.

Lall, G. S., Revell, V. L., Momiji, H., Al Enezi, J., Altimus, C. M., Güler, A. D., Aguilar, C., Cameron, M. A., Allender, S., Hankins, M. W. and Lucas, R. J. (2010) 'Distinct contributions of rod, cone, and melanopsin photoreceptors to encoding irradiance', *Neuron*, 66(3), pp. 417–428.

Leak, R. K., Card, J. P. and Moore, R. Y. (1999) 'Suprachiasmatic pacemaker organization analyzed by viral transynaptic transport', *Brain Research*, 819(1–2), pp. 23–32.

Leak, R. K. and Moore, R. Y. (2001) 'Topographic organization of suprachiasmatic nucleus projection neurons.', *The Journal of comparative neurology*, 433(3), pp. 312–34.

LeGates, T. A., Fernandez, D. C. and Hattar, S. S. (2014) 'Light as a central modulator of circadian rhythms, sleep and affect', *Nat Rev Neurosci*, 15(7), pp. 443–454.

Lesage, F., Guillemare, E., Fink, M., Duprat, F., Lazdunski, M., Romey, G. and Barhanin, J. (1996) 'TWIK-1, a ubiquitous human weakly inward rectifying K+ channel with a novel structure.', *The EMBO journal*, 15(5), pp. 1004–11.

Linden, A.-M., Sandu, C., Aller, M. I., Vekovischeva, O. Y., Rosenberg, P. H., Wisden, W. and Korpi, E. R. (2007) 'TASK-3 knockout mice exhibit exaggerated nocturnal activity, impairments in cognitive functions, and reduced sensitivity to inhalation anesthetics.', *The Journal of pharmacology and experimental therapeutics*, 323(3), pp. 924–934.

Liu, C., Au, J. D., Zou, H. L., Cotten, J. F. and Yost, C. S. (2004) 'Potent activation of the human tandem pore domain K channel TRESK with clinical concentrations of volatile anesthetics', *Anesthesia and Analgesia*, 99(6), pp. 1715–1722.

Liu, W. and Saint, D. A. (2004) 'Heterogeneous expression of tandem-pore K+ channel genes in

adult and embryonic rat heart quantified by real-time polymerase chain reaction', *Clinical and Experimental Pharmacology and Physiology*, 31(3), pp. 174–178.

Logan, R. W., Zhang, C., Murugan, S., O'Connel, S., Levitt, D., Rosenwasser, A. M. and Sarkar, D. K. (2012) 'Chronic shift-lag alters the circadian clock of natural killer cells and promotes lung cancer growth in rats', *The Journal of Immunology*, 188(6), pp. 2583–2591.

López-Otín, C., Blasco, M. A., Partridge, L., Serrano, M. and Kroemer, G. (2013) 'The hallmarks of aging', *Cell*, 153(6), p. 1194.

Lu, B., Su, Y., Das, S., Liu, J., Xia, J. and Ren, D. (2007) 'The Neuronal Channel NALCN Contributes Resting Sodium Permeability and Is Required for Normal Respiratory Rhythm', *Cell*, 129(2), pp. 371–383.

Lu, J., Zhang, Y. H., Chou, T. C., Gaus, S. E., Elmquist, J. K., Shiromani, P. and Saper, C. B. (2001) 'Contrasting effects of ibotenate lesions of the paraventricular nucleus and subparaventricular zone on sleep-wake cycle and temperature regulation.', *Journal of neuroscience*, 21(13), pp. 4864–4874.

Lucas, R. J., Douglas, R. H. and Foster, R. G. (2001) 'Characterization of an ocular photopigment capable of driving pupillary constriction in mice', *Nat Neurosci*, 4(6), pp. 621–626.

Lucas, R. J., Hattar, S. S., Takao, M., Berson, D. M., Foster, R. G. and Yau, K.-W. (2003) 'Diminished Pupillary Light Reflex at High Irradiances in Melanopsin - Knockout Mice', *Science*, 299(5604), pp. 245–247.

Lucas, R. J., Lall, G. S., Allen, A. E. and Brown, T. M. (2012) 'How rod, cone, and melanopsin photoreceptors come together to enlighten the mammalian circadian clock', *Progress in Brain Research*, 199(September 2016), pp. 1–16.

Magnusson, K. R. (2012) 'Aging of the NMDA receptor: From a mouses point of view', *Future Neurology*, 7(5), pp. 627–637.

Markwell, E. L., Feigl, B. and Zele, A. J. (2010) 'Intrinsically photosensitive melanopsin retinal ganglion cell contributions to the pupillary light reflex and circadian rhythm', *Clinical and Experimental Optometry*, 93(3), pp. 137–149.

Masland, R. H. (2012) 'The Neuronal Organization of the Retina', *Neuron*. Elsevier Inc., 76(2), pp. 266–280.

Mathie, A. (2007) 'Neuronal two-pore-domain potassium channels and their regulation by G protein-coupled receptors.', *The Journal of physiology*, 578(Pt 2), pp. 377–385.

Mathie, A., Al Moubarak, E. and Veale, E. L. (2010) 'Gating of two pore domain potassium channels.', *The Journal of Physiology*, 588(Pt 17), pp. 3149–3156.

Mayer, M. L. (2005) 'Crystal structures of the GluR5 and GluR6 ligand binding cores: Molecular mechanisms underlying kainate receptor selectivity', *Neuron*, 45(4), pp. 539–552.

Maynard, S., Fang, E. F., Scheibye-Knudsen, M., Croteau, D. L. and Bohr, V. A. (2015) 'DNA damage, DNA repair, aging, and neurodegeneration', *Cold Spring Harbor Perspectives in Medicine*, 5(10).

Maywood, E. S., Fraenkel, E., McAllister, C. J., Wood, N., Reddy, A. B., Hastings, M. H. and Morton, A. J. (2010) 'Disruption of peripheral circadian timekeeping in a mouse model of Huntington's disease and its restoration by temporally scheduled feeding', *Journal of Neuroscience*, 30(30), pp. 10199–10204.

Maywood, E. S. and Mrosovsky, N. (2001) 'A molecular explanation of interactions between photic and non-photic circadian clock-resetting stimuli', *Gene Expression Patterns*, 1(1), pp. 27–31.

Maywood, E. S., Mrosovsky, N., Field, M. D. and Hastings, M. H. (1999) 'Rapid down-regulation of mammalian Period genes during behavioral resetting of the circadian clock', *Proceedings of the National Academy of Sciences*, 96(26), pp. 15211–15216.

Maywood, E. S., Okamura, H. and Hastings, M. H. (2002) 'Opposing actions of neuropeptide Y and light on the expression of circadian clock genes in the mouse suprachiasmatic nuclei', *European Journal of Neuroscience*, 15(1), pp. 216–220.

McNeill, D. S., Sheely, C. J., Ecker, J. L., Badea, T. C., Morhardt, D., Guido, W. and Hattar, S. S. (2011) 'Development of melanopsin-based irradiance detecting circuitry.', *Neural development*, 6(1), p. 8.

Meijer, J. H., Colwell, C. S., Rohling, J. H. T., Houben, T. and Michel, S. (2012) *Dynamic neuronal network organization of the circadian clock and possible deterioration in disease*. 1st edn, *Progress in Brain Research*. 1st edn. Elsevier B.V.

Meijer, J. H., van der Zee, E. A. and Dietz, M. (1988) 'Glutamate phase shifts circadian activity rhythms in hamsters', *Neuroscience Letters*, 86(2), pp. 177–183.

Meredith, A. L., Wiler, S. W., Miller, B. H., Takahashi, J. S., Fodor, A. a, Ruby, N. F. and Aldrich, R. W. (2006) 'BK calcium-activated potassium channels regulate circadian behavioral rhythms and pacemaker output.', *Nature neuroscience*, 9(8), pp. 1041–1049.

Moga, M. M. and Moore, R. Y. (1997) 'Organization of neural inputs to the suprachiasmatic nucleus in the rat', *Journal of Comparative Neurology*, 389(3), pp. 508–534.

Mohawk, J. A., Green, C. B. and Takahashi, J. S. (2012) 'Central and Peripheral Circadian Clocks in Mammals', *Annual Review of Neuroscience*, 35(1), pp. 445–462.

Mohawk, J. A. and Takahashi, J. S. (2011) 'Cell autonomy and synchrony of suprachiasmatic nucleus circadian oscillators', *Trends in Neurosciences*. Elsevier Ltd, 34(7), pp. 349–358.

Moore, R. Y. and Eichler, V. B. (1972) 'Loss of a circadian adrenal corticosterone rhythm following suprachiasmatic lesions in the rat', *Brain Research*, 42(1), pp. 201–206.

Moore, R. Y. and Speh, J. C. (1993) 'GABA is the principal neurotransmitter of the circadian system', *Neuroscience Letters*, 150(1), pp. 112–116.

Moore, R. Y., Speh, J. C. and Card, J. P. (1995) 'The retinohypothalamic tract originates from a distinct subset of retinal ganglion cells', *Journal of Comparative Neurology*, 352(3), pp. 351–366.

Moore, R. Y., Speh, J. C. and Leak, R. K. (2002) 'Suprachiasmatic nucleus organization', *Cell and Tissue Research*, 309(1), pp. 89–98.

Morin, L. P. (2013a) 'Neuroanatomy of the extended circadian rhythm system', *Experimental Neurology*. Elsevier Inc., 243, pp. 4–20.

Morin, L. P. (2013b) 'Nocturnal light and nocturnal rodents: Similar regulation of disparate functions?', *Journal of Biological Rhythms*, 28(2), pp. 95–106.

Mrosovsky, N. (1999) 'Masking: History, Definitions, and Measurement', *Chronobiology International*, 16(4), pp. 415–429.

Mrosovsky, N. and Hattar, S. (2003) 'Impaired Masking Responses to Light in Melanopsin-Knockout Mice', *Chronobiology International*, 20(6), pp. 989–999.

Mrosovsky, N. and Thompson, S. (2008) 'Negative and positive masking responses to light in retinal degenerate slow (rds/rds) mice during aging', *Vision Research*, 48(10), pp. 1270–1273.

Myung, J., Hong, S., DeWoskin, D., De Schutter, E., Forger, D. B. and Takumi, T. (2015) 'GABA-mediated repulsive coupling between circadian clock neurons in the SCN encodes seasonal time.', *Proceedings of the National Academy of Sciences of the United States of America*, 112, pp. E3920-3929.

Nahm, S.-S., Farnell, Y. Z., Griffith, W. and Earnest, D. J. (2005) 'Circadian Regulation and Function of Voltage-Dependent Calcium Channels in the Suprachiasmatic Nucleus', *The Journal*

of Neuroscience, 25(40), pp. 9304–9308.

Nakamura, T. J., Nakamura, W., Yamazaki, S., Kudo, T., Cutler, T., Colwell, C. S. and Block, G. D. (2011) 'Age-Related Decline in Circadian Output', *Journal of Neuroscience*, 31(28), pp. 10201–10205.

Nanou, E., Kyriakatos, A., Kettunen, P. and El Manira, A. (2009) 'Separate signalling mechanisms underlie mGluR1 modulation of leak channels and NMDA receptors in the network underlying locomotion', *Journal of Physiology*, 587(12), pp. 3001–3008.

Nash, H. A., Scott, R. L., Lear, B. C. and Allada, R. (2002) 'An Unusual Cation Channel Mediates Photic Control of Locomotion in Drosophila', *Current Biology*, 12(2), pp. 2152–2158.

Niswender, C. M. and Conn, P. J. (2010) 'Metabotropic Glutamate Receptors: Physiology, Pharmacology, and Disease', *Annual Review of Pharmacology and Toxicology*, 50(1), pp. 295–322.

Ohta, H., Yamazaki, S. and McMahon, D. G. (2005) 'Constant light desynchronizes mammalian clock neurons', *Nature Neuroscience*, 8(3), pp. 267–269.

Ono, D., Honma, K. ichi, Yanagawa, Y., Yamanaka, A. and Honma, S. (2018) 'Role of GABA in the regulation of the central circadian clock of the suprachiasmatic nucleus', *Journal of Physiological Sciences*. Springer Japan, 68(4), pp. 333–343.

Paoletti, P. and Neyton, J. (2007) 'NMDA receptor subunits: function and pharmacology', *Current Opinion in Pharmacology*, 7(1), pp. 39–47.

Partch, C. L., Green, C. B. and Takahashi, J. S. (2014) 'Molecular architecture of the mammalian circadian clock', *Trends in Cell Biology*. Elsevier Ltd, 24(2), pp. 90–99.

Patton, A. P. and Hastings, M. H. (2018) 'The Suprachiasmatic Nucleus', *Current Biology*. Elsevier, 28(15), pp. R816–R822.

Pergel, E., Lengyel, M., Enyedi, P. and Czirják, G. (2019) 'TRESK (K2P18.1) background potassium channel is activated by novel-type protein kinase C via dephosphorylation', *Molecular Pharmacology*, 95(6), pp. 661–672.

Pittendrigh, C. S. and Daan, S. (1976a) 'A functional analysis of circadian pacemakers in nocturnal rodents - I. The stability and lability of spontaneous frequency', *Journal of Comparative Physiology*, 106(3), pp. 223–252.

Pittendrigh, C. S. and Daan, S. (1976b) 'A functional analysis of circadian pacemakers in nocturnal rodents - IV. Entrainment: Pacemaker as clock', *Journal of Comparative Physiology*,

106(3), pp. 291–331.

van den Pol, A. N. (1994) 'Metabotropic glutamate receptor mGluR1 distribution and ultrastructural localization in hypothalamus', *Journal of Comparative Neurology*, 349(4), pp. 615–632.

Prolo, L. M. (2005) 'Circadian Rhythm Generation and Entrainment in Astrocytes', *Journal of Neuroscience*, 25(2), pp. 404–408.

Rajan, S., Preisig-Muller, R., Wischmeyer, E., Nehring, R., Hanley, P. J., Renigunta, V., Musset, B., Schlichthorl, G., Derst, C., Karschin, A. and Daut, J. (2002) 'Interaction with 14-3-3 proteins promotes functional expression of the potassium channels TASK-1 and TASK-3.', *The Journal of physiology*, 545(Pt 1), pp. 13–26.

Reddy, A. B., Field, M. D., Maywood, E. S. and Hastings, M. H. (2002) 'Differential resynchronisation of circadian clock gene expression within the suprachiasmatic nuclei of mice subjected to experimental jet lag.', *The Journal of neuroscience : the official journal of the Society for Neuroscience*, 22(17), pp. 7326–7330.

Reddy, P., Zehring, W. A., Wheeler, D. A., Pirrotta, V., Hadfield, C., Hall, J. C. and Rosbash, M. (1984) 'Molecular analysis of the period locus in Drosophila melanogaster and identification of a transcript involved in biological rhythms', *Cell*, 38(3), pp. 701–710.

Redlin, U. (2001) 'Neural basis and biological function of masking by light in mammals: Suppression of melatonin and locomotor activity', *Chronobiology International*, 18(5), pp. 737–758.

Refinetti, R. (2004) 'Non-stationary time series and the robustness of circadian rhythms', *Journal of Theoretical Biology*, 227(4), pp. 571–581.

Refinetti, R. (2006) *Circadian physiology*. 2nd Editio. London: CRC Press.

Renigunta, V., Schlichthorl, G. and Daut, J. (2015) 'Much more than a leak: structure and function of K2P-channels', *Pflugers Archiv European Journal of Physiology*, pp. 867–894.

Reppert, S. M. and Weaver, D. R. (2001) 'Molecular analysis of mammalian circadian rhythms', *Physiology*, 63, p. 647.

Rietveld, W. J., Minors, D. S. and Waterhouse, J. M. (1993) 'Circadian rhythms and masking: An overview', *Chronobiology International*, 10(4), pp. 306–312.

Roenneberg, T., Hut, R., Daan, S. and Merrow, M. (2010) 'Entrainment concepts revisited.', *Journal of biological rhythms*, 25(5), pp. 329–339.

Roseboom, P. H., Namboodiri, M. a. A., Zimonjic, D. B., Popescu, N. C., R. Rodriguez, I., Gastel, J. A. and Klein, D. C. (1998) 'Natural melatonin "knockdown" in C57BL/6J mice: Rare mechanism truncates serotonin N-acetyltransferase', *Molecular Brain Research*, 63(1), pp. 189–197.

Ruby, N. F., Brennan, T. J., Xie, X., Cao, V., Franken, P., Heller, C. and Hara, B. F. O. (2002) 'Role of Melanopsin in Circadian Responses to Light', *Science*, 298(5601), pp. 2211–2213.

Rusak, B., Robertson, H. A., Wisden, W. and Hunt, S. P. (1990) 'Light Pulses That Shift Rhythms Induce Gene Expression in the Suprachiasmatic Nucleus', *Science*, 248(4960), pp. 1237–1240.

Sack, R. L. (2009) 'The pathophysiology of jet lag', *Travel Medicine and Infectious Disease*, 7(2), pp. 102–110.

Sano, Y., Inamura, K., Miyake, A., Mochizuki, S., Kitada, C., Yokoi, H., Nozawa, K., Okada, H., Matsushime, H. and Furuichi, K. (2003) 'A novel two-pore domain K+ channel, TRESK, is localized in the spinal cord', *Journal of Biological Chemistry*, 278(30), pp. 27406–27412.

Sauer, B. and Henderson, N. (1988) 'Site-specific DNA recombination in mammalian cells by the Cre recombinase of bacteriophage P1', *Proceedings of the National Academy of Sciences*, 85(14), pp. 5166–5170.

Schewe, M., Nematian-Ardestani, E., Sun, H., Musinszki, M., Cordeiro, S., Bucci, G., De Groot, B. L., Tucker, S. J., Rapedius, M. and Baukrowitz, T. (2016) 'A Non-canonical Voltage-Sensing Mechanism Controls Gating in K2P K+ Channels', *Cell*, 164(5), pp. 937–949.

Schmidt, T. M., Chen, S. K. and Hattar, S. S. (2011) 'Intrinsically photosensitive retinal ganglion cells: Many subtypes, diverse functions', *Trends in Neurosciences*. Elsevier Ltd, 34(11), pp. 572–580.

Schmittgen, T. D. and Livak, K. J. (2008) 'Analyzing real-time PCR data by the comparative CT method', *Nature Protocols*, 3(6), pp. 1101–1108.

Sekaran, S., Foster, R. G., Lucas, R. J. and Hankins, M. W. (2003) 'Calcium Imaging Reveals a Network of Intrinsically Light-Sensitive Inner-Retinal Neurons Sumathi', *Current Biology*, 13, pp. 1290–1298.

Sepulveda, F. V, Pablo Cid, L., Teulon, J. and Niemeyer, M. I. (2015) 'Molecular aspects of structure, gating, and physiology of pH-sensitive background K2P and Kir K+-transport channels', *Physiol Rev*, 95(1), pp. 179–217.

Sherwood, L. (1993) *Human Physiology: From Cells to Systems*. Second Edi. West publishing

company.

Shuboni, D. D., Cramm, S., Yan, L., Nunez, A. A. and Smale, L. (2012) 'Acute behavioral responses to light and darkness in nocturnal Mus musculus and diurnal Arvicanthis niloticus', *Journal of Biological Rhythms*, 27(4), pp. 299–307.

Steinberg, E. A., Wafford, K. A., Brickley, S. G., Franks, N. P. and Wisden, W. (2014) 'The role of K2P channels in anaesthesia and sleep', *Pflugers Archiv European Journal of Physiology*, 467(5), pp. 907–916.

Stephan, F. K. and Zucker, I. (1972) 'Circadian rhythms in drinking behavior and locomotor activity of rats are eliminated by hypothalamic lesions.', *Proceedings of the National Academy of Sciences of the United States of America*, 69(6), pp. 1583–6.

Talley, E. M., Solorzano, G., Lei, Q., Kim, D. and Bayliss, D. a (2001) 'CNS distribution of members of the two-pore-domain (KCNK) potassium channel family.', *The Journal of neuroscience : the official journal of the Society for Neuroscience*, 21(19), pp. 7491–7505.

Thomas, D. and Goldstein, S. A. N. (2010) 'Two-P-Domain (K 2P) Potassium Channels: Leak Conductance Regulators of Excitability', *Encyclopedia of Neuroscience*, 1, pp. 1207–1220.

Thompson, S., Foster, R. G., Stone, E. M., Sheffield, V. C. and Mrosovsky, N. (2008) 'Classical and melanopsin photoreception in irradiance detection: Negative masking of locomotor activity by light', *European Journal of Neuroscience*, 27(8), pp. 1973–1979.

Tso, C. F., Simon, T., Greenlaw, A. C., Puri, T., Mieda, M. and Herzog, E. D. (2017) 'Astrocytes Regulate Daily Rhythms in the Suprachiasmatic Nucleus and Behavior', *Current Biology*. Elsevier Ltd., 27(7), pp. 1055–1061.

Tulleuda, A., Cokic, B., Callejo, G., Saiani, B., Serra, J. and Gasull, X. (2011) 'TRESK channel contribution to nociceptive sensory neurons excitability: modulation by nerve injury.', *Molecular pain*, 7(1), p. 30.

Ukai-Tadenuma, M., Yamada, R. G., Xu, H., Ripperger, J. A., Liu, A. C. and Ueda, H. R. (2011) 'Delay in feedback repression by cryptochrome 1 Is required for circadian clock function', *Cell*, 144(2), pp. 268–281.

Viswanathan, N. and Davis, F. C. (1995) 'Suprachiasmatic nucleus grafts restore circadian function in aged hamsters', *Brain Research*, 686(1), pp. 10–16.

Vujovic, N., Gooley, J. J., Jhou, T. C. and Saper, C. B. (2015) 'Projections from the subparaventricular zone define four channels of output from the circadian timing system',

Journal of Comparative Neurology, 523(18), pp. 2714–2737.

Wang, Y. C. and Huang, R. C. (2006) 'Effects of sodium pump activity on spontaneous firing in neurons of the rat suprachiasmatic nucleus', *J Neurophysiol*, 96(0022–3077 (Print)), pp. 109–118.

Weir, G. A. and Cader, Z. M. (2011) 'New directions in migraine', *BMC Medicine*. BioMed Central Ltd., 9(1), p. 116.

Weir, G. A., Pettingill, P., Wu, Y., Duggal, G., Ilie, A.-S., Akerman, C. J. and Cader, Z. M. (2019) 'The Role of TRESK in Discrete Sensory Neuron Populations and Somatosensory Processing', *Frontiers in Molecular Neuroscience*, 12(July), pp. 1–11.

Welsh, D. K., Logothetis, D. E., Meister, M. and Reppert, S. M. (1995) 'Individual Neurons Dissociated From Rat Suprachiasmatic Nucleus Express Independently Phased Circadian Firing Rhythms', *Neuron*, 14(4), pp. 697–706.

Welsh, D. K., Takahashi, J. S. and Kay, S. A. (2010) 'Suprachiasmatic Nucleus: Cell Autonomy and Network Properties', *Annual Review of Physiology*, 72(1), pp. 551–577.

Willard, S. S. and Koochekpour, S. (2013) 'Glutamate, glutamate receptors, and downstream signaling pathways', *International Journal of Biological Sciences*, 9(9), pp. 948–959.

Wolff, G., Duncan, M. J. and Esser, K. a (2013) 'Chronic phase advance alters circadian physiological rhythms and peripheral molecular clocks.', *Journal of applied physiology (Bethesda, Md. : 1985)*, 115(3), pp. 373–82.

Yan, L., Karatsoreos, I., LeSauter, J., Welsh, D. K., Kay, S., Foley, D. and Silver, R. (2007) 'Exploring spatiotemporal organization of SCN circuits', *Cold Spring Harbor Symposia on Quantitative Biology*, 72, pp. 527–541.

Yan, L. and Silver, R. (2002) 'Differential induction and localization of mPer1 and mPer2 during advancing and delaying phase shifts', *European Journal of Neuroscience*, 16(8), pp. 1531–1540.

Yannielli, P. C. and Harrington, M. E. (2000) 'Neuropeptide Y applied in vitro can block the phase shifts induced by light in vivo', *NeuroReport*, 11(7), pp. 1–5.

Yellen, G. (2002) 'The voltage-gated potassium channels and their relatives.', *Nature*, 419(6902), pp. 35–42.

Yoo, S.-H., Yamazaki, S., Lowrey, P. L., Shimomura, K., Ko, C. H., Buhr, E. D., Siepka, S. M., Hong, H.-K., Oh, W. J., Yoo, O. J., Menaker, M. and Takahashi, J. S. (2004) 'PERIOD2::LUCIFERASE real-time reporting of circadian dynamics reveals persistent circadian oscillations in mouse

peripheral tissues', *Proceedings of the National Academy of Sciences*, 101(15), pp. 5339–5346.

Zhao, J., Warman, G. R. and Cheeseman, J. F. (2019) 'The functional changes of the circadian system organization in aging', *Ageing Research Reviews*. Elsevier, 52(December 2018), pp. 64–71.

Zuniga, L. and Zuniga, R. (2016) 'Understanding the cap structure in K2P channels', *Frontiers in Physiology*, 7(June), p. 228.

Appendix 1

[REDACTED]

Appendix 2

[REDACTED]